Dynamically reconfigurable optical access network

Dynamically Reconfigurable Optical Access Network

PROEFSCHRIFT

ter verkrijging van de graad van doctor aan de
Technische Universiteit Eindhoven, op gezag van de
rector magnificus, prof.dr.ir. C.J. van Duijn, voor een
commissie aangewezen door het College voor
Promoties in het openbaar te verdedigen
op maandag 16 november 2009 om 16.00 uur

door

Patryk Jan Urban

geboren te Szczecin, Polen

Dit proefschrift is goedgekeurd door de promotor:

prof.ir. A.M.J. Koonen

Copromotoren:
dr.ir. H. de Waardt
en
dr. G.N. van den Hoven

A catalogue record is available from
the Eindhoven University of Technology Library

Urban, Patryk

Dynamically Reconfigurable Optical Access Network
Proefschrift. - ISBN 978-90-386-2093-0
NUR 959
Trefw.: optische telecommunicatie / lokale telecommunicatie
Subject headings: optical fibre communication / local area networks

Typeset using LaTeX, printed in The Netherlands.

(...) I need the truth
Ryszard Riedel

Marcie
Moim Rodzicom

Summary

Dynamically Reconfigurable Optical Access Network

This dissertation presents the research results on a fiber-optic high bit-rate access network which enables dynamic bandwidth allocation as a response to varying subscribers' demands and bandwidth needs of emerging services.

The motivation of the research is given in **Chapter 1 "Introduction"** together with a brief comparative discussion on currently available and future access networks. The idea of wavelength reconfigurability in the last-mile networks is described as a solution for more efficient bandwidth utilization and a subject of the Broadband Photonics project.

Chapter 2 "Reconfigurable WDM/TDM access network - architecture" provides a comprehensive description of the proposed solution with each network element being analyzed in terms of its functionalities. This includes a colorless optical network unit and a reconfigurable optical add/drop multiplexer. An estimation of power budget is followed by the choice of wavelength set and network control and management layer overview.

In **Chapter 3 "Reflective transceiver module for ONU"** after discussing different communication schemes and modulation formats three approaches to a colorless high bit-rate transmitter are analyzed in detail. This includes experiment and simulation results on a reflective semiconductor optical amplifier, reflective electro-absorption modulator and a Michelson-interferometer modulator. The Chapter is concluded with a comparative discussion.

Chapter 4 "Reconfigurable optical add/drop multiplexer" discusses another key element in the proposed network architecture which is an integrated structure of micro-ring resonators providing wavelength reconfigurability. The measured characteristics assess the applicability of the device able to support unicast and multicast transmission.

A range of possible sources of signal degradation in the access links are analyzed in **Chapter 5 "Transmission and network impairments in the access network"**. An estimation of potential power penalties resulting from such impairments in the proposed system follows afterwards.

Special attention is paid to optical in-band crosstalk penalties and improvement methods in **Chapter 6 "Interferometric crosstalk in the access network with an RSOA"**. This subject is treated extensively with the support of mathematical considerations and experimental results.

Proof-of-concept experiments of the proposed network architecture are presented in **Chapter 7 "Reconfigurable WDM/TDM access network - experiments"**. The results of bidirectional transmission of high bit-rate WDM signals in different wavelength allocation schemes are discussed in detail. From there, the behavior of a full-scale network is assessed by means of simulations.

In **Chapter 8 "Migration towards WDM/TDM access network"** the migration scenario from currently deployed fiber-optic access networks towards the novel solution is proposed. Afterwards, a short dispute on the economics of last-mile fiber technologies is included.

Finally, the work is concluded and potential future research ideas based on this thesis are given in **Chapter 9 "Conclusions and further work"**.

Contents

Summary **i**

1 Introduction **1**
1.1 Rationale . . . 1
1.2 Next-generation access architectures . . . 3
1.2.1 Wavelength reconfigurability . . . 8
1.3 Overview of fiber-to-the-x market . . . 9
1.4 The Broadband Photonics Access project . . . 11
1.5 Contributions of the dissertation and thesis overview . . . 12

2 Reconfigurable WDM/TDM access network - architecture **13**
2.1 General specifications . . . 13
2.2 Central office . . . 16
2.3 Optical network unit . . . 16
2.4 Remote node . . . 17
2.5 Power budget . . . 19
2.6 Wavelength set . . . 24
2.7 Network control and management . . . 25

3 Reflective transceiver module for ONU **27**
3.1 CO-ONU communication schemes . . . 27
3.1.1 Modulation format . . . 28
3.1.2 Wavelength demultiplexing at ONU . . . 29
3.2 Reflective semiconductor optical amplifier . . . 30
3.2.1 MQW-RSOA characterization . . . 31
3.3 Reflective electro-absorption modulator . . . 36
3.3.1 REAM characterization . . . 37
3.3.2 R-SOA-EAM characterization . . . 38
3.4 Michelson-interferometer modulator . . . 39
3.5 Comparison of reflective modulators . . . 42

4 Reconfigurable optical add/drop multiplexer 45
4.1 ROADM architecture . . . 45
4.2 Static characterization . . . 48
4.3 Dynamic characterization . . . 53

5 Transmission and network impairments in the access network 63
5.1 Limited extinction ratio . . . 63
5.2 Intrachannel crosstalk . . . 64
5.3 Interchannel crosstalk . . . 67
5.4 Accumulation of ASE noise . . . 68
5.5 Other sources of power penalties . . . 70
5.5.1 Dispersion . . . 70
5.5.2 Frequency chirping in the transmitter . . . 71
5.5.3 Narrow effective passband . . . 71
5.5.4 Nonlinearities . . . 72
5.5.5 PDL, component aging and power margin . . . 73
5.6 Power penalties in the BBPhotonics network . . . 74

6 Interferometric crosstalk in the access network with an RSOA 75
6.1 Crosstalk scenario . . . 75
6.2 Analytical models . . . 77
6.2.1 Coherent crosstalk and RSOA bias dithering . . . 77
6.2.2 Incoherent crosstalk and RSOA bias dithering . . . 81
6.2.3 Coherent crosstalk and external phase modulation . . . 82
6.2.4 Incoherent crosstalk and external phase modulation . . . 83
6.3 Experimental results . . . 84
6.3.1 Coherent crosstalk and RSOA bias dithering . . . 85
6.3.2 Incoherent crosstalk and RSOA bias dithering . . . 87
6.3.3 Coherent crosstalk and external phase modulation . . . 87
6.3.4 Incoherent crosstalk and external phase modulation . . . 92
6.4 Discussion . . . 92

7 Reconfigurable WDM/TDM access network - experiments 97
7.1 1.25 Gbit/s transmission . . . 97
7.1.1 Testbed structure . . . 98
7.1.2 Measurement and simulation results . . . 100
7.2 10 Gbit/s transmission . . . 102
7.2.1 Testbed structure . . . 102
7.2.2 Measurement results . . . 105
7.3 Full-scale network transmission model . . . 109
7.3.1 Model description . . . 110
7.3.2 Simulation results . . . 119
7.4 Summary . . . 122

8 Migration towards WDM/TDM access network 123
8.1 Hardware upgrade 123
8.2 Economics of WDM-PON 126

9 Conclusions and further work 131
9.1 Conclusions 131
9.2 Further work 135

A Optical code division multiple access-extended BBPhotonics network architecture 137
A.1 Two-dimensional incoherent optical coding 138
A.2 Implementation of two-dimensional OCDMA in BBPhotonics network architecture 139

B RSOA simulation model 143

C The BBPhotonics testbed 145

References 147

Acronyms 161

Acknowledgements 167

Curriculum vitae 169

List of publications 171

Chapter 1

Introduction

In 1841, a Swiss physicist Daniel Colladon, demonstrated that light can use internal reflection to follow a specific path. In his experiment he directed a beam of sunlight at the stream of water flowing through the spout of one container to another. The light beam followed a zigzag path inside the curved path of the water. This is considered to be the first research into the guided transmission of light [1].

A hundred years later another milestone was set by Brian O'Brien from the American Optical Company and his colleagues from the Imperial College of Science and Technology in London who developed a fiberscope, which used the first practical all-glass fiber, and a few years later, an externally coated glass fiber.

In 1990, only 40 years after bringing the term "fiber optics" to life, engineers at Bell Laboratories succeeded in soliton transmission of a 2.5 Gbit/s signal over 7500 km without regeneration using an erbium-doped fiber amplifier (EDFA) and less than a decade afterwards they reached another record of sending a hundred of 10 Gbit/s wavelength channels for a distance of 400 km thanks to wavelength division multiplexing (WDM) [2].

Today the technology chase has brought the WDM technology closer to the end-user. After conquering long-haul transport networks and metro networks it is entering the area of access networks.

1.1 Rationale

59 % to 64 % of the downstream traffic is web- or web media-related which is mainly because of photo and video communication and real-time streaming. Peer-to-peer (P2P) traffic covers over one-fifth of downstream and over 60 % of upstream traffic. Services alternative to P2P like file hosting and remote storage are gaining more interest [3]. Also the growing interest in voice, video and data delivery on the same infrastructure (triple-play) has changed the common way of network usage - a necessity of running many application on several devices connected si-

Table 1.1: Downstream bandwidth consumption for future access networks.

Service	Bandwidth
SDTV	2 Mbit/s per channel
HDTV	8 Mbit/s per channel
3D SDTV	63 Mbit/s per channel
3D HDTV	187 Mbit/s per channel
Basic HSI	5 Mbit/s average
Gaming	10 Mbit/s average
Multimedia surfing	8 Mbit/s average
Video-conf. and learning	3 Mbit/s per session
Home-working	4 Mbit/s average
VoIP	110 Kbit/s

multaneously to a single access point has arisen [4]. Furthermore, when mature high-definition TV (HDTV) products become available the situation will get even worse. Changing from the standard-definition TV (SDTV) to HDTV, 1-3 Mbit/s to 8 Mbit/s per channel respectively, even not including services like video-on-demand (VoD), P2P and online gaming will exceed the capabilities of currently most popular digital subscriber lines (DSLs) drastically [5]. Although the transmission speed offered by the asymmetric DSL (ADSL) technology has improved significantly from 512 Kbit/s (2001) up to 20 Mbit/s (2006), the most sophisticated protocols ADSL2+ and very high speed DSL 2 (VDSL2) are not able to satisfy the next-generation users' bandwidth hunger. This forces the efforts towards not only near-future solutions but also towards future-proof networks which can last for next 25 years and more [6].

Table 1.1 shows the bandwidth requirements for some example services [7, 8], and fig. 1.1 gives the flavor of time required to download a file depending on the access technology. Besides multi-session applications, e. g. multi HDTV channels transmission to one home, the traffic pattern changes, for instance, from the before-noon business-centric file transfer and video-conference to afternoon entertainment-centric VoD and voice-over-IP (VoIP) communication. Therefore, the location of the traffic congestion changes on a specific time-scale basis [9].

This bandwidth-hungry scenario created by both content providers and consumers stimulates the development of novel components and network architectures which should not only be capable of transmitting data at high bit-rates but should also be cost-efficient. Latter is a necessity to make them particularly attractive for network operators and service providers (SP). The physical layer of such network has to be capable of providing bandwidth on-demand, and, since the destination

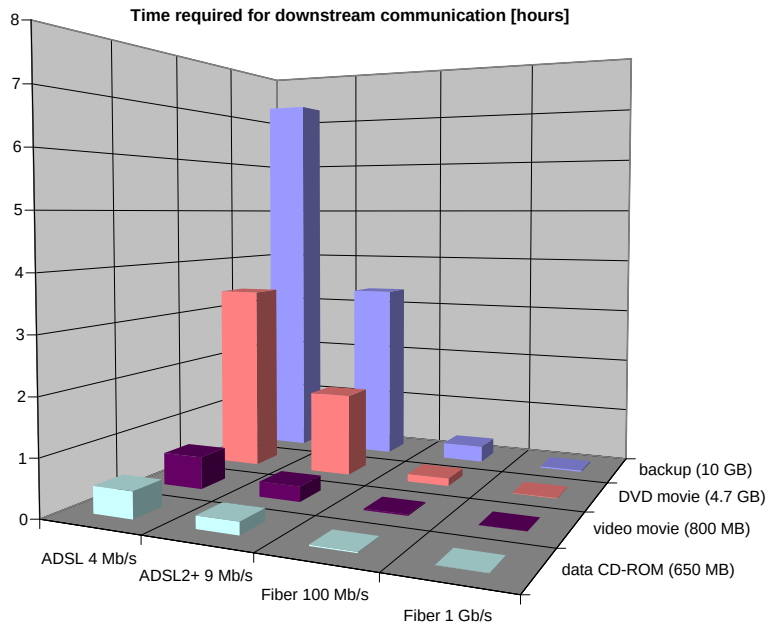

Figure 1.1: Examples of downstream services (calculation performed with [10]).

of the traffic load may change in time, the provision of the bandwidth should be made reconfigurable.

The great majority of current copper-based and point-to-point fiber-based access installations do not comprise these features and need to be changed into advanced fiber architectures [11, 12].

Although installing optical fiber in the access area is a great challenge, e. g. in terms of capital expenses (CAPEX), next question comes immediately: which network solution should be chosen in order to succeed in low operational expenses (OPEX), so the end-user can enjoy instantaneous large bandwidth connectivity without upgrades in the next decades?

The so-called next-generation access (NGA) network can provide the answer for the requirements in the "last mile".

1.2 Next-generation access architectures

The basic general architectures of optical access networks are point-to-point (PtP) and point-to-multipoint (PtMP) [13] as depicted in fig. 1.2. Because of different possible placements of the optical network unit (ONU) there are several topologies for access networks, for instance fiber to the home (FTTH a. k. a. fiber home-run), fiber to the node/curb/bulding (FTTN/C/B), in general FTTX. In case of

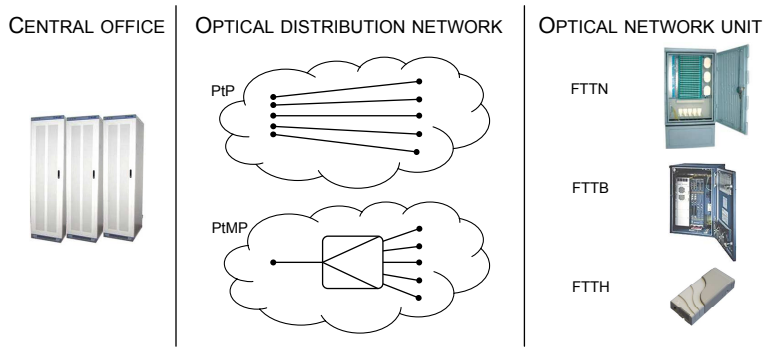

Figure 1.2: Access network architectures.

Table 1.2: Overview of access network standards.

	Standard	Date	Bandwidth
APON	inc. in ITU-T G.983	1998	625 Mbit/s
BPON	ITU-T G.983	2002	625 Mbit/s
EPON	IEEE 802.3ah	2004	1.25 Gbit/s
GPON	ITU-T G.984	2005	2.4 Gbit/s
10GPON	none	to be ratified in 2010	10 Gbit/s
WDM-PON	none	unknown	1-10 Gbit/s per wav.

FTTN/C/B a copper cable is provided in the very last section from the ONU to the user's home which gives the maximum capacity of 100 Mbit/s at 300 m (for VDSL2). FTTN also holds for hybrid fiber-coax (HFC) which provides lower bandwidth. FTTH is a completely optical connection reaching the user's home, thus it can provide the largest bandwidth. In some exceptions, like rural areas due to low population density, ONU can be equipped with a radio base station providing wireless connectivity to the home (fixed-wireless access, FWA).

Currently deployed broadband access networks together with the solutions being considered for NGA are given in table 1.2, where an evident trend of increasing the aggregated bandwidth can be noticed.

DSL exploits the existing copper infrastructure that was originally deployed for plain old telephone services (POTS) and the maximum available bit-rate is achieved at a range of few hundred meters as mentioned before [14].

The growing popularity of fiber as an efficient transmission medium in terms of achievable bit-rate and reach has brought several standards for passive optical

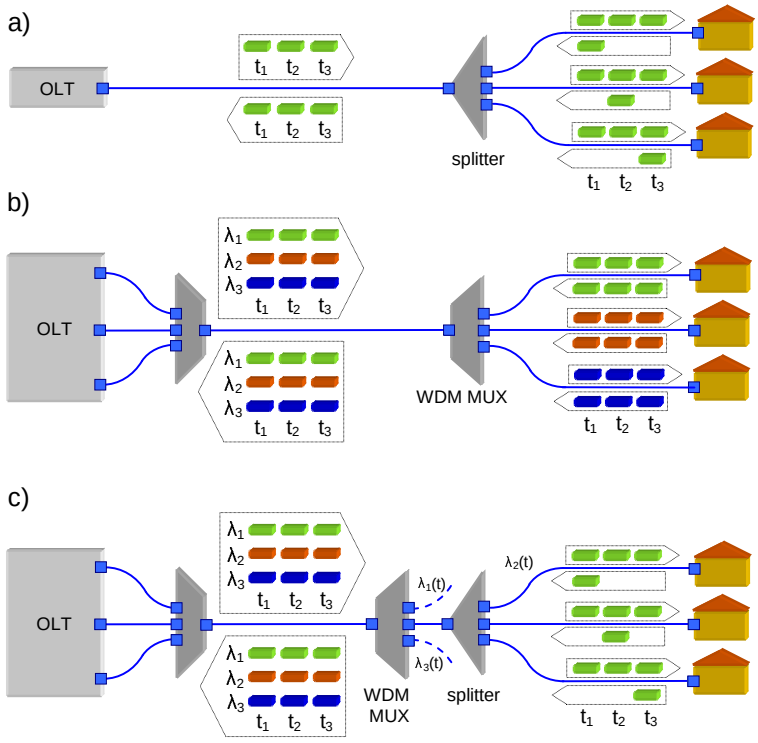

Figure 1.3: Passive optical network architectures: a) TDM-PON, b) WDM-PON and c) WDM/TDM-PON.

access networks (PONs). A PON consists of an optical line termination (OLT, situated in the central office, CO), ONUs and an optical distribution network (ODN) which includes fiber spans and splitters between OLT and ONUs. The CO provides the interface between the PON and the backbone network. The ONU terminates the optical link and provides interfaces at the user side for different services. In a PON system downstream encrypted signals are broadcast to each ONU on a shared fiber plant. Upstream signals are combined using time division multiple access (TDMA) such that every ONU is assigned a time slot for transmission, fig. 1.3a. PONs are attractive for their low outside plant (OSP) maintenance costs, for instance no power supply in the cabinet is needed and in case of a fiber-cable rupture between OLT and the distribution cabinet fewer splices are needed than in a multi-fiber installation.

Asynchronous transfer mode PON (ATM-PON or APON) was the first PON standard and it was intended for business applications. Further improvements to the original APON concept led to broadband PON (BPON) which provides an asymmetric bandwidth of typically 622 Mbit/s downstream and 155 Mbit/s

upstream [15]. The ethernet PON (EPON) uses standard ethernet frames with symmetric 1.25 Gbit/s upstream and downstream rates. It is applicable for networks in data centers as well as access networks with triple-play service [16]. The gigabit PON (GPON) standard is a great improvement with respect to BPON. It uses variable-length packets which gives larger aggregated bandwidth (2.5 Gbit/s) and exploits the bandwidth more efficiently. To allow for higher quality of service (QoS) for delay-sensitive applications a GPON encapsulation method (GEM) is implemented in the standard [17]. 10GPON (10 gigabit PON) is a GPON natural successor, which provides larger bandwidth. However, it requires expensive components a. o. high-bandwidth burst-mode receivers. Wavelength division multiplexing PON (WDM-PON) exploits multiple optical wavelengths to increase available bandwidth. In such system each ONU receives and transmits data on a dedicated (unshared) wavelength channel, therefore the strict time-scheduling due to time division multiplexing (TDM) transmission is not required any longer, fig. 1.3b.

10GPON and WDM-PON are a subject of an intensive discussion on their pros and cons [18,19]. However, a general conclusion is that a WDM-PON, which in fact provides a wavelength-based PtP connectivity, combines the advantages of fiber-based PtP communication and PtMP infrastructure as summarized in table 1.3.

Besides providing the end-users with much larger bandwidth in downstream and upstream, WDM-PON systems can cover larger areas since the power budget is significantly extended. For instance, in case of a system with 32-ONUs a multiplexer/demultiplexer in a WDM-PON will introduce around 4 dB loss, and a power splitter in a TDM-PON will introduce over 15 dB loss. Both networks can be extended to long-reach PONs, beyond 20-25 km, through a single amplification module placed in the ODN [20]. Another advantage of a WDM-PON system over TDM-PON is the ease of scalability. Adding an extra ONU in the former one requires launching another wavelength which is done without any disruption to the other active users, whereas in a TDM-PON connecting additional ONU reduces average bandwidth available per each user in the system. Apparently, both upgrades are feasible as long as the distribution points, like multiplexer or passive splitter, are equipped with sufficient amount of free ports. Another issue in a TDM-PON is the capability of upgrading to higher bit-rate. Since each ONU in a TDM scheme has to work at the same bit-rate, an upgrade of even a single ONU implies the upgrade of the complete system, whereas in WDM or fiber-diversified scheme it can be introduced on a per-wavelength or per-fiber, thus per ONU, basis. A great advantage of TDM-PON system is the reduction of energy consumption. Since it scales together with the number of OLT ports, a TDM-PON architecture which uses a single port at OLT to provide the communication to the complete PON system, is more energy-efficient than a wavelength-PtP or fiber-PtP [21,22]. From a SP's viewpoint the key advantage of the WDM-PON is the capability of the local-loop unbundling (LLU), which means the possibility to introduce several SPs on the same network infrastructure simply by assigning different wavelength channels, thus corresponding ONUs, to a given SP. The benefits of LLU, for instance cost-reduction, are not only directed to SPs, also the end-users gain in richer

Table 1.3: Advantages and disadvantages of different optical access architectures.

	fiber PtP	TDM-PON (PtMP)	WDM-PON (wavelength PtP)
LLU	+	-	+
Upscale to more ONUs	+	-	+
Upgrade to higher bit-rate	+	-	+
Power budget	+	-	+/-
Energy consumption	-	+	+/-
Fiber plant reduction	-	+	+

and more competitive offers.

In a WDM-PON system a single wavelength pair can provide a separate TDM-PON, e. g. GPON. Such architecture is referred to as a hybrid WDM/TDM-PON and a single wavelength-specific PON is very often referred to as a virtual PON or colored PON, fig. 1.3c. The wavelengths can be also used in a flexible manner to provide efficient bandwidth allocation which brings the benefit of increased average bandwidth available per user [12, 13, 23–25]. Although wavelength-flexible and wavelength-fixed WDM/TDM-PON can scale up to a much larger number of active users than WDM-PON they have lower power budget and limited range with respect to the latter one. However, the main issue related to WDM and WDM/TDM systems is the high cost of components, a. o. wavelength-specific transmitters. This can be solved if more functionalities are integrated on a single optical chip which enables mass production to eventually provide a lower cost per device [26, 27]. The critical problems for a 10GPON system are dispersion management and a high-speed burst-mode receiver with sufficient sensitivity.

The NGA covers a large area of research subjects from physical layer up to the protocol layer and involves numerous development aspects, e. g. network capacity, reach and coverage as well as network reliability, survivability and scalability. The recent decade has brought numerous PON-related research projects [11, 28] and an evolutionary trend towards a hybrid WDM/TDM-PON can be noticed. Different architectures have been considered such as splitter-based PON, (cascaded) arrayed waveguide grating (AWG)-based PON, amplified PON and PONs based on different wavelength spacings [29,30] as well as different topologies such as bus-and-tree or ring [31–33], integrated metro-access architectures [34] and long-reach large-scale solutions [35–37]. In those works only fixed wavelength assignment has been considered. However, as access networks tend to connect a higher number of users each with fluctuating bandwidth demands, this growing amount of traffic should be dynamically managed which brings the strong need for reconfigurability in the access domain as addressed in [23, 24].

1.2.1 Wavelength reconfigurability

In a short-term evolution scenario a demand of on average 60-70 Mbit/s per ONU is expected which includes multiple HDTV channels, and in a long-term evolution it can reach 300 Mbit/s and beyond when including 3D HDTV [7, 8]. As a result traffic congestion will increase. In a multiwavelength transmission system it can be reduced by routing wavelength carriers from areas with lower bandwidth requirements to areas with higher bandwidth requirements, fig. 1.4. As a result, the number of ONUs sharing the same wavelength channel is adapted dynamically [13, 38].

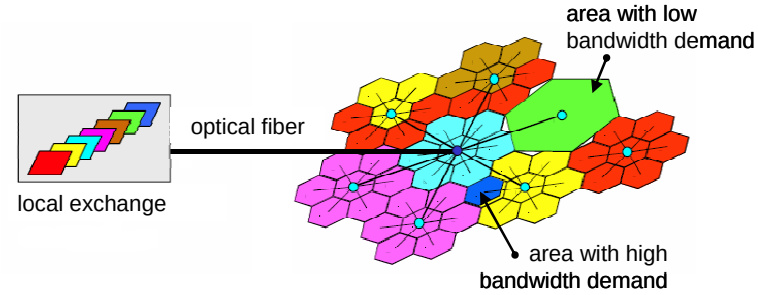

Figure 1.4: Wavelength reallocation [13].

The advantage of flexible capacity reallocation can be demonstrated by analyzing the call blocking probability. Given the actual traffic loads on all the wavelength channels, the call request of an ONU may not fit into its default wavelength channel, but may fit into an other wavelength channel which still has sufficient capacity available. In the static wavelength assignment case this call of an ONU would have been blocked, whereas using the flexible wavelength assignment it can be accepted. Therefore, the on-demand bandwidth allocation will decrease the call blocking probability remarkably which implies that more calls can be accepted.

Fig. 1.5 shows the system blocking probability versus relative system load, after [38]. The example system comprises eight wavelength channels with a capacity of 1.25 Gbit/s each, and 256 ONUs, which generate Poisson-distributed calls with a data-rate of 63 Mbit/s or 125 Mbit/s. The length of a call is assumed to be exponentially distributed. This may be a realistic model for exchanging files through the network. The relative system load ρ_n of the network is then defined in eq. 6.2, where N is number of active users, Δf is bandwidth of a call and B is the aggregate capacity of all wavelength channels.

$$\rho_n = \frac{N \cdot \Delta f}{B} \tag{1.1}$$

Taking these assumptions, the number of users active at any given moment follows a discrete binomial distribution. Using the Chernoff's upper bound approximation the system blocking probability versus relative system load has been

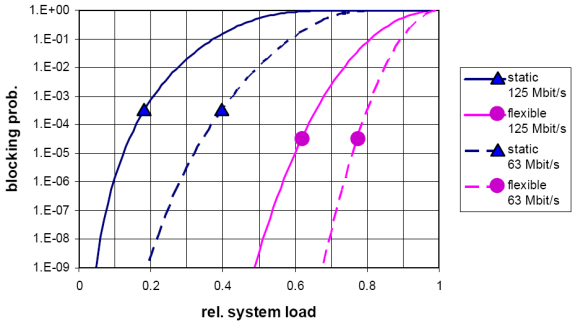

Figure 1.5: System blocking probability versus relative system load for static and dynamic capacity allocation [38].

calculated, under the assumption that granularity effects are negligible, which is a reasonable assumption when the call bandwidth is much smaller than the wavelength channel bandwidth. It can be seen that the flexible capacity allocation reduces the blocking probability with respect to the fixed capacity allocation. For instance, for a blocking probability of 10^{-3}, the system load may be doubled for 63 Mbit/s calls, and more than doubled for 125 Mbit/s calls.

The above consideration shows that a higher loading factor for a given blocking probability is allowed in the wavelength flexible network, and thus the resources at the OLT are exploited more efficiently. This implies that the network operator has to install less equipment in the OLT, which results in cost reduction. Moreover, for a given amount of OLT equipment the network operator can accept more calls, and thus increase the revenues.

From the network hardware viewpoint such routing may be performed by e. g. adjustable wavelength-multicasting routers, which settings are optimized and adjusted to current bandwidth demands through a management protocol. Besides such routers, wavelength-agile transceiver modules are required since every ONU in such network should be capable of detecting and transmitting any wavelength channel.

1.3 Overview of fiber-to-the-x market

Increasing the available bandwidth per user allows for more terminals at home. However, since there are more terminals and each of them may evolve its bandwidth needs, the bandwidth needed per home is higher, which on its turn pushes the network operator... to increase the bandwidth [39]. Regardless this vicious circle, there are more factors influencing the pace of broadband development.

Depending on the market of broadband services, legislation issues, competition in hardware development, wealth and density of population and the involvement of

local authorities NGA penetration ratio is foreseen to reach 20 % (United Kingdom and Spain), 40 % (USA, Denmark, Italy, France and Germany) and up to 80 % (Japan, South Korea, Sweden and the Netherlands) in 2015 [5, 40]. According to [41] by the end of 2011 the number of FTTH subscribers in Japan will grow to around 30 million, whereas in USA deployment of FTTP will reach 16 million links. In Europe by the same time it is foreseen that FTTH will reach 33 %, 32 %, 22.5 % and 15 % of all broadband access links in Denmark, Sweden, the Netherlands and France, respectively, which brings the French to a leading position in Europe with 3.7 million FTTH links [42, 43].

Some European broadband providers have already started to sell 100 Mbit/s FTTH links for € 30 [44], and on the other hand it is forecasted that around € 20 billion will be invested in new access technologies [45]. The decrease of pricing and, in parallel, the increase of investment in NGA is caused not only by the users willing to explore emerging services but also by the network operators to whom the regulations are becoming more transparent and thus they can start mass FTTH roll-outs.

Whereas most of the operators continue to invest in fiber PtP and few other in TDM-PON topologies, some predictions were published that in the year of 2013 the end-user will be given a dedicated wavelength channel [46].

From the users' viewpoint the attractiveness of broadband access originates from the diversity of the provided services, and not from the advancement in network technology itself. To enable a palette of competitive offers multiple providers should be allowed to share the same well-developed open access infrastructure. Thanks to the open access model in the Western European countries, where the network infrastructure is owned by an incumbent or a third party (e. g. municipality), the leading role of national operators is being limited while enabling the alternative operators and SPs to develop. E. g. in the Dutch city of Enschede the infrastructure is owned by the leading national operator KPN, and the end-users can choose their preferred SP. Orange, the large French operator, is taking steps towards building and opening the network in newly-built dwellings. In other countries, like Poland, although the position of the incumbent remains very strong, the first open access networks are given a chance, e. g. owned by local authorities Broadband Network of Małopolska is operated by Telekomunikacja Polska SA (incumbent) and Telefonia Dialog (alternative operator) [47].

It is important to note that the increase of broadband penetration causes a natural development of information and communication technologies (ICT). This contributes to the extension of industry and trade via stimulation of leading services and more effective production, logistics, resource management etc. Thanks to video-conferencing and home-working it also helps to reduce population migration from rural to metropolitan areas. Eventually, it also enables the citizens to communicate with governmental agencies (e-government) which contributes to the development of democracy and reduces the administration-related expenses of public financial resources [48].

1.4 The Broadband Photonics Access project

As justified in Section 1.1, current optical access networks will not be able to efficiently handle the avalanche-like growth of traffic and need to be upgraded in terms of higher bit-rate and on-demand bandwidth provision as well as coverage and scalability.

The Freeband Broadband Photonics Access (BBPhotonics) project vision encompasses congestion-free access for the user to virtually unlimited amounts of information, which is available to the user at any time, anywhere [49].

Obviously, this vision can only be realized with an access network infrastructure of which the communication power exceeds any present and foreseeable user communication need. A brute-force solution could be to provide abundant communication power everywhere, no matter whether it is needed at that instant or not. However, excessive overprovisioning of capacity leads to poor utilization efficiency of network equipment and high infrastructure costs, which is severe problem in the access network where costs need to be low because of the low per-user network sharing factor.

In the BBPhotonics project, it is therefore proposed to build intelligence in the access network, which enables to provide an adequate adjustable amount of communication power tailored to the actual instantaneous and temporal user needs. Optical fibre carrying multiple wavelength channels is chosen for the broadband flexible network infrastructure. Putting emphasis on low costs, which is a crucial factor for success in the market of access network products, reconfigurable architectures and access network modules are investigated. Compact low-power photonic integrated circuits and intelligent network reconfiguration mechanisms are key research items in the project.

Concrete project results envisaged towards this next-generation access network goal are:

- System concepts for congestion-free wideband access networks, capable of accommodating fluctuating capacity demands
- Definition of a universal wideband access network platform supporting ethernet-based traffic up to 10 gigabit ethernet (GbE)
- Migration strategies for upgrading (fibre-based) access networks towards wideband
- Low-cost advanced opto-electronics modules for wideband access
- Trial testbeds for assessing technical feasibility of reconfiguration mechanisms and advanced modules.

1.5 Contributions of the dissertation and thesis overview

The key contributions of this dissertation are given below:

- Design and proof-of-principle of a dynamically reconfigurable 25 km-reach WDM/TDM-PON-based architecture which can provide the bandwidth of 1.25-10 Gbit/s per wavelength channel to minimum 64 ONUs
- Novel design of a high bit-rate wavelength-agile transceiver based on a reflective semiconductor optical amplifier (RSOA), a reflective electro-absorption modulator (REAM) and a Michelson-interferometer modulator (MIM)
- Assessment of a tunable micro-ring resonator structure for dynamic wavelength reconfiguration
- Realization of an efficient method for interferometric crosstalk mitigation in a WDM-PON environment employing reflective ONUs.

The thesis is organized as follows. The architecture of the proposed novel network is given in Chapter 2. This is followed by the description of design, realization and test results of individual network modules in Chapters 3 and 4. Afterwards, possible network and transmission impairments are discussed in Chapter 5. Interferometric crosstalk is treated separately in Chapter 6 where efficient suppression methods are discussed as well. Chapter 7 provides comprehensive experimental results on a network testbed and a full-scale network simulation results. In Chapter 8, the migration scenario from currently deployed fiber-optic access networks towards the proposed novel solution is given together with a discussion on the economics of last-mile fiber technologies. Finally, the work is summarized and suggestions for further research are given in Chapter 9.

Chapter 2

Reconfigurable WDM/TDM access network - architecture

In this Chapter based on [50] the network architecture is discussed. A general network description is given in Section 2.1. In Sections 2.2, 2.3 and 2.4 central office (CO), ONU and remote node (RN) are described, respectively. The downstream (DS) and upstream (US) power budget for the longest light-path is estimated in Section 2.5 after which the wavelength panel applied in the network and the required network control and management are discussed in Sections 2.6 and 2.7, respectively.

2.1 General specifications

The BBPhotonics network is a dynamically reconfigurable novel solution for the access domain. It provides the end-users with high bandwidth which is available on demand thanks to dynamic wavelength reallocation. For this purpose wavelength-flexible switching nodes and wavelength-agile high bit-rate ONUs have been designed.

The BBPhotonics access network architecture is characterized with a powerful set of features [51]:

- delivery of multiple wavelength channels per home (up to all system wavelengths) enabling service separation e. g. in terms of QoS (latency and bandwidth requirements) and tariff, SP separation e. g. to flexibly lease the capacity by the network operator, traffic rerouting e. g. connection restoration via alternative, and higher capacity e. g. to provide more of the same services.
- n ONUs connected to a RN
- m RNs, each equipped with tunable wavelength router

- multiple wavelength channels grouped in DS/US pairs placed on ITU 200 GHz grid, in 1530-1561 nm range
- protected feeder fiber ring architecture with of standard single-mode fiber (SSMF) between the RNs (L_{RN-RN}), CO and RN (L_{CO-RN}) and from RN to ONU (L_{RN-ONU})
- wavelength-agnostic ONU (by deploying a reflective modulator)
- up to 10 Gbit/s per wavelength channel
- embedded control channel for remote network reconfiguration.

The designed network architecture does not determine whether the traffic should go along the upper or lower branch of the ring, since bidirectional transmission over a single fiber is provided via bidirectional RNs. The optical splitter with variable optical split ratio at the CO enables protection against breaks in a ring feeder fiber. It is connected to a circulator which splits/combines the US and DS. Such architecture allows the network to be extended with another RN simply by proper re-routing of the data traffic and adding more wavelength channels (more transceivers in the CO) without interrupting the operation of any part of the network.

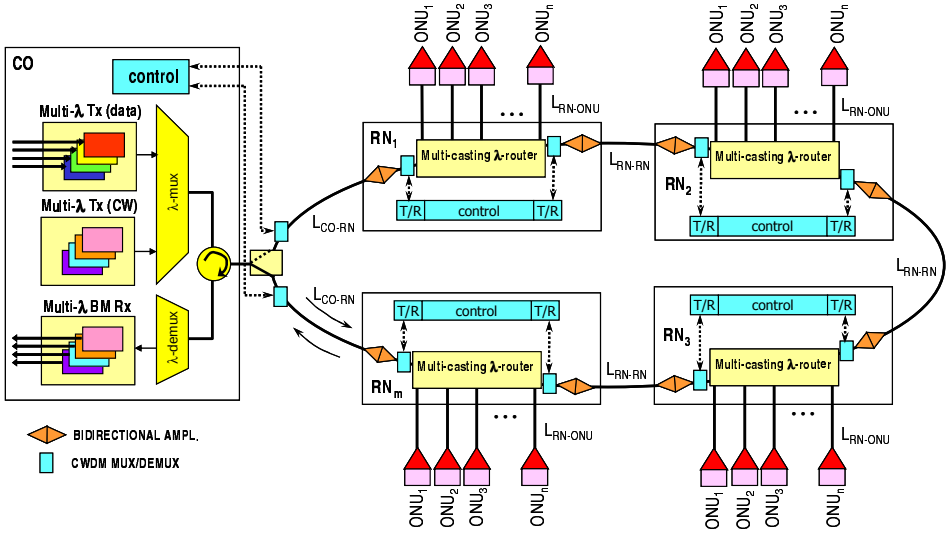

Figure 2.1: BBPhotonics network architecture.

To reduce the gap with todays FTTH practices it has been decided to relax the above requirements, which, in general, reduces the functionality of the network. However, it also constitutes a first realistic migration step which entails

less demanding specifications for the system modules, which can be simpler and thus potentially lower cost[1]. The specified parameters for the network architecture considered here are as follows [52]:

- delivery of a single DS/US wavelength pair to the subscriber
- $n = 16$ ONUs per RN
- $m = 4$ RNs, each equipped with tunable OADM
- 16 wavelength channels (8 DS/US pairs) placed on ITU 50 GHz C-band grid; up- and down-channel in a pair spaced by 500 GHz
- protected feeder fiber ring architecture with 20 km of L_{CO-RN}, 1 km of L_{RN-RN} and L_{RN-ONU}
- wavelength-agnostic ONUs
- up to 10 Gbit/s per wavelength channel
- 300 Mbit/s to 1.25 Gbit/s or 10 Gbit/s of available bandwidth per user.

FlexPON

In the FlexPON approach[2], the complexity of the system is substantially reduced which is associated with a small penalty in the network functionality, e. g. two wavelength channels can be sent to a single ONU. This is in the interest of realizing a practical working demonstrator providing a proof-of-feasibility of the concepts envisaged in the BBPhotonics project. The FlexPON demonstrator is foreseen to deliver GbE per wavelength channel (1.25 Gbit/s) to two end-users in total. The network characteristics for the demonstrator are:

- delivery of 2 wavelength channels per subscriber (1 DS and 1 US)
- 1 GbE capacity per wavelength channel
- 1 RN and 2 ONUs
- 4 wavelength channels (2 DS/US pairs) placed on ITU 200 GHz C-band grid
- 20 km of L_{CO-RN} and 5 km L_{RN-ONU}.

[1] An upgrade of the discussed network with optical code division multiplexing (OCDM) has been considered as well and it is discussed in Appendix A based on [50].

[2] The FlexPON is a subject of development activities led by Genexis BV (http://www.genexis.eu), a BBPhotonics Project partner, and it is out of the scope of this dissertation.

2.2 Central office

The CO contains a set of transmitters generating continuous-wavelength (CW) carriers and amplitude-modulated (non return to zero, NRZ) data signals for DS transmission and a set of receivers for US termination, as shown in fig. 2.1. Two AWGs are used as WDM multiplexer and WDM demultiplexer for DS and US, respectively. The DS and US traffic transmitted over a single fiber is split by a circulator. No direct communication between ONUs has been foreseen in this network which means that all traffic is terminated at the CO. A variable optical splitter at the CO is added for protection and restoration purposes. When power loss is detected, for example, in the upper branch of the ring it enables the transmission via lower branch. Therefore, a break of the ring fiber causes a connection loss only during the switching operation. Also any maintenance or inserting a new RN will not seriously disturb network operation. Coarse-WDM (CWDM) multiplexers are used to provide a control channel which is situated out-of-band with respect to the data signal channels in order not to interfere with or depend on these. It is used to control the OADM functions in the RNs.

2.3 Optical network unit

The ONU contains a Mach-Zehnder (MZ) duplexer which demultiplexes a modulated signal and a CW signal at its two outputs by means of wavelengths diversity. As shown in fig. 2.2a a photodetector is connected to the lower output and an RSOA to the upper output of the MZ duplexer.

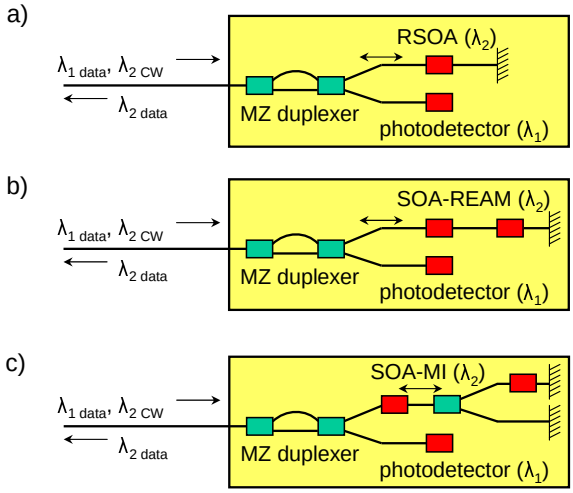

Figure 2.2: Solutions for the optical network unit: (a) based on RSOA, (b) based on REAM, (c) based on MIM.

The CW signal is amplified and intensity modulated in the RSOA. It is reflected at the end facet of the RSOA and sent back to the CO with modulated US data. The capability to provide gain and modulation at the same time reduces the need for additional amplification and the wide amplification bandwidth of the RSOA provides wavelength-independency of the ONU.

Since its electrical bandwidth is low ($\ll 10$ Gbit/s), other solutions for fast integratable wavelength-agnostic reflective modulators are studied, namely, an REAM fig. 2.2b and an MIM as shown in fig. 2.2c. The REAM works on the basis of a voltage-controlled change in light absorption and the MIM works on the basis of phase-to-amplitude conversion. These are discussed in detail in Chapter 3.

2.4 Remote node

In the original BBPhotonics access network design the RN is based on a wavelength router (a. k. a. λ-router), fig. 2.1a, which can deliver multiple wavelength channels to a single subscriber. Since the system requirements have been reduced, as discussed earlier, the wavelength router has been changed to an OADM, fig. 2.1b.

The RN also includes bidirectional optical amplification stage and CWDM multiplexers for control channel detection and transmission at each side as schematically shown in fig. 2.1.

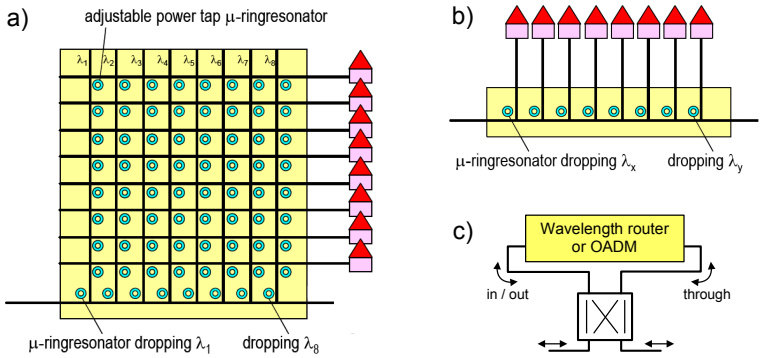

Figure 2.3: An eight-port wavelength router (a), an OADM (b) and the position of the switch (c).

The wavelength router and OADM are equipped with thermally tunable microring resonators [53] as shown in fig. 2.3 for an eight-port device. The temperature dependency of the refractive index is used to apply a phase shift to the optical field. The thermal-optic effect is a slow process (ms), thus, it is only suitable for relatively slow circuit switching (routing) applications. Using this device a single wavelength channel can be dropped to multiple users or a single user can be assigned a wavelength at any given time. Fig. 2.4 schematically illustrates the

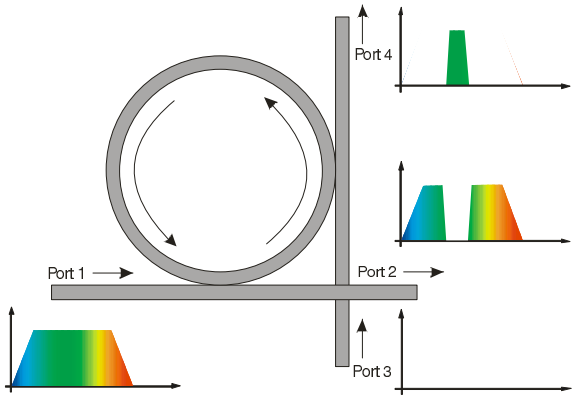

Figure 2.4: Basic operation of a micro-ring resonator.

operation of a single micro-ring resonator. The ring is connected to two waveguides in a four port configuration (two inputs and two outputs). The waveguides are situated orthogonally to enable the micro-ring resonators to be placed in a matrix array as indicated in fig. 2.3.

Consider a broadband input (multiple wavelength channels) at port 1. When the ring is in resonance for λ_{drop}, the wavelength channel λ_{drop} is dropped on port 4 together with all wavelengths which are separated by an integral multiple of the free spectral range (FSR) of the micro-ring resonator. The FSR is defined as the distance between two consecutive fringes (resonance peaks) in the spectral response of a single micro-ring resonator. The remaining (non-resonant) wavelengths are transferred to port 2. It is also possible to drop a single wavelength to multiple ports by a deliberate detuning of the ring resonator from a nominal wavelength of the channel. That way part of the power is dropped and the remaining power is transmitted to the adjacent ring resonator.

The micro-ring resonator structure is unidirectional in terms of common-input to through-port transmission. Therefore, in order to maintain the bidirectional traffic in the ring fiber a 2×2 switch is necessary to keep optical signals running in the same direction through the OADM as shown in fig. 2.3c. If the traffic on the fiber ring changes direction, because of a protection switching in the CO, this switch changes from bar-state to cross-state or vice versa.

The bidirectional amplification can be provided either by a two unidirectional EDFAs or SOAs depending on gain and noise requirements as shown in fig. 2.5. The preference is given to gain-clamped amplifiers which can reduce cross-gain modulation and provide high output saturation power[3]. Although, to satisfy the gain requirements, as shown in the next Section, it is enough to apply a single amplification module, two such modules are applied at every RN and they are

[3]CIP, SOA-L-OEC-1550, saturation output power specified as 16 dBm

switched on and off (by proper optical switch states) depending on the network configuration (e. g. traffic direction change due to switching at the CO).

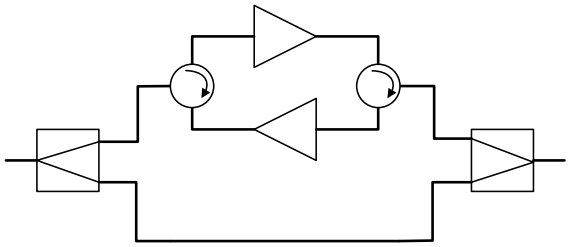

Figure 2.5: Bidirectional amplification module.

2.5 Power budget

The calculation of the power budget is performed for the longest light-path as explained graphically in fig. 2.6. A fiber break is assumed between the last RN and CO and all traffic goes via the upper branch of the ring. In this calculation the aggregate capacity (8 wavelength pairs) is distributed uniformly among all ONUs (64) in such a way that each wavelength pair feeds two ONUs per RN as indicated in fig. 2.6. This means that each wavelength channel experiences a total power-split ratio of 8.

In table 2.1 and table 2.2 the power budget is calculated for downstream and upstream path, respectively[4]. The CO loss includes the insertion loss of a WDM DS multiplexer and US demultiplexer (4.0 dB each), a CWDM coupler (1.0 dB), a circulator (0.8 dB), a switch (1.0 dB) and connectors (0.6 dB in total). The through loss in RN_1, RN_2 and RN_3 each includes OADM insertion loss (6 dB)[5], OADM split loss (1.25 dB)[6], connectors (0.6 dB in total), two times insertion loss of a CWDM coupler (1.0 dB) and a switch (1.0 dB), and an additional attenuator at stage B as explained later. The drop loss in RN_4 includes OADM insertion loss (6 dB), OADM split loss (9.0 dB), connectors (0.6 dB in total), a CWDM coupler and a switch. For the applied wavelength range (1540 nm to 1550 nm) the fiber loss is 0.2 dB/km. The insertion loss in ONU (8.5 dB) includes connector, fiber/chip coupling, MZ duplexer and waveguide losses. It has to be noticed that different transmission impairments (discussed in Chapter 5) will accumulate (e. g. ASE noise) and cause

[4]All values used in table 2.1 and table 2.2 are working assumptions. The realistic values based on characterization of the ONU and the OADM are given in Chapter 3 and Chapter 4. Moreover, this estimation concerns only power levels, and noise properties of the complete system are discussed in Chapter 5.

[5]The insertion loss of the OADM includes fiber/chip coupling and waveguide loss.

[6]25 % of power of each wavelength channel is tapped-off at each RN as it feeds two subscribers per RN.

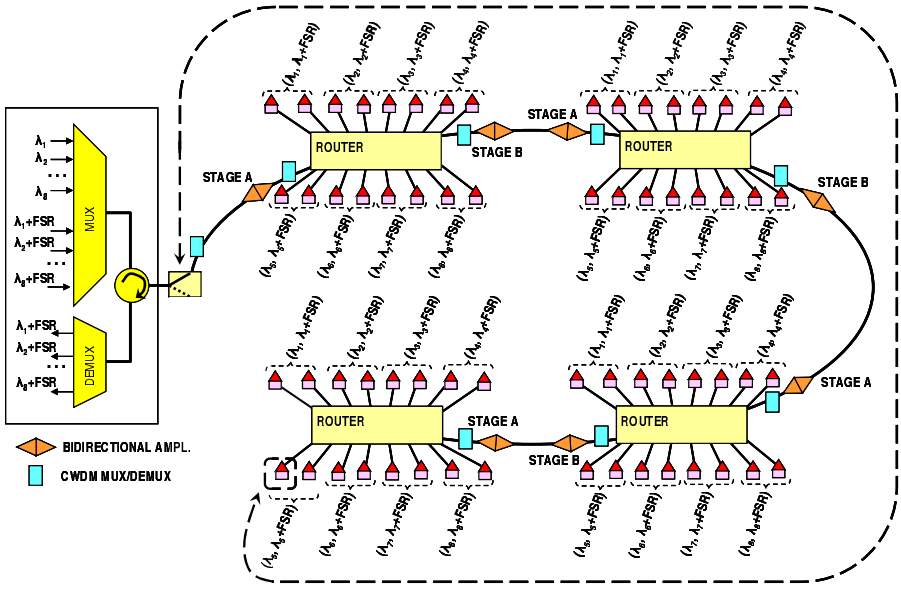

Figure 2.6: The longest light-path.

higher power penalties at ONUs, for instance, at RN_4 than at RN_1. This drives the requirement for sufficiently high power margin to be maintained across all ONUs in the network. Here, the margin is 5.0 dB for downstream and 6.0 dB for upstream as indicated in table 2.1 and table 2.2, respectively. The sensitivity of 1.25 Gbit/s is better than a 10 Gbit/s which extends the available power budget significantly (6-8 dB). For the purpose of the power budget estimation discussed here we assume all wavelength channels are modulated at 10 Gbit/s and the receiver sensitivity is -24 dBm which is close to the value specified in [54] for a receiver with an avalanche photodiode.

It can be noticed in table 2.1 that in the downstream direction the required gain (stage A) RN_4 is lower than in other RNs. This is caused by the fact that at RN_4 the signal power is completely dropped to two ONUs receiving 50% of the optical power restored by the amplifier at the input of this node. In RN_1-RN_3 the ONUs receive the same amount of power, however the split ratio is different due to the through port power requirements of those RNs. In order to avoid additional amplification (stage B) and, therefore, maintain low total noise figure, the split ratio there is adjusted to pass through 75% power and divide the remaining power equally over two ONUs.

In upstream direction, table 2.2, the gain requirements are higher as the input powers are lower. This is because of the fact that the signals transmitted by ONUs first experience the high OADM losses and then they enter the amplifiers.

In the discussed calculation, each wavelength channel feeds exactly the same

Table 2.1: System power budget for downstream path (data and CW channel).

	Parameter	loss/gain [dB] or power [dBm]
(1)	Transmitted power per wav. channel	6.0
(2)	CO loss	- 7.4
(3)	CO-RN_1 fiber att.	- 4.0
	RN_1 input power	- 5.4
(4)	RN_1 stage A gain/att.	12.7
(5)	RN_1 through loss	- 11.9
(6)	RN_1 stage B gain/att.	- 0.7
(7)	RN_1-RN_2 fiber att.	- 0.2
	RN_2 input power	- 5.4
(8)	RN_2 stage A gain/att.	12.7
(9)	RN_2 through loss	- 11.9
(10)	RN_2 stage B gain/att.	0.7
(11)	RN_2-RN_3 fiber att.	- 0.2
	RN_3 input power	- 5.4
(12)	RN_3 stage A gain/att.	12.7
(13)	RN_3 through loss	- 11.9
(14)	RN_3 stage B gain/att.	0.7
(15)	RN_3-RN_4 fiber att.	- 0.2
	RN_4 input power	- 5.4
(16)	RN_4 stage A gain/att.	6.7
(17)	RN_4 drop loss	- 11.6
	RN_4 power at drop port	- 10.3
(18)	RN_4-ONU fiber att.	- 0.2
(19)	ONU loss	- 8.5
	Received power	- 19.0
(20)	10 Gbit/s receiver sens./refl. mod. sens.	- 24.0
(21)	Power budget, [(1)-(20)]	30.0
	Remaining power margin [(2)+(3)+...+(19)+(21)]	5.0

Table 2.2: System power budget for upstream.

	Parameter	loss/gain [dB] or power [dBm]
	Refl. mod gain	22.0
	ONU fiber-to-fiber gain	5.0
(1)	Refl. mod. transmitted power	3.0
(2)	ONU loss	- 8.5
(3)	RN_4-ONU fiber att.	- 0.2
	RN_4 power at add port	- 5.7
(4)	RN_4 add loss	- 11.6
(5)	RN_4 stage A gain/att.	10.7
(6)	RN_4-RN_3 fiber att.	- 0.2
	RN_3 input power	- 6.8
(7)	RN_3 stage B gain/att.	- 4.7
(8)	RN_3 through loss	- 11.9
(9)	RN_3 stage A gain/att.	16.6
(10)	RN_3-RN_2 fiber att.	- 0.2
	RN_2 input power	- 6.8
(11)	RN_2 stage B gain/att.	- 4.7
(12)	RN_2 through loss	- 11.9
(13)	RN_2 stage A gain/att.	16.6
(14)	RN_2-RN_1 fiber att.	- 0.2
	RN_1 input power	- 6.8
(15)	RN_1 stage B gain/att.	- 4.7
(16)	RN_1 through loss	- 11.9
(17)	RN_1 stage A gain/att.	16.6
(18)	RN_1-CO fiber att.	- 4.0
	CO input power	- 10.6
(19)	CO loss	- 7.4
	Received power	- 18.0
(20)	10 Gbit/s receiver sensitivity	- 24.0
(21)	Power budget, [(1)-(20)]	27.0
	Remaining power margin [(2)+(3)+...+(19)+(21)]	6.0

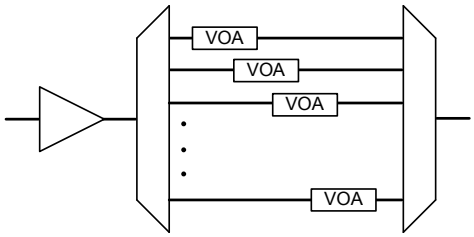

Figure 2.7: The wavelength-dependent amplification module.

number of subscribers per RN. However, different split ratios are possible thanks to flexible wavelength assignment in the OADM. For instance, a given wavelength pair may feed 2 ONUs at RN_1, 6 ONUs at RN_2, 3 ONUs at RN_3 and 16 ONUs at RN_4, whereas the remaining wavelength pairs cover the bandwidth requirements of the remaining ONUs[7]. In the worst case it may also happen that one wavelength pair feeds all subscribers in the network. These different wavelength allocation schemes cause different split losses per wavelength channel. Also the gain variation caused by the ASE spectrum of cascaded amplifiers may substantially influence the power distribution among the wavelength channels. Moreover, the attenuation due to different CO-ONU distances will contribute to the packet-to-packet power level differences upon reception at the OLT. Hence, the amplification values of the optical amplifiers at the RNs are set to balance the losses in the RNs in such a way that each ONU receives the same optical power. This requires proper gain settings at the input of the OADM (stage A in fig. 2.6). Furthermore, in order to enable a modular upgrade of the network by adding another RN each wavelength channel needs to have the same power at through port of each RN. This requires proper power adjustment at the output of the OADM (stage B in fig. 2.6).

This, so called, unity-gain approach (the resultant RN loss is 0 dB at a through port) also enables easier network reconfiguration/restoration in case of protection switching [55]. However, it yields the requirement for tunable wavelength-dependent gain which can be achieved in the setup depicted in fig. 2.7. After demultiplexing the wavelength channels, the electrically-driven variable optical attenuators (VOA) are adjusted according to the required power level which is set by the control unit. In order to provide high output power gain-clamped SOAs are proposed which also helps to suppress cross-gain modulation effects and the resultant interchannel crosstalk. Currently available gain-clamped SOAs are not yet capable of satisfying these requirements. However, models of such devices reveal gain over 15 dB and saturation output power over 22 dBm [56].

[7]This is discussed for the FlexPON design in [55] where detailed power budget specifications for different capacity distribution cases together with the power budget for a control channel are given.

2.6 Wavelength set

In the BBPhotonics network architecture 64 ONUs are served by 8 wavelength channel pairs. This provides the end-user with an average available bandwidth of 300 Mbit/s to 1.25 Gbit/s depending if a given wavelength pair serves a GPON or 10GPON system. The network can be configured in such manner that some users are assigned the complete (symmetrical) capacity of a single wavelength channel. In this case the bandwidth available for the rest of the users is decreased accordingly.

The wavelength set has to match with the FSR of the micro-ring resonators in the OADM (FSR_{OADM}) and to the periodicity of a MZ interferometer in the ONU (FSR_{MZI}). It also has to correspond to the ITU standard wavelength grid such that commercially available equipment can be employed. For this network the optical band of 1540-1550 nm is used and the channels are spaced by 50 GHz. The channels are grouped into two subbands as shown in fig. 2.8a where the DS subband contains modulated wavelength channels and the US subband contains CW carriers for remote modulation at the ONU. An US-DS channel pair, which is to be dropped to the same ONU, is spaced by a single FSR_{OADM} (here: 500 GHz). As shown in fig. 2.8b the FSR_{MZI} has to be twice the FSR_{OADM}, that is 1 THz, in order to separate the two channels.

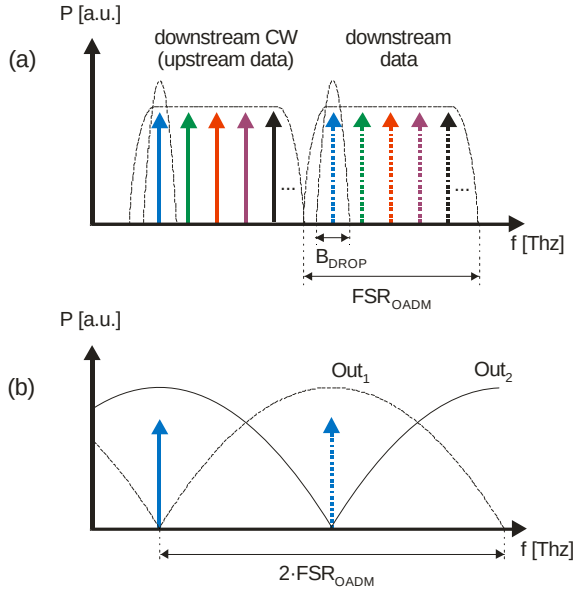

Figure 2.8: Wavelength architecture at the OADM (a) and at the MZ duplexer outputs in the ONU (b).

Initially, another wavelength set has been considered. It concerned interleaving upstream and downstream channels. However, it led to stricter requirements

on the design of the micro-ring resonators-based OADM, which would need to be tuned across much broader optical bandwidth (up to 30 nm in case of 200 GHz channel spacing) which would cause higher electrical power dissipation. In the chosen wavelength set the OADM has to be tuned across 10 nm bandwidth only. However, it requires the wavelength duplexer at the ONU to be fine-tuned whenever the wavelength channels assigned to a given ONU are changed as discussed in [57].

2.7 Network control and management

The BBPhotonics network is considered as a stack of quasi-independent logical PONs. The concept of bandwidth reallocation is shown in fig. 2.9. The network from headend (HE) to customer premises equipment (CPE) is depicted as a two stage switch. The first stage switching is done by a GbE switch which can route traffic to and from every OLT from any of the ports towards the wide area network (WAN) interface. The second stage switch is the reconfigurable network itself which can associate any ONU to any OLT based on the wavelength configuration.

Fig. 2.9 shows two OLTs which are operating on a unique wavelength pair. Each OLT and the associated ONUs form a logical PON namely the "Red" PON and the "Blue" PON. The nominal bandwidth available to an ONU depends on

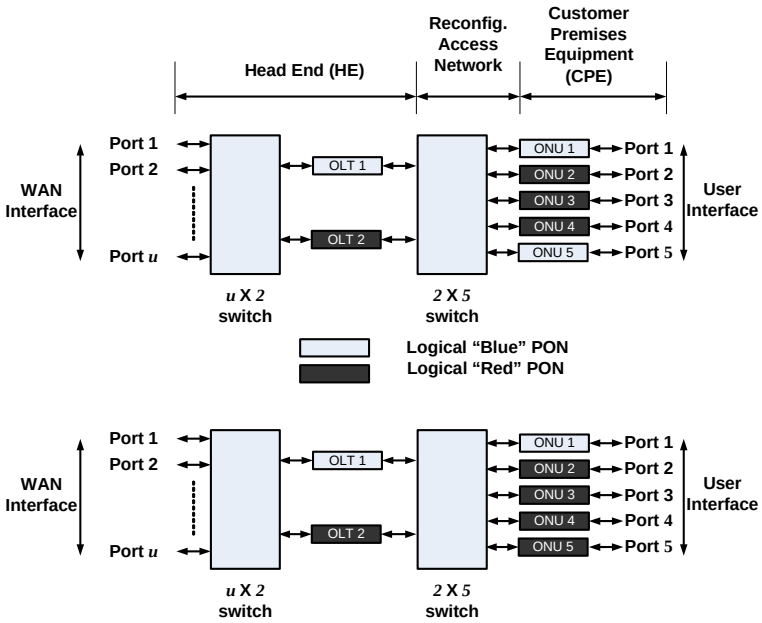

Figure 2.9: Concept of bandwidth reallocation [50].

the number of ONUs supported by each logical PON. If the number of ONUs supported by a logical PON is increased then the nominal bandwidth available per ONU reduces while it increases when the number of ONUs is decreased. This is an effect of using time slots in the network. The increase in the nominal bandwidth available to ONU1 in the "Blue" PON is achieved by changing the wavelength assigned to ONU5, as shown in fig. 2.9.

The network reconfiguration and hence the consequent reallocation of the ONUs is done in such a way, that the bandwidth distribution in the network is optimized [58]. A master controller (MC) monitors the network load and sets a configuration that is optimal for bandwidth availability to the end-user. The MC communicates with the GbE switch and OLTs at the HE as well as with local controllers (LC) at the RNs. The LCs act as slave devices to the MC and perform status monitoring and reconfiguration. The LCs are based on microcontrollers or embedded microcontrollers.

All control and management for the network is done on an out of data band communication channel. This channel works on 1310/1490 nm optics based on a 100Base-X communication link between the MC at the CO and LCs at the RNs. A two-fiber diversity in the link connection between the CO and every RN ensures fail-safe communication for up to a single link failure [59]. This out of band communication channel for the network ensures independence in operation of EPON or any other standard MAC protocol for such a network.

Chapter 3

Reflective transceiver module for ONU

Several source-free ONU architectures using reflective modulators have been proposed in Chapter 2. In this Chapter, based on [50, 60–64], different solutions for a wavelength-agile remotely-seeded reflective modulator are discussed.

An overview of possible CO-ONU communication methods is given in Section 3.1. In Sections 3.2, 3.3 and 3.4 ONUs based on RSOA, REAM and MIM, respectively, are characterized. This is followed by a brief comparison of the reflective modulators in Section 3.5.

3.1 CO-ONU communication schemes

The ONU is situated at the user-end and has two major tasks. Firstly, it terminates the optical path and converts the DS data into the electrical domain and, secondly, it transmits the US data after converting it from the electrical to the optical domain.

Since the size of the ODN is critical when deploying an access network, it is important to reduce the number of fiber links and optical splices. Although the topology which uses two unidirectional fibers in parallel is the most tolerant to backscattering and reflections, fig. 3.1a, it requires a relatively large number of components with respect to single-fiber communication. The same applies even if the same wavelength is used for DS and US transmission (a. k. a. wavelength reusage), fig. 3.1b. Bidirectional transmission using a single bidirectional fiber, fig. 3.1c and fig. 3.1d, reduces the amount of fiber needed by half, but the crosstalk issues are increased in such topology (Chapter 6). Nevertheless, it enables the utilization of a single-port ONU, which leads to simple and cost-efficient packaging technology. Although, dedicating a separate wavelength for upstream transmission requires an additional light source at the CO and a wavelength duplexer at the

ONU, it is favorable in terms of upstream modulation performance and, therefore, the scheme depicted in fig. 3.1c is chosen when designing the BBPhotonics access network.

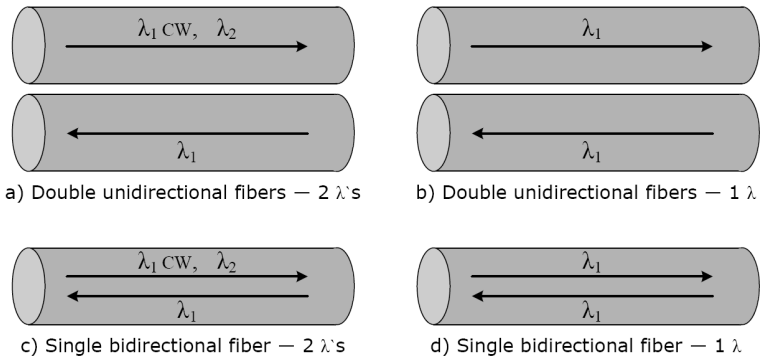

Figure 3.1: Communication schemes [63].

3.1.1 Modulation format

The most straightforward manner to provide the upstream communication is to send a CW carrier from the CO to the reflective modulator at the ONU. It is not a bandwidth-efficient method as each ONU needs two wavelengths[1]. Furthermore, it is sensitive to backscattering which is discussed in detail in Chapter 6 together with improvement methods. However, if intensity modulation in both directions is chosen it becomes very attractive for access networks in terms of costs as it requires only simple direct receivers. Therefore, this modulation format is applied in the BBPhotonics access network.

Recently, transmission of 10 Gbit/s was achieved with a modulator based on an EAM monolithically integrated with SOAs [66, 67]. Transmission experiments using a monolithically integrated reflective modulator comprising a concatenated SOA and an EAM section (R-SOA-EAM) have been demonstrated at a bit-rate up to 7.5 Gbit/s in [68]. Architectures using an RSOA [69–71] for 1.25 Gbit/s upstream transmission or a wavelength-locked Fabry-Perot laser diode (FP-LD) as the 622 Mbit/s reflective modulator in the ONU have also been proposed [72–75].

[1] Time partitioning can be used to separate the DS and US signals [65] if a single wavelength is used to provide DS and US communication. In such case the modulated DS signal from the CO is alternated with a CW optical carrier. At the ONU a portion of the light is detected by a receiver, and the remaining light is looped back through a modulator to the CO.

3.1.2 Wavelength demultiplexing at ONU

In a WDM/TDM-PON each ONU operates on a dedicated or shared wavelength which is transmitted over a shared CO-RN and a dedicated RN-ONU fiber-links. Therefore, the ONU is supposed to operate at any wavelength which can be assigned statically (fixed) or dynamically by the CO. Both require wavelength-independent performance of the ONU within a broad wavelength range.

In order to decouple the two DS wavelengths as indicated in fig. 3.1c, a cost-efficient wavelength duplexer has to be provided. For this purpose different solutions are possible. Some of those are shown in fig. 3.2.

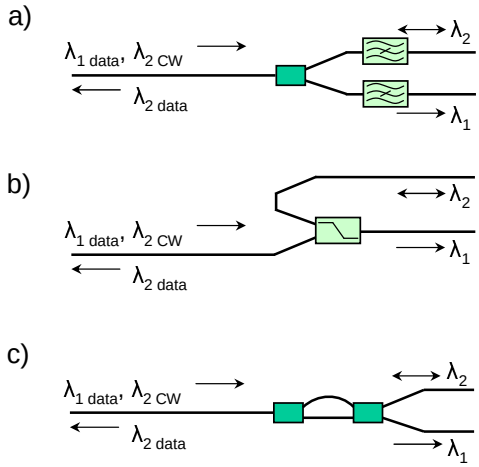

Figure 3.2: Wavelength duplexers for ONU: (a) power splitter and bandpass filter (BPF), (b) banded skip filter and (c) MZ interferometer [63].

The architecture in fig. 3.2a uses a combination of a passive power splitter and bandpass filters to separate the wavelengths. The incoming signal is split into two arms. In the upper arm the DS CW channel is selected by filtering before it reaches a reflective modulator. The filter in the lower arm selects the DS data channel and sends the signal to the receiver. The device can be integrated and it does not require active control for tuning since the passband can be large enough to let through all DS CW channels or all DS data channels depending on the arm of the splitter. The disadvantage is the substantial power loss caused by the splitter. The DS data signal will have a loss of 3 dB. The other channel passes the splitter twice, which will result in a power loss of 6 dB. Another disadvantage is that such a wideband filter will not suppress amplified spontaneous emission (ASE) noise well enough. This ASE noise may come from the in-line amplifiers or from the reflective modulator which can be based on e. g. RSOA, and such unsuppressed noise will deteriorate the amplitude of the signal.

The duplexer presented in fig. 3.2b is a passive red/blue filter a. k. a. banded

skip filter. The part of the input signal containing the DS data band is reflected to the photodetector and the rest of the input signal (DS CW) is sent through to the reflective modulator. Similarly to the earlier design, the disadvantage of this device is that due to the large optical bandwidth it is not filtering the ASE noise effectively.

Although the third solution, fig. 3.2c, which is based on a MZ interferometer requires active control to tune to the desired wavelengths, it is advantageous in terms of integration capability. Therefore, this solution is chosen for the duplexer [76] to be integrated with the photodetector [77, 78] and the reflective modulator [79] in the transceiver module [57, 80] in the BBPhotonics network.

3.2 Reflective semiconductor optical amplifier

An SOA has the same structure as a semiconductor laser but without feedback mirror. The gain is realized via stimulated emission induced by electrical pumping. In bulk material, the drive current is directly injected in the active region, while in multiple quantum well (MQW) material the drive current generates carriers in the separate confinement heterostructure (SCH) which are captured in the quantum wells area. Spontaneous emission is also present in the amplification process, therefore, the output signal is accompanied by additive noise, known as ASE.

If the SOA is driven by an amplitude-modulated current it becomes an amplified modulator. The internal gain of such a device compensates for splitting and coupling losses. However, the frequency response of the SOA is governed by three major factors: the relaxation oscillation frequency, cavity travel time and the parasitic capacitance.

The relaxation oscillation results from the interplay between the photon field and the population inversion in the active region of the SOA. The modulation response is relatively flat for $\omega_m \ll \Omega_R$, peaks near $\omega_m = \Omega_R$ and drops sharply for $\omega_m > \Omega_R$, where ω_m is the modulation frequency and Ω_R is the relaxation oscillation frequency. The damping of the resonance is governed by the spontaneous emission at low photon densities and by the gain suppression factor at high photon densities. For the purpose of high frequency modulation a large increase of the relaxation oscillation is desired but it will be severely limited at high photon densities by the damping introduced by the gain suppression [81].

The other factor limiting the electrical bandwidth of an SOA is the cavity travel time. Suppose an instantaneous change in gain at t_0 is applied to an amplifier with a continuous optical input power. The output signal will reach its steady state output power when the photons that entered the amplifier at t_0 exit the amplifier at $t_0 + \Delta t$. All photons exiting the amplifier before $t_0 + \Delta t$ will undergo the new gain for a shorter time (or length), so the output power before $t_0 + \Delta t$ will be smaller. After $t_0 + \Delta t$ the output power will be stable. The Δt causes an unavoidable delay between modulation input and optical output power, thus a rise-time and a fall-time. The value of Δt depends on the effective refractive index

n_{eff} and the lightpath length ΔL.

$$\Delta t = \frac{\Delta L}{v_g} = \frac{n_{eff}\Delta L}{c} \tag{3.1}$$

To give an idea about the influence of this phenomenon, the cavity travel time is calculated for estimated values of n_{eff} (3.7) and L (700 μm). Therefore, ΔL is equal to $1.4 \cdot 10^{-3}$ m ($2 \cdot L$), and the cavity travel time becomes 17.3 ps. With a modulation speed of 1.25 Gbit/s this is 2.16 % of the bit period, while for 10 Gbit/s modulation speed it is 17.3 % of the bit period. In the latter case this phenomena will cause a serious decrease in signal quality.

The last factor which may significantly influence the frequency response of the SOA modulator is the parasitic capacitance, which is located between the active layer (top) contact and the substrate contact of the device. When changing the drive current the device parasitic capacitance limits the achievable modulation speed. To decrease the parasitic capacitance, the area of the active layer contact can be decreased or the distance between the two contacts, mostly dominated by the substrate thickness, can be enlarged. The material permittivity is directly linked with the refractive index, so changing the permittivity is not feasible. For higher bit-rates the degradation of the electric signal due to the parasitic capacitance can cause problems, so attention has to be paid on the electrical design of the RSOA module. The length of the device, which is inherently necessary to obtain high enough gain, is limiting the achievable minimum parasitic capacitance. A more extensive description of the effect of this capacitance, and a possible solution by adjusting the drive current pulse shape is presented in [82].

When one of the facets of the SOA is coated with a high reflectivity mirror, the SOA becomes reflective and combines modulation and gain of the optical carrier in a single-port geometry. The light enters the cavity after which it is modulated-amplified, reflected and leaves the cavity via the entrance facet.

3.2.1 MQW-RSOA characterization

The MQW-RSOA[2] is characterized in terms of static and dynamic properties[3].

It has an integrated impedance matching circuit and an SMA connector for the drive current supply. Temperature control is provided via 7 regular connector pins, and the bias current is supplied to the device via a bias-tee, which enables superposition of the DC and AC current, fig. 3.3.

The measurement system used to perform static characterization is shown in fig. 3.4. Because the reflective SOA has only one fiber pigtail, the input power and output power run through the same fiber. In the static measurement they are separated by a 3 dB coupler. The part with the optical source consists of a

[2]CIP, SOA-R-OEC-1550, serial no. 02852.

[3]Further in this work, Chapter 6, the RSOA is also characterized in terms of the influence of interferometric crosstalk on its performance.

Figure 3.3: RSOA with MQW material [62].

CW laser (1 MHz linewidth), an isolator and an in-line power meter/attenuator. Also a polarization controller is applied right before the RSOA. The input power is measured from the second output of the coupler, while the second input of the coupler is used to measure the output power after a 3 nm-BPF.

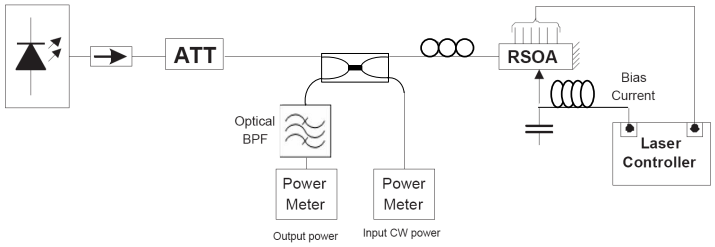

Figure 3.4: Experimental setup for static characterization of an MQW-RSOA [62].

The static measurement results are shown in fig. 3.5. All measurements are done for a polarization state optimized for the highest output power[4]. The saturation output power is 1, 5 and 7 dBm for drive current of 30, 50 and 80 mA, respectively. The transparency current is around 10 mA, which is in agreement with the specified values in the datasheet of the device.

The low transparency current for MQW device is explained by the small active area. Also, a lower gain is required to compensate for the lower background loss, which also reduces the transparency current.

[4]According to the datasheet the polarization dependent gain of the examined device is 20 dB

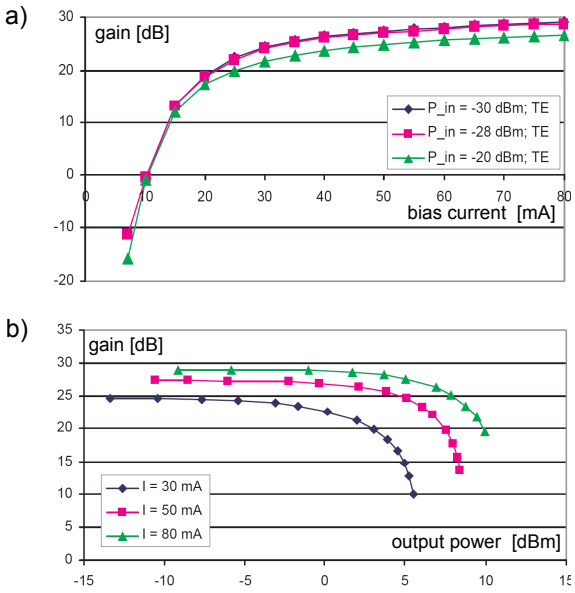

Figure 3.5: Static characterization results of an RSOA with MQW material: (a) gain in function of the bias current and (b) gain in function of the output power characteristics [62].

The slope of the MQW device starts steep (fig. 3.5) and reduces fast. This can be explained by the higher linear material gain. Higher gain also leads to saturation at lower drive current.

Because of its potential advantages in high bit-rate amplitude modulation, MQW-RSOA is also characterized in terms of dynamic properties. The measurement system used to perform dynamic characterization is shown in fig. 3.6. A tunable laser source generates the CW input signal (1552.56 nm) for the RSOA. The signal goes via the in-line power meter/attenuator and a circulator to a 50/50 coupler. The output power is first ASE-filtered before it is measured. A polarization controller is used to optimize the polarization of the CW input signal. The amplified, modulated and reflected signal passes the coupler before the circulator separates the signal from the input CW-signal. A demultiplexer is used to filter the signal (0.88 nm bandwidth) like it would happen in the eventual system. After the filter an attenuator is placed which will be used to investigate the minimum received optical power (ROP) for error-free detection. A lightwave converter (regular photodiode with a transimpedance amplifier) converts the optical signal into the electrical signal, which is detected by a bit error-rate tester (BERT). The bias current and temperature control are provided from a laser diode controller/temperature controller (LD/TE) module. The amplitude is provided by a pulse pattern generator (PPG), driven by a pseudo-random bit sequence (PRBS)

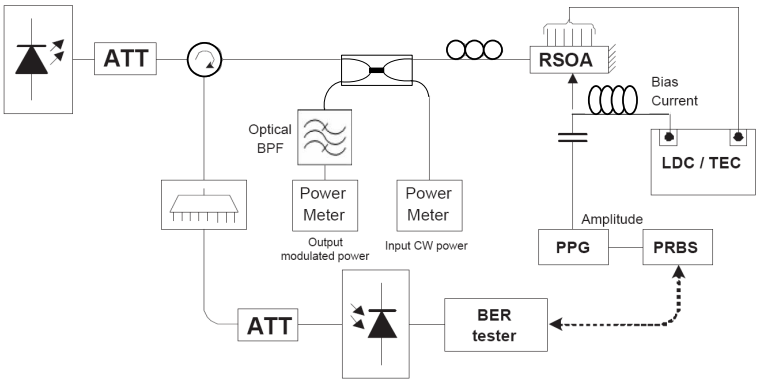

Figure 3.6: Experimental setup for dynamic characterization of an MQW-RSOA [62].

generator. The output of the PRBS generator is also linked to the BER tester for a reference signal. In this system it is no longer necessary to apply an isolator, because the circulator has high isolation (>60 dB), high directivity (>40 dB) and high return loss (>60 dB). The total loss of this setup is around 6 dB for the modulated signal and almost 4 dB for the CW signal, which is mainly caused by the coupler and the insertion loss of the demultiplexer.

The length of the PRBS codeword applied in these measurements is $2^{31} - 1$. The amplitude of the drive current provided by the PPG is limited to approximately 40 mA (maximum output of the PPG is 2 V in 50 Ω) and it is applied centered around the bias current. From the static measurements on this device the transparency current appeared to be 10 mA, which is the value corresponding with a logic '0'. Thus, the bias current provided by the LDC is set to 30 mA. The input CW signal power is -28 dBm. Under these conditions a very open eye diagram at 500 Mbit/s is obtained, fig. 3.7a. An eye diagram of 1.25 Gbit/s ($2^{31} - 1$ PRBS) is also very open, fig. 3.7b. To improve the performance even further the bias current is adjusted to obtain higher extinction ratio. A '0' level current of 8.7 mA and a corresponding '1' level current of 47.3 mA give optimum extinction ratio. This means that the '0' current is below transparency current, which is plausible, because the eye diagram from fig. 3.7a already shows a slower falling edge than the rising edge. If now the '0' current is decreased, the carrier-density for a '0' drops below transparency, which leads to a quicker falling edge, while the rising edge will become slightly slower. This trade-off has an optimum value for the drive currents given earlier, fig. 3.7b. The spectrum of 1.25 Gbit/s modulated signal reveals slightly wavy nature, which is due to the cavity resonances inside the RSOA, fig. 3.7c. The error-free transmission (BER equal to 10^{-9}) is easily achieved even in the system with a simple lightwave converter, fig. 3.7d. The time-averaged fiber-to-fiber gain of the RSOA in this case is around 20 dB. The 1.5 dB power

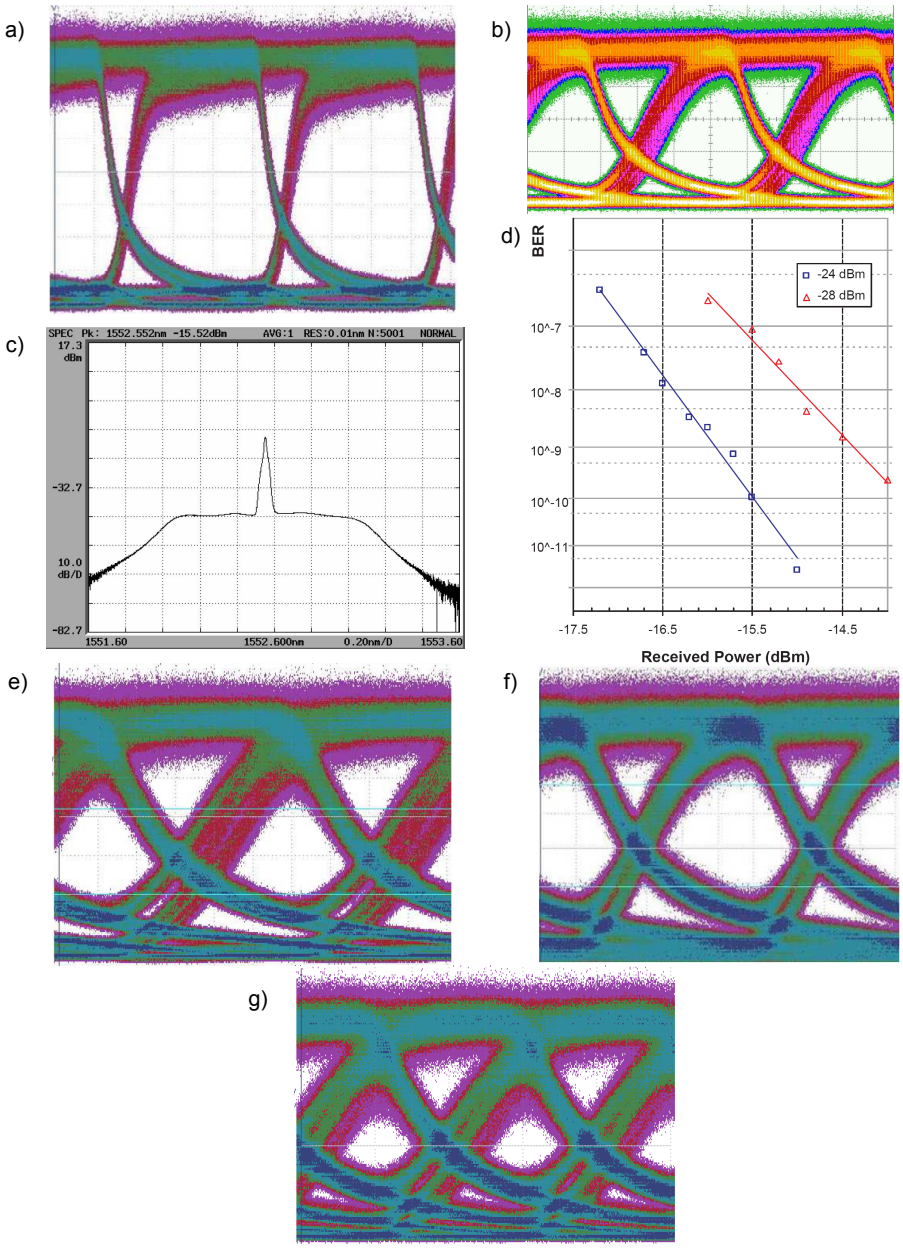

Figure 3.7: Dynamic characterization results of an RSOA with MQW material: (a) eye diagram of the 500 Mbit/s signal, (b) eye diagram of the 1.25 Gbit/s signal, (c) spectrum of the 1.25 Gbit/s signal, (d) BER results for the 1.25 Gbit/s signal, (e) eye diagram of the 2 Gbit/s signal (30 mA bias), (f) eye diagram of the 2 Gbit/s signal (40 mA bias) and (g) eye diagram of the 2.5 Gbit/s signal [62].

penalty is caused by poorer extinction ratio and larger ASE noise contribution in the case with lower input power.

If higher bit-rates are applied, pattern effects arise, fig. 3.7e ($2^7 - 1$ PRBS, -28 dBm input power), which causes degradation of BER results. In this case the extinction ratio is not the most important parameter. Since the highest possible bit-rate with error-free reception is investigated, the symmetry of the eye and the eye-opening become indications of performance. In order to improve the eye diagram the bias current is changed from 30 mA to 40 mA. The pattern effect decreases and the crossing of the rising and trailing edge becomes more centered, fig. 3.7f. The eye-opening increases until a maximum is reached, fig. 3.7g, and beyond this point the eye-opening decreases because of a larger saturation in the gain-current characteristic. Probably higher bit-rates could be reached if the system loss would be lower and the amplitude of the modulating signal would be higher.

3.3 Reflective electro-absorption modulator

The EAM operates through a voltage-controlled change in light absorption. The waveguide absorbs the light when it is reversely biased and it is transparent when no bias is applied. The absorption coefficient of the EAM varies with the wavelength of the incident light and with the electric field in the active region imposed by the reverse bias voltage.

The semiconductor EAMs operate through either the Franz-Keldysh effect in bulk semiconductor layers, or the quantum-confined Stark effect in MQW layers. In the bulk material under the external electric field the probability of lateral carrier tunneling of an electron from the valence band to the conduction band via absorption of a photon with an energy below the material band gap energy is increased. This results in a red-shift of the absorption edge. In an MQW-EAM, when an external electric field perpendicular to the wells is applied, the energy of the well states is reduced, resulting in a lower effective band gap. Compared with bulk material EAMs, the MQW-EAMs have higher modulation efficiencies and lower drive voltages, because the band gap in QW structures can change significantly faster than the absorption near the band gap in a comparable bulk structures.

The significant intrinsic optical propagation loss in the EAM can be compensated with the gain of an SOA. The adoption of an all semiconductor/integrated approach enhances the prospects for low-cost manufacture of the ONU at high volume, which is necessary for applications in the access domain. The modulator described in [83] is based on a semiconductor EAM monolithically integrated with an SOA. Such a device is capable of modulation at 10 Gbit/s [84]. Recently, also single-port monolithically integrated amplified reflective EAMs (R-SOA-EAM) have been proposed [66, 85]. These devices can work at 10 Gbit/s over a large spectral bandwidth up to 40 nm.

3.3.1 REAM characterization

Two REAMs are characterized[5]: REAM-A[6] and REAM-B[7], fig. 3.8a. They are packaged with a Peltier element driven by a temperature controller. The modulation signal and the bias current are provided via 50 Ω-impedance SMA connector.

The setup used to measure the attenuation of the REAMs, fig. 3.8b, contains a tunable DFB laser, a circulator which directs the return signal from REAM to a power meter and a polarization controller which adjusts the polarization to the highest attenuation. The polarization dependent loss (PDL) at 4.5 V reverse bias is 4 dB for REAM-A and 2 dB for REAM-B. The reverse voltage is applied to the REAM by a voltage source.

Fig. 3.8d shows the normalized ($P_{out} - P_{in}$) attenuation values for REAM-A. The longer wavelengths have a relatively smaller absorption at a low reverse voltage region, which can be explained with a lower density of states at such a voltage. The measurement in the high voltage region shows different behavior for this device only: the attenuation at wavelength 1540 nm is smaller than that at wavelength 1550 nm. This is probably due to polarization changes. The insertion loss (attenuation at 0 V) for the shorter wavelengths is much higher than for the longer wavelengths (specified as 4.5 dB typically). Based on fig. 3.8d it can be concluded that the extinction ratio has a maximum absolute value at a certain reverse voltage between 0 V and -4.5 V. The largest extinction ratio is at the shortest wavelength 1530 nm. Similar behavior can be noticed in fig. 3.8e, which represents the REAM-B.

The setup applied for BER measurements is based on the previous setup, fig. 3.8c. In front of the 10 Gbit/s receiver there is an in-line attenuator and a power meter to adjust and measure the ROP. It is followed by the BER tester. The REAM is provided with a 10 Gbit/s modulation signal with the maximum available amplitude of 2 V, which is superposed on a reverse bias voltage of around 1 V. This gives the optimum extinction ratio for the provided amplitude of the modulation signal.

The resulting BER curves for REAM-A, fig. 3.8f, indicate that the receiver is the most sensitive to the wavelength 1545.32 nm and the least sensitive to the wavelength 1562.23 nm. This, in general, corresponds to the attenuation measurements, fig. 3.8d, which shows that wavelength 1540 nm has a larger extinction ratio than wavelength 1550 nm at reverse voltage of 2 V. The results also show that the receiver sensitivity at a BER equal to 10^{-9} slightly differs (<0.5 dB) for different input powers. Similar trends are observed for REAM-B, fig. 3.8g.

[5]Most of the results included in this Section cannot be compared to the values specified in the datasheets of the devices as the characterization here was performed under different working conditions determined by the laboratory equipment parameters (RF voltage amplitude was 2 V, whereas in the datasheet it was 4 V). The provided datasheet did not include the measurement of attenuation in function of wavelength.

[6]CIP, R-EAM-1550, serial no. 03185.

[7]CIP, R-EAM-1550, serial no. 03272.

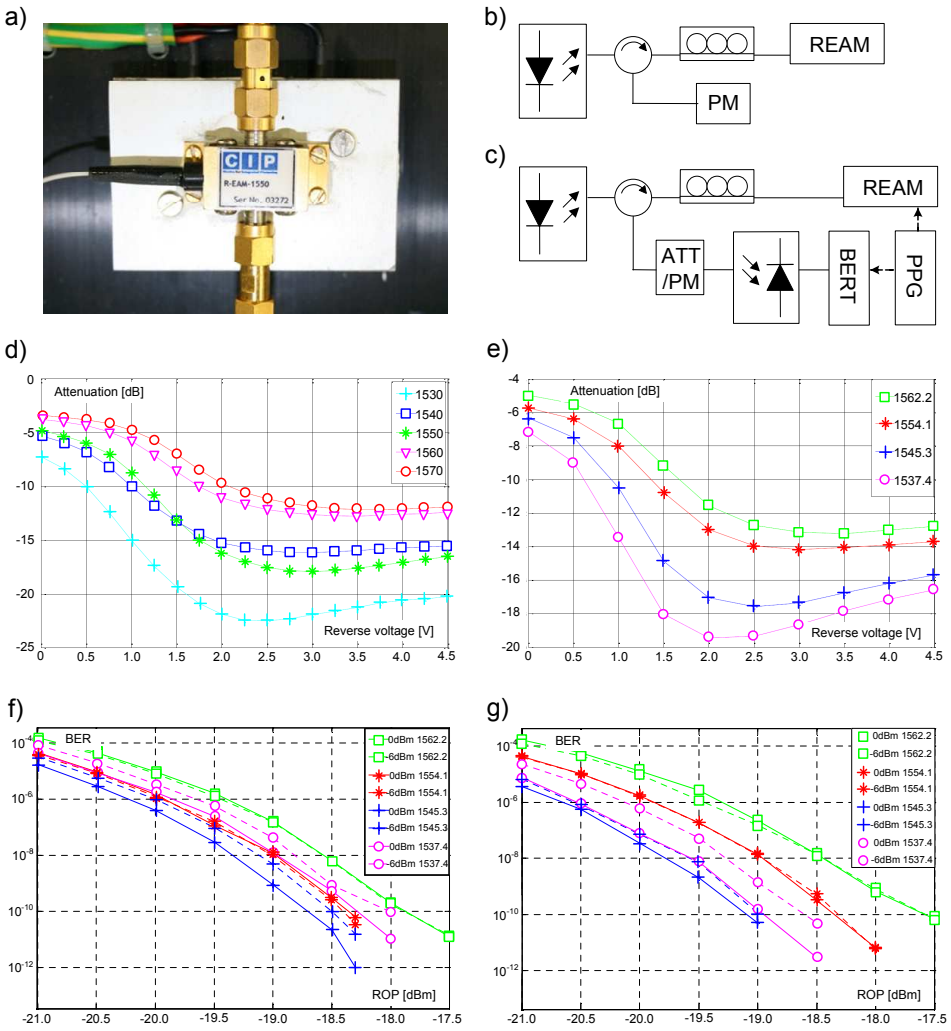

Figure 3.8: REAM characterization: (a) an example REAM, (b) setup for static characterization, (c) setup for BER characterization, attenuation in function of bias current for (d) REAM-A and (e) REAM-B, BER results for (f) REAM-A and (g) REAM-B [64].

3.3.2 R-SOA-EAM characterization

As mentioned earlier, the high intrinsic loss of the REAM has to be overcome with a bidirectional optical amplifier. The transmission properties of such an R-SOA-EAM combination (based on REAM-B) are investigated here.

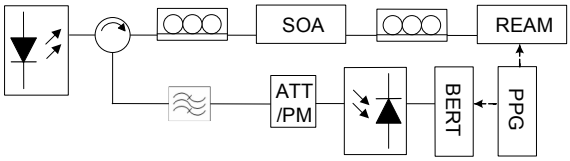

Figure 3.9: Setup for the characterization of the R-SOA-EAM [64].

The setup used in this measurement is depicted in fig. 3.9. The polarization controller before the SOA is adjusted until the highest optical power is provided to the REAM. The other polarization controller guarantees a stable system by adjusting the polarization of the modulated light returned from the REAM. If this polarization state is not well-adjusted it was observed that the received optical signal fluctuates in an unexpected way due to cross-gain modulation in the SOA (interaction between the CW input of the SOA and the modulated output of the REAM). After tuning the bias of the SOA the stability is achieved for orthogonal polarizations. Due to the presence of the ASE noise in this system a BPF is applied in front of the receiver (0.8 nm).

The measurements are performed for four different wavelengths, fig. 3.10 - 3.13. The reference lines are the lines from the back-to-back (BtB) measurements obtained by averaging BER values for input power levels of 0 dBm and -6 dBm.

Regardless the wavelength, if a higher input power is applied to the ONU, a larger driving current and, thus, a higher gain of the ONU results in a larger power penalty. This happens because the overshot due to the gain saturation of the SOA is larger at the high driving current. In the case of lower input power, the power penalty decreases as the driving current increases. It might be because more ASE noise of the SOA is suppressed by the higher optical signal returned from REAM. For the measurements with an input of -20 dBm and driving current of 100 mA not enough power was received at the receiver to reach a BER of 10^{-9}.

3.4 Michelson-interferometer modulator

The MZM is the most widely used type of interferometric modulator, fig. 3.14a. It consists of two phase modulators and two Y-branches. Light launched into a single-mode input waveguide is split equally between the arms of a symmetric input Y junction. The two beams are phase-modulated by the field between the planar electrodes and reach the second Y branch. When the phases of the two light beams are the same at this point, the light propagates to the single-mode waveguide output. When the phases are opposite, the light goes out of the waveguide.

If an MZM device is half-terminated by a reflective surface, an MIM is formed, fig. 3.14b [61, 86, 87]. The incident light splits equally into the two branches of the interferometer at the Y junction. Both signals travel through the waveguides

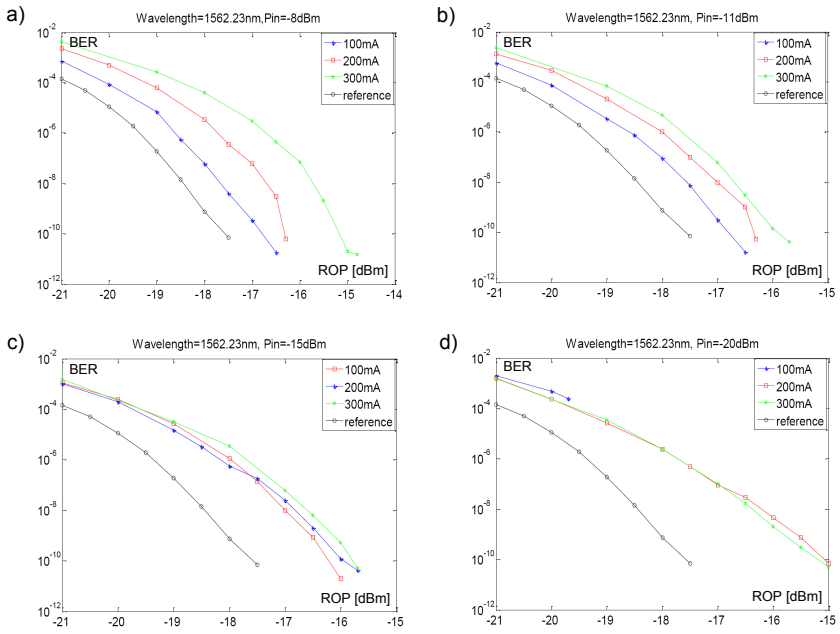

Figure 3.10: BER results for wavelength 1562.23 nm [64].

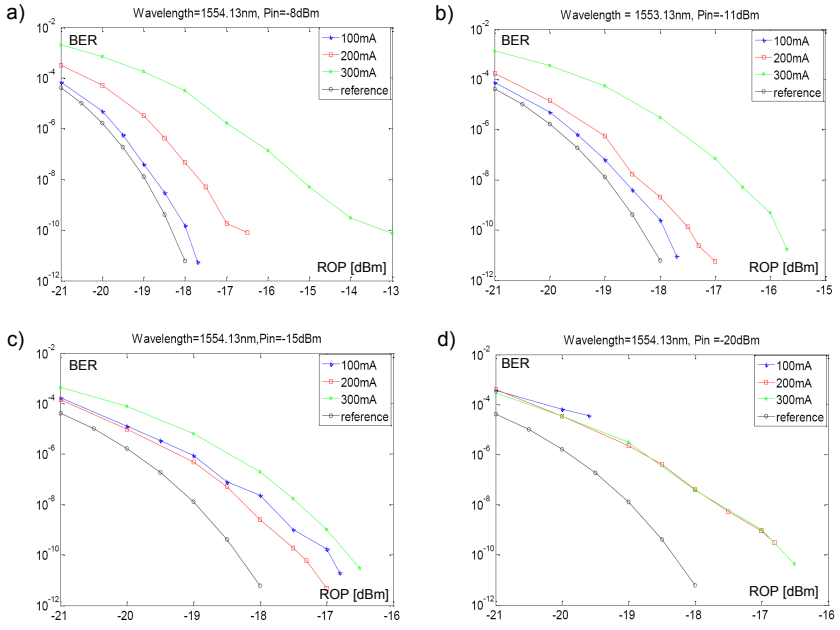

Figure 3.11: BER results for wavelength 1554.13 nm [64].

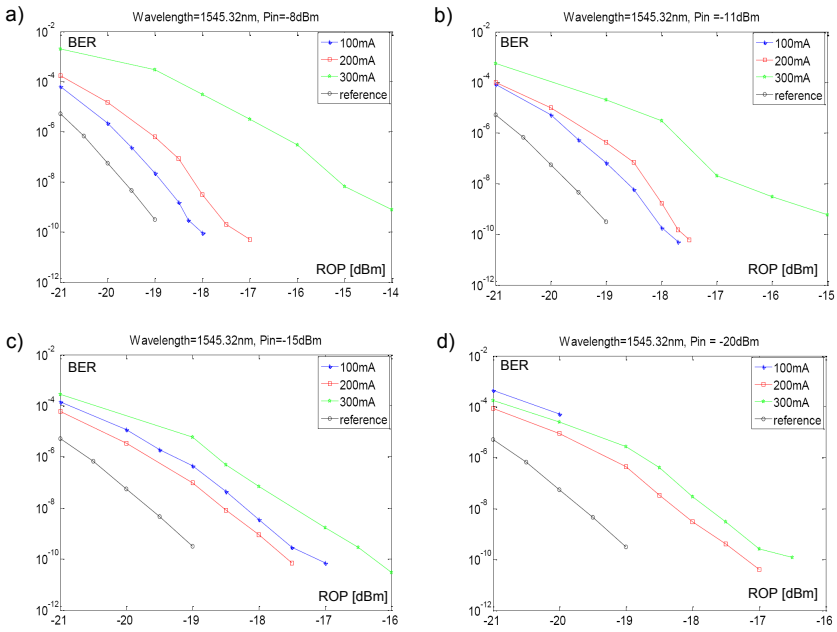

Figure 3.12: BER results for wavelength 1545.32 nm [64].

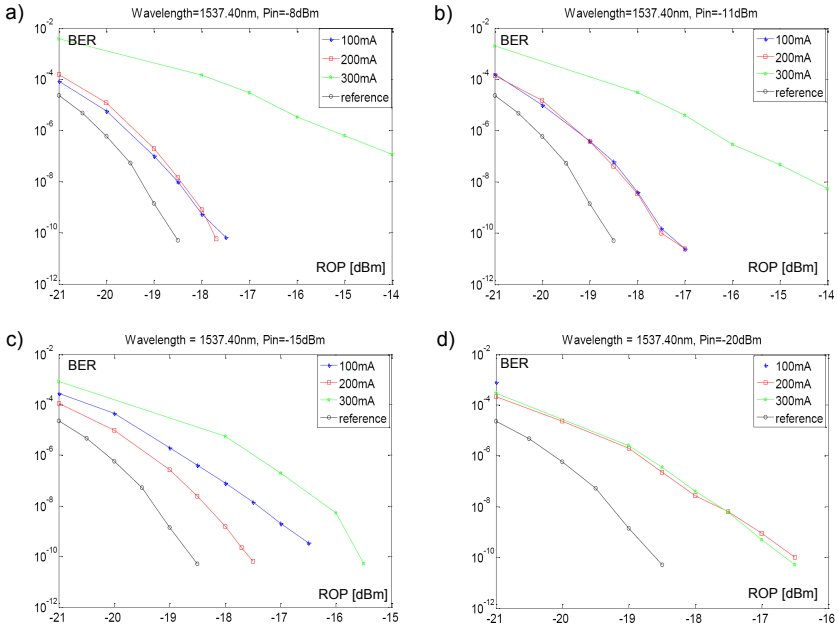

Figure 3.13: BER results for wavelength 1537.40 nm [64].

to the mirror and are reflected back to the junction to recombine. By applying a differential voltage to the electrodes deposited on top of the two waveguides, a difference of refractive index in the two branches is created similar as in the case of the MZM. This causes a phase difference between the two reflected signals and, based on the degree of this phase shift, light from the two segments interferes at the recombining Y-junction destructively or constructively. Consequently, phase-to-amplitude modulation conversion is realized. For the best destructive interference the induced phase shift must be π at the recombination junction yielding a logic '0'. Constructive interference yields a logic '1' and it happens when the phase shift is 0.

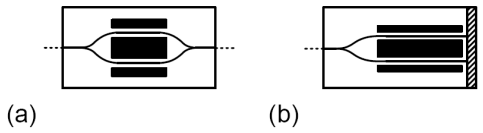

Figure 3.14: Structure of (a) a Mach-Zehnder interferometer and (b) a Michelson interferometer.

Since an MZM can be monolithically integrated with a laser source [88], the integration of an MIM with an SOA is also possible. A virtual model of an SOA-MIM-based reflective module is designed, fig. 3.15a, and simulated [89]. In the simulation setup a 0.8 nm optical filter was used followed by the 15 GHz receiver. When comparing the obtained eye diagrams, fig. 3.15b, to the eye diagrams of the RSOA, fig. 3.7, the SOA-MIM device shows great potential in high speed modulation. The rising and falling slopes do not limit the performance of the device as the eye remains widely and symmetrically open.

Similarly to an R-SOA-EAM, the SOA-MIM can provide modulation and amplification in a single chip, very high bit-rate modulation and large optical bandwidth.

3.5 Comparison of reflective modulators

The intensity modulators like the EAM or the MIM have the largest electrical bandwidth and reach 10 Gbit/s easily. The electrical bandwidth of the RSOA is limited to around 3 Gbit/s.

The required input power into the RSOA is lower than for the REAM. However, if the intensity modulator (REAM, MIM) is integrated with an optical amplifier the required input power is also low.

The unavoidable ASE noise present in all discussed designs will decrease the achievable Q-factor of the modulated signal mainly through the signal-ASE beat noise. The ASE-ASE beat noise can be effectively filtered out by an optical BPF.

All presented modulators have large optical bandwidth to provide colorless operation of the ONU and are capable of being integrated with a photodiode.

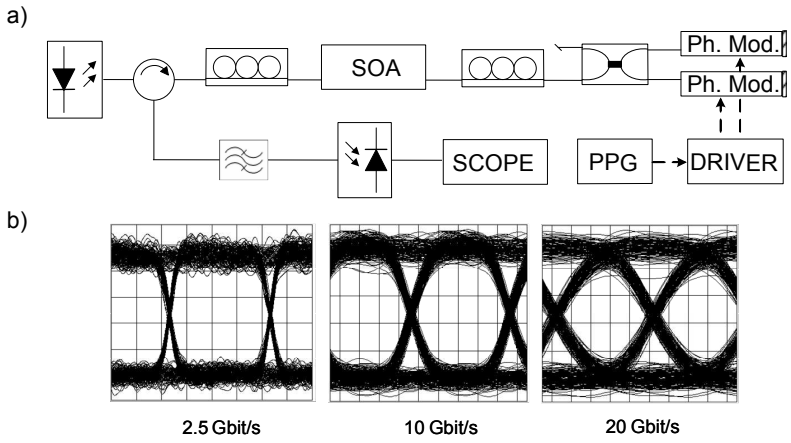

Figure 3.15: MIM simulation (a) model and (b) results.

The fabrication cost of an RSOA and an MIM can be low when they are produced in large volumes. The cost of an EAM and an integrated SOA-EAM, is higher due to its complex semiconductor structure.

Chapter 4

Reconfigurable optical add/drop multiplexer

In this Chapter, the reconfigurable OADM (ROADM) based on the micro-ring resonator structure is characterized [53, 90, 91].

In Section 4.1 the BBPhotonics ROADM architecture, as introduced in Chapter 2, is described and characterized in terms of passive and dynamic performance in Section 4.2 and Section 4.3, respectively[1].

4.1 ROADM architecture

The dynamic wavelength allocation in the access domain has been already considered in earlier projects [23, 24, 95–99]. Wavelength selection can be performed either at the ONU or through wavelength routing in the ODN [13]. The most common solution is to realize the wavelength channel selection by combination of cyclic AWGs and tunable laser sources. Providing tunability in the ONU requires advanced and expensive components at the user-side, whereas setting the wavelength-flexible ROADM in the shared part of the network, i. e. CO or ODN, reduces significantly the overall initial investment.

The ROADM in the BBPhotonics network is placed at the RN. It is remotely controlled (from CO) based on the requested bandwidth per user and provides the user with exactly one wavelength-pair via a single drop-port. The principle of operation is given in Section 2.4. For the purpose of the proof-of-concept experiment the number of add/drop ports in the ROADM is downscaled to four.

The structure of the ROADM is based on thermally tunable micro-ring resonators fabricated in the Si_3N_4/SiO_2 materials system. The application of a high

[1]The device characterized in this Chapter was also applied as a label extractor/eraser in optical signal processing experiments as described in [92–94].

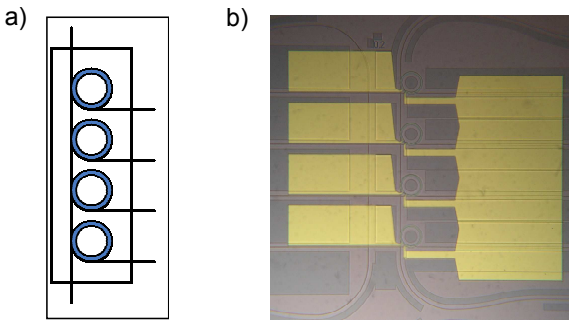

Figure 4.1: Architecture of the ROADM: (a) schematic and (b) mask; after [53].

contrast materials system ($\Delta n = 0.55$) for the highly selective filters allows for the creation of complex devices on a small footprint [90, 91, 100].

As it can be seen in fig. 4.1 the ROADM consists of a central bus waveguide which is coupled with four resonators. These resonators can be used to add/drop channels from/to the four ports. The design is based on a single resonator unit cell, fig. 4.2, which is copied a certain number of times to create the desired component. Such cell consists of a ring resonator that is vertically coupled to its port waveguides. On top of each resonator there is a thin-film omega-shaped chromium heater, which enables thermal tuning.

Because of the material stress the maximum thickness of the Si_3N_4 layers is about 340 nm and, since the transverse magnetic (TM) modes will typically have a significantly lower effective refractive index and higher losses in resonator waveguides with a low aspect ratio, it is impossible to create a polarization-independent resonator with this technology. The structure is optimized for the transverse electric (TE) modes polarization only. However, the device can be made polarization-independent if the TriPleX^{TM} technology is used [101]. It enables matching the effective indices for TE and TM by fabricating non-square waveguides. Another approach, suggested in [90], is based on the polarization diversity scheme. Although, it preserves the same amount of ring resonators thanks to the exploitation of the bidirectionality of a single resonator cell, it requires more complex design including polarization beam splitters and polarization converters. Moreover, it suffers from the interference induced by reflected signals.

The complete fabrication process is explained in [90]. The device is packaged with the complete driving circuit involving a. o. a universal serial bus (USB) interface and digital-to-analog converters (DAC), fig. 4.3. The USB interface is driven with user-friendly software which enables separate tuning of each resonator by changing the individual voltages. The DACs convert the digital signal to a corresponding analog voltage.

Several ROADMs based on the design described above have been fabricated

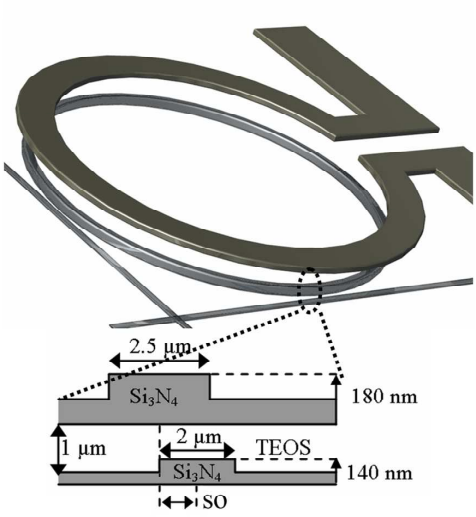

Figure 4.2: Top view and coupling region cross-section of the MR unit cell; after [53].

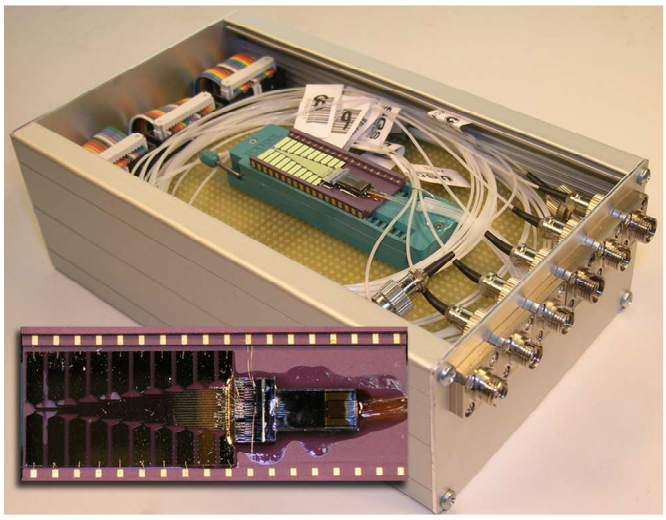

Figure 4.3: An example of packaged ROADM and the pigtailed chip in the inset; after [53].

within the BBPhotonics project[2]. In general, the requirements like passband and tuning range have been satisfied. However, remaining issues are the high polarization dependence and insertion loss, low return loss and thermal instability.

As mentioned earlier the PDL can be addressed by e. g. TriPleX^{TM} technology. The high insertion loss and low return loss result in a very low signal-to-crosstalk ratio (SCR) in a single bidirectional fiber system. The return loss and insertion loss may be improved if, in addition to the small core fiber butt-coupled to the chip, a transparent adhesive would be used for index-matching. For further improvement tapered fiber with coated chip or slanted fiber and chip are recommended.

Thermal instability, which is mainly a result of thermal crosstalk between neighboring heaters, causes an unwelcome detuning of a ring from its desired resonant wavelength and a higher power loss observed at a corresponding drop-port. In extreme cases, when high voltages are applied, it may even lead to inter-band (inter-wavelength or inter-channel) crosstalk resulting in serious degradation of the received data signal. The thermal crosstalk is an unavoidable fundamental issue, since the waveguide material is thermo-active and the rings are placed very close to each other. This issue may only be addressed by voltage-wavelength look-up table with correction factors for different heater configurations. The other issue contributing to the thermal instability is the influence of the ambient temperature, which is far lower than the thermal crosstalk between the heaters and can be managed by proper packaging of the optical chip.

In the following Sections a complete characteristic of the fabricated device with the best properties is given.

4.2 Static characterization

The main static parameters of the ROADM are: the insertion loss (IL), the PDL, the return loss (RL), the FSR, and the filter response. The IL, PDL and RL are measured (1550 nm band) in the setups given in fig. 4.4a-4.4c with the ROADM completely passive (no voltages applied to the heaters) unless mentioned differently. The results are summarized in table 4.1[3].

Table 4.1: Measured loss parameters of the ROADM

Parameter	Input-port	Port 1	Port 2	Port 3	Port 4	Through-port
IL [dB]		11.3	12.5	15.5	16.2	14.6
PDL [dB]		> 30	> 30	> 30	> 30	> 30
RL [dB]	21.6	22.6	18.5	13.6	21.6	18.5

[2]LioniX BV (http://www.lionixbv.nl), a BBPhotonics Project partner.
[3]IL measurement is optimized for the best polarization (the highest transmission).

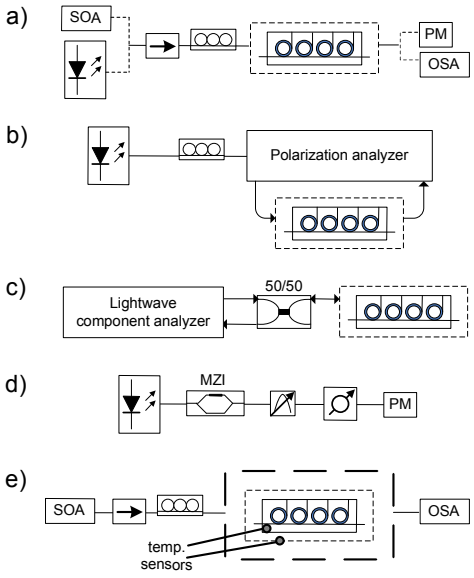

Figure 4.4: Setups for static characterization of the ROADM: (a) IL, FSR, filter response, (b) PDL, (c) RL, (d) detuning-induced power loss and (e) ambient temperature-induced wavelength shift.

The increasing trend of IL can be explained by the higher waveguide losses and waveguide-ring coupling losses which the signal encounters while passing by the consecutive ring resonators. This is also clearly visible in fig. 4.5, where for the purpose of only this measurement 0 V, 2.85 V, 3.9 V and 4.88 V are applied to the resonator heater 1, 2, 3 and 4, respectively, in order to tune to 50 GHz spaced channels. Drop-port 3 shows an excessive insertion loss with respect to the other ports. This, together with the exceptionally low return loss for this port, can be explained with the misalignment of the fiber array which is attached to the drop-ports of the optical chip.

The FSR is measured in the setup shown in fig. 4.4a with 0.02 nm-resolution OSA attached to the through port of the ROADM when all rings are passive (not tuned). The measured FSR is 4.31 nm as indicated in fig. 4.6. The FSR deviation from the desired value of 4.0 nm is caused by inaccuracy of the waveguide resonator diameter (5 μm).

The same setup, fig. 4.4a, was used to measure the filter response of an example single resonator by sweeping the tunable laser over 4 nm around the resonant frequency of a passive ring resonator and measuring the output power at a drop-port 1 with polarization set to maximum transmission, fig. 4.7. In the same figure, this is compared with the drop-port response to a broadband input recorded with the OSA, which shows an acceptable matching. The filter response shows around

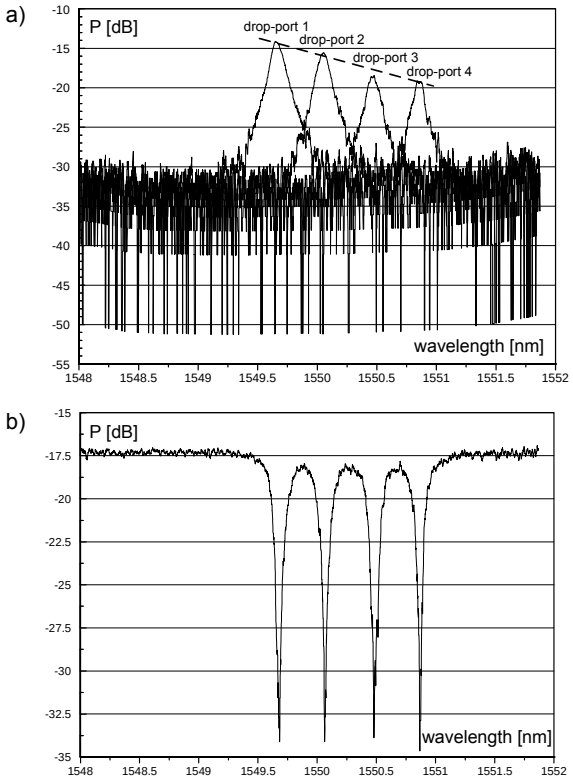

Figure 4.5: Spectral response of (a) the drop-ports and (b) the through port.

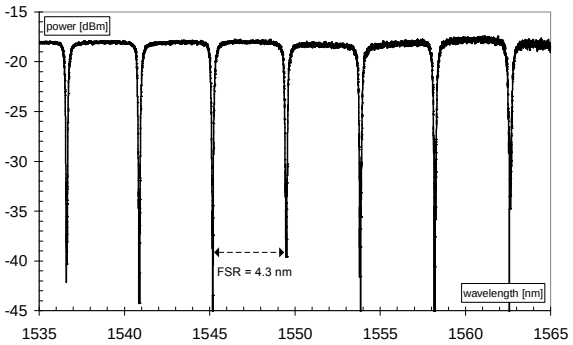

Figure 4.6: Free spectral range of the ROADM.

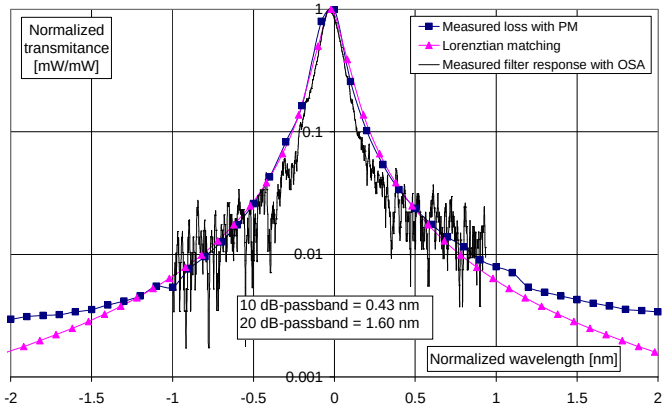

Figure 4.7: Filter response of port 1 of the ROADM.

15 dB suppression ratio for 50 GHz wavelength grid, which should result in less than 0.2 dB power penalty induced by interchannel crosstalk[4], as discussed in Chapter 5.

In order to provide PtMP operation, the ring-resonator has to work in a drop-and-continue mode. This is achieved after some deliberate detuning of a ring-resonator from the nominal wavelength, which potentially may introduce chirp-induced intensity variations. The power loss at the drop-port caused by such detuning is checked in the simulation setup using VPI TransmissionMaker [89], fig. 4.4d, where the Lorentzian-matched filter characteristic is applied. The simulation allows for elimination of any additional instabilities, e. g. thermal crosstalk between the heaters, which may cause large inaccuracy during the measurement on the real device. The simulation results are given in fig. 4.8.

Also, some undesired detuning may happen due to the ambient temperature changes, since the device is not equipped with a temperature control circuit, or thermal crosstalk between the neighboring heaters. Therefore, the ROADM is also tested in terms of the thermal stability. For this purpose the whole aluminium box with the RAODM is placed in a temperature-controlled chamber. The box of the ROADM is partly opened, just as in fig. 4.3, to allow for the air convection. Two temperature sensors are applied: one measures the air temperature inside the ROADM box and the second one is placed on the ROADM aluminium box, as indicated in fig. 4.4e. For this measurement the OSA with the highest resolution of 0.01 nm is used. The temperature of the chamber is changed from -10 ^oC to 42 ^oC, the measurements are performed three times in around 12 hours intervals and the temperature-up cycle is 4, 3 and 2 hours. The averaged results show 0.0147 $nm/^oC$ shift, fig. 4.9. Based on this result and the results in fig. 4.8, one

[4]This applies only to PtP (add/drop) configurations of the ROADM, which means that the wavelength channels are not power-split as in PtMP configurations.

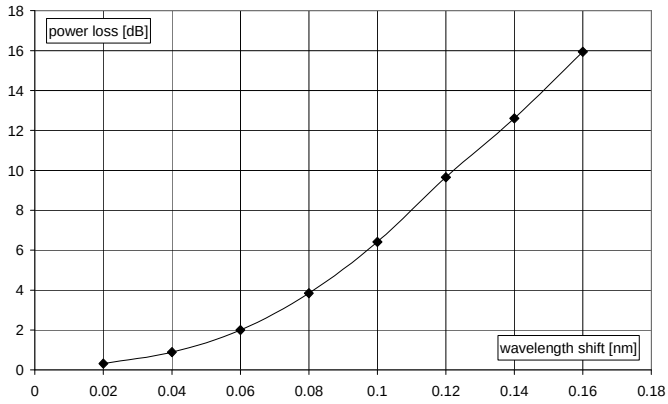

Figure 4.8: Power loss due to detuning.

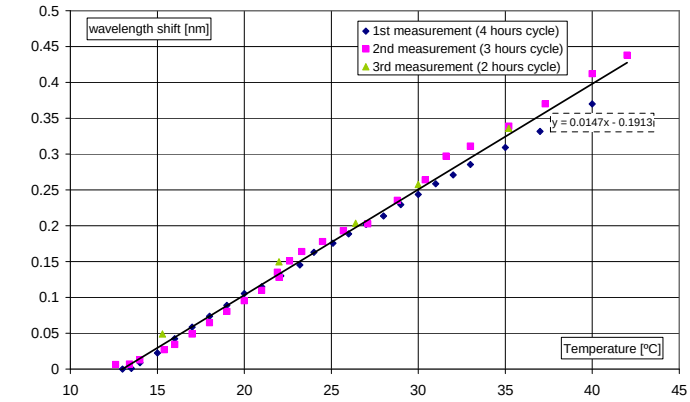

Figure 4.9: Wavelength shift due to ambient temperature changes measured at the through-port.

can conclude that the temperature change of 4 ^oC, resulting in 0.06 nm detuning from the desired wavelength brings minimum 2 dB additional loss at the given drop-port. Therefore, it is recommended that the device is stabilized within 1 ^oC in terms of ambient temperature changes in order to keep the power loss lower than 0.3 dB. The thermal crosstalk between the heaters will be discussed in the next Section.

4.3 Dynamic characterization

For the dynamic characterization the voltage to the heaters is applied.

In order to prove the proper filter function of the ROADM a 1.25 Gbit/s amplitude-modulated wavelength channel is sent from the input-port to the drop-port 1 in the setup given in fig. 4.10a. For this measurement a different device with the same design but slightly better loss characteristics operating in 1300 nm band was available[5]. The reference measurement showed the receiver sensitivity of around -35.5 dBm at $BER = 10^{-9}$, fig. 4.11. To drop the 1305.2 nm wavelength channel drop-port 1 is tuned with 2.6 V. As it can be seen in the results of BER measurements for PRBS equal to $2^{31} - 1$, fig. 4.11, no significant power penalty was measured. The negligible difference of around 0.12 dB is assigned to the polarization instability in the measurement system and the remaining ASE noise. The received eye diagrams show no negative influence of the OADM on the eye parameters, as can be expected from the 46 GHz bandwidth of the MRs [102] that offers the possibility of even higher bit-rates [103].

Although no dispersion effect can be observed in fig. 4.11 for 1.25 Gbit/s and even for modulation at 10 Gbit/s in fig. 4.12, the wavelength-dependent optical delay in the OADM needs to be explained. The micro-ring resonator is a resonant filter and, therefore, the delay will be dependent on the position of the nominal wavelength of the transmitted signal with respect to the resonance frequency of the filter. Since the amplitude-modulated signal has a relatively wide spectrum, different components of the modulated signal experience different delay causing pulse-spreading and inter-symbol interference (ISI). In the case of micro-ring resonators only the structural dispersion can be critical and the other dispersion types (material and waveguide dispersions) can be neglected [104, 105]. The modal dispersion can be also neglected, since all waveguides are designed to be single-mode. The structural dispersion is determined by the layout of the structure and the resulting coupling constants, which is discussed in detail in [91]. There, the simulated and measured group delay at the drop-port after the 10 Gbit/s amplitude-modulated signal is transmitted through a single micro-ring resonator is 5 ps and the resulting dispersion is 25 ps/nm. This is less than the dispersion after 2 km of SSMF, which definitely will not cause any visible power penalty or eye diagram degradation, fig. 4.12.

[5]Due to the problems with mask alignment the device performed better at 1300 nm than in 1550 nm as initially designed.

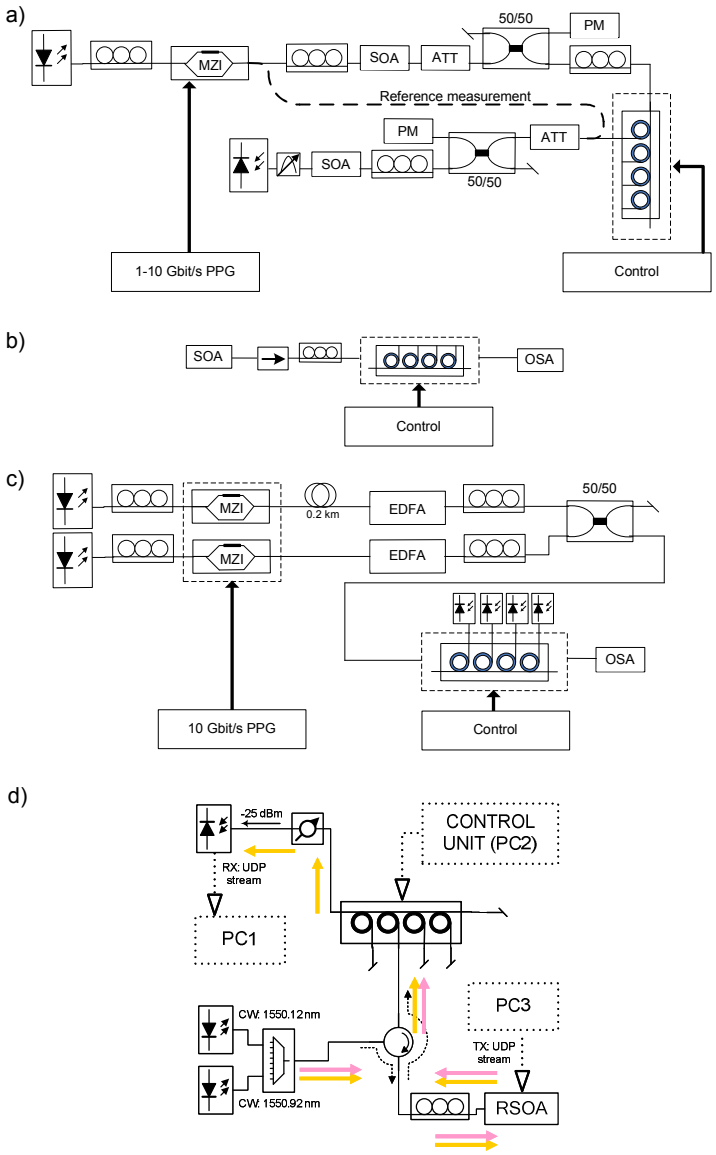

Figure 4.10: Setups for dynamic characterization of the ROADM: (a) filter function, (b) tuning range, (c) interchannel crosstalk and (d) switching time.

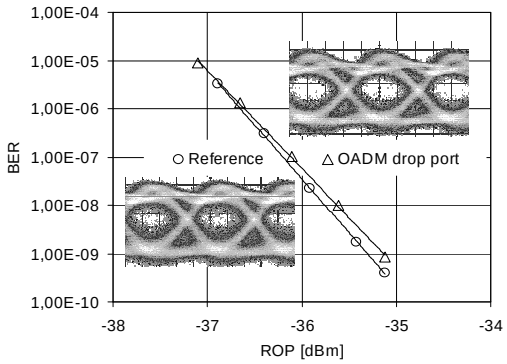

Figure 4.11: Measurement of the 1.25 Gbit/s data signal dropped at the ROADM.

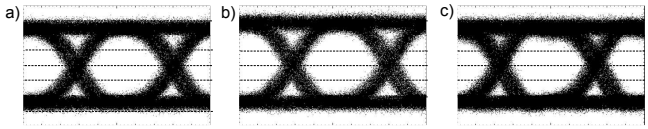

Figure 4.12: Eye diagrams of the 10 Gbit/s wavelength channel dropped at a single drop-port for different positions of the resonant frequency with respect to the nominal signal wavelength: (a) 0 GHz, (b) 13 GHz, and (c) 25 GHz shift.

The eye diagrams of a 10 Gbit/s wavelength channel dropped by a single resonator detuned with 0 GHz, 13 GHz and 25 GHz are given in fig. 4.12. In the situation when a number of ring resonators in a row share the same wavelength channel, every next ring resonator will see the through-response of the earlier ring resonator with accompanying phase delay and dispersion. Still, no visible dispersion-induced ISI in the eye diagram is recorded as shown in fig. 4.13. The system used for this experiment is depicted in fig. 4.10c[6].

Next, the tuning range of each resonator was checked in the setup as depicted in fig. 4.10b. The measurement was taken from the through-port response to a broadband input. In principle, the tuning range should cover the complete FSR. However, in order not to overdrive the heaters, the tests for maximum ratings are not performed. All rings reveal comparable tunability, and the measured tuning range is sufficient to accommodate wavelength channels on a 50 GHz standard wavelength grid, fig. 4.14. The slight differences in the graph are caused by the lead length differences from the bondpad to the heater on the chip which results in higher resistance and a lower current reaching the heater.

The dynamic operation of the ROADM splitting two wavelength channels to

[6]The micro-ring resonator-based structures can be also used for dispersion compensation. For that purpose proper coupling coefficients and the position of the resonant frequency with respect to the signal nominal wavelength has to be chosen [91].

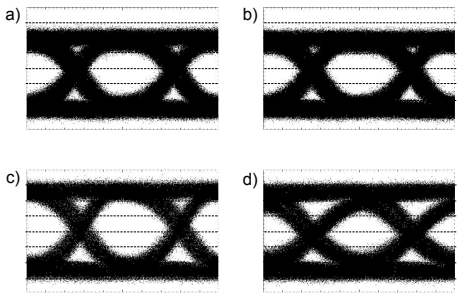

Figure 4.13: Eye diagrams of the 10 Gbit/s wavelength channel shared among four drop-ports detuned from the nominal signal wavelength with (a) -25 GHz at drop-port 1, (b) +13 GHz at drop-port 2, (c) -13 GHz at drop-port 3 and (d) 0 GHz at drop-port 4.

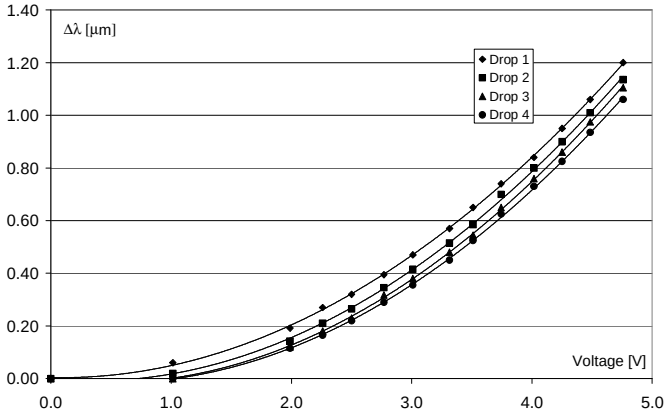

Figure 4.14: Tuning range of the rings.

two different drop-ports is checked in the setup as given in fig. 4.10a. The first ring is set to drop $\lambda_0 = 1549.61$ nm which corresponds to the required voltage of 1.4 V applied to the heater. The second, third or fourth ring is set to drop a wavelength channel 100 GHz apart from λ_0 which corresponds to 0.8 nm wavelength shift and the required voltage of around 4.0 V, 4.1 V and 4.2 V, respectively, based on fig. 4.14. As indicated in the recorded drop-port responses to a broadband input in fig. 4.15a-4.15c, after activation of the second, third or fourth drop port a passband shift can be noticed at the first drop-port, which is due to the undesired cross-heating between the heaters[7]. This cross-heating is caused by substrate thermal conductivity and it is lower if the distance between the heaters is larger. In order to compensate for this instability and the resulting excess power loss (1-2 dB at minimum according to fig. 4.8) a correction has to be applied to the voltage driving the primary ring as indicated in table 4.2. Due to the fact that all the heaters influence each other a voltage-wavelength look-up table with proper correction factors has to be implemented for numerous wavelength configurations which the ROADM is supposed to support in a given application.

Table 4.2: Corrected voltages required due to inter-heater thermal crosstalk.

Active drop-ports	Original voltage for drop-port 1 [V]	Voltage for crosstalk drop-port [V]	$\Delta\lambda$ [nm]	Corrected voltage for drop-port 1 [V]
1 and 2	1.4	4.0	0.050	0.82
1 and 3	1.4	4.1	0.048	0.86
1 and 4	1.4	4.2	0.045	0.92

If a ring resonator has to work in a drop-and-continue configuration only a certain power level has to be tapped off from the broadcast wavelength channel. It requires detuning of the ring resonator depending on the power level which has to be dropped or let through to the next ring. Consider a situation where a single wavelength channel is shared over two ONUs and, therefore, it has to be divided into equal power levels. Again, drop-port responses to a broadband input signal are recorded using the setup in fig. 4.10b. First, drop-port 2 is tuned to drop completely wavelength channel at 1549.667 nm, which requires 1.482 V provided to the corresponding heater. Then, drop-port 1 is tuned to drop the same power as drop-port 2. That way the effective 50/50 splitting factor (including the different IL for drop-port 1 and drop-port 2) is achieved[8], fig. 4.16a. It takes a few seconds to

[7]The passband shift is defined as the shift measured at FWHM on the graphs in fig. 4.15.

[8]Since equal drop power levels can be achieved, and the IL is not the same for each drop-port in the prototype device as shown in fig. 4.5, the contribution of split loss to the total loss also differs per drop-port.

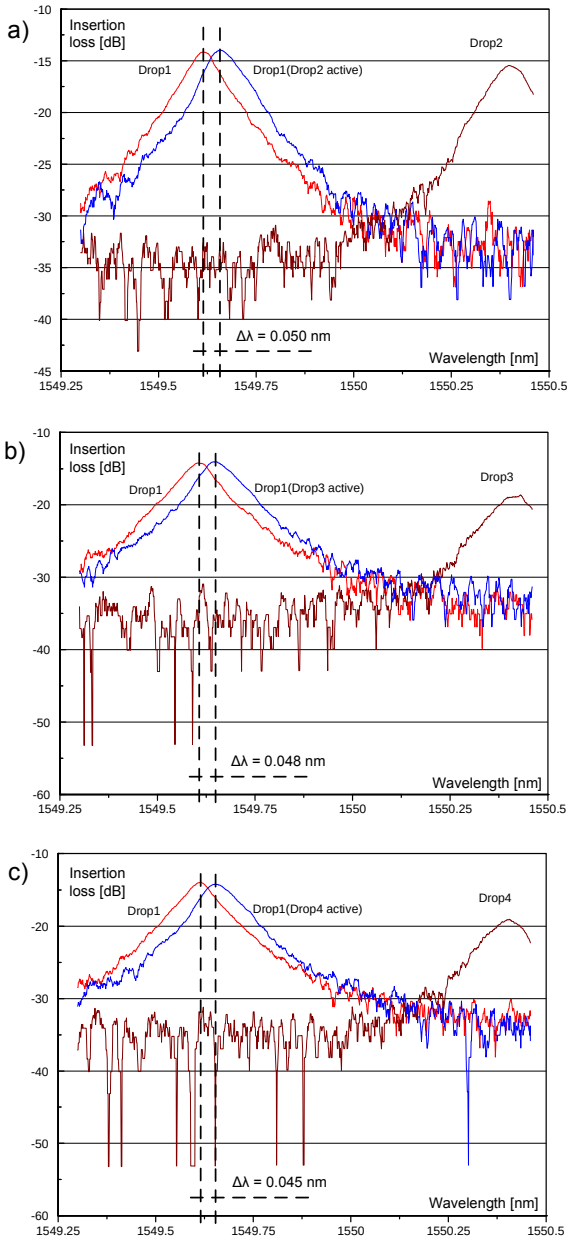

Figure 4.15: Undesired wavelength shift in drop-port 1 resulting from the thermal crosstalk after switching on (a) drop-port 2, (b) drop-port 3 and (c) drop-port 4.

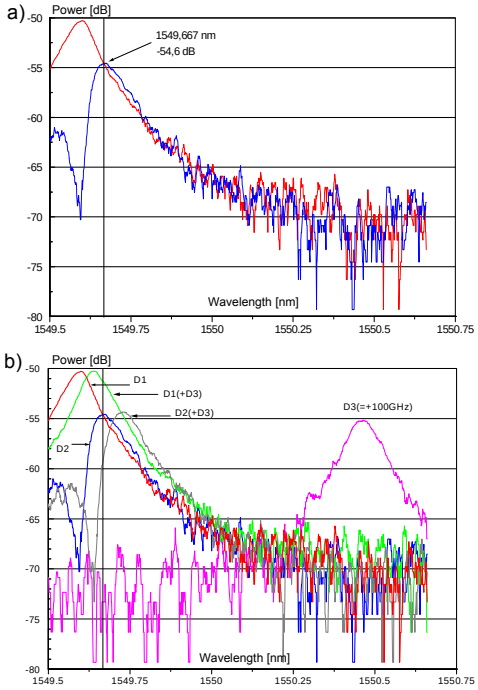

Figure 4.16: ROADM configuration: (a) drop-and-continue and (b) drop-and-continue with extra drop.

stabilize the situation as both heaters influence each other. The total loss (L_{total}) for a given drop-port can be written as follows (dB):

$$L_{total} = IL + L_{split} \tag{4.1}$$

where L_{split} is the splitting loss.

As discussed earlier, if an additional heater is activated it causes an undesired wavelength shift to the primary ring. In a drop-and-continue scenario the two drop-ports sharing the same wavelength are a subject to thermal crosstalk and significant power loss if a third heater is switched on. This requires correction of their voltages. Such a situation is depicted in fig. 4.16b. It may happen that the thermal crosstalk is so large that the required correction cannot be performed even if the voltage of the primary ring is set to 0 V. In order to be able to compensate for the wavelength shift in a sufficiently wide bandwidth around the desired wavelength all rings should be biased (pretuned) in the start-up situation. This should be taken into account in the look-up table, which was mentioned earlier.

The partial filtering of the data channel will cause suppression of higher frequency components in the electrical domain and, as a consequence, lengthen the

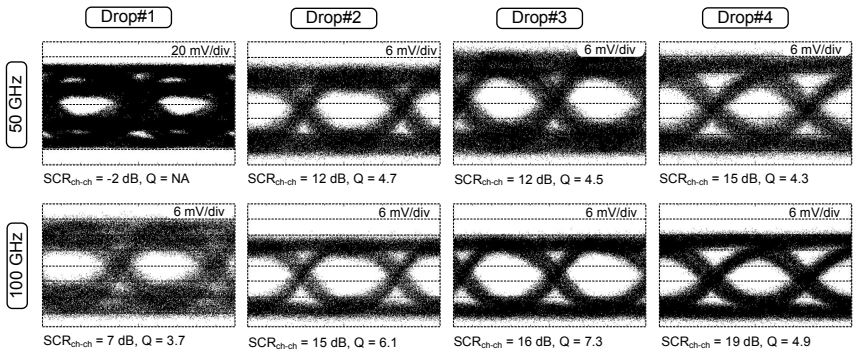

Figure 4.17: Results for two different wavelength channel spacings of the ROADM in a 1x4 configuration.

rise and fall slopes of the eye diagram. Moreover, if a 50 GHz wavelength grid is applied, interchannel crosstalk may become an issue for higher split-ratio configurations requiring further detuning of wavelength-sharing drop-ports. Such a situation is recorded in the setup shown in fig. 4.10c, where one of two 10 Gbit/s amplitude-modulated wavelength channels entering the ROADM is shared over 4 drop-ports. The same modulation signal was applied to both external modulators and the output modulated signals were decorrelated by means of an optical delay (0.2 km SSMF). The eye diagrams of the photodetected signals for 50 GHz and 100 GHz channel spacings are shown in fig. 4.17 together with the SCR and Q-factor measured by the OSA and the digital analyzer, respectively. The presented 1x4 configuration requires the last ring in the row to be tuned exactly to the nominal wavelength (drop mode), whereas the earlier rings operate in a drop-and continue mode. The first ring is -25 GHz detuned from the nominal wavelength, the second and the third ring are detuned with -13 GHz and +13 GHz, respectively. For the 50 GHz channel spacing the signal dropped at the first ring suffers from substantial interchannel crosstalk, fig. 4.17. The situation can be improved if the channel spacing is increased to 100 GHz, as shown in fig. 4.17, or if the filter characteristic of a drop port is upgraded by implementing higher order filters consisting of 2 or more micro-ring resonators [104]. However, in such a case the phase response and, therefore, the dispersion properties are different from those for a single micro-ring resonator filter [106]. No chirp-induced amplitude-variations due to the operation on the slope of the filter have been observed.

One of the most important parameters related to the dynamic performance of the ROADM is the switching time [107]. In the setup used for this measurement two CW signals are inserted into the RSOA using a circulator after the OADM to avoid backreflections induced by poor return loss as mentioned earlier in this Section, fig. 4.10d. Both CW signals are modulated simultaneously in the RSOA with the data generated by personal computer 1 (PC1). Only one channel at a

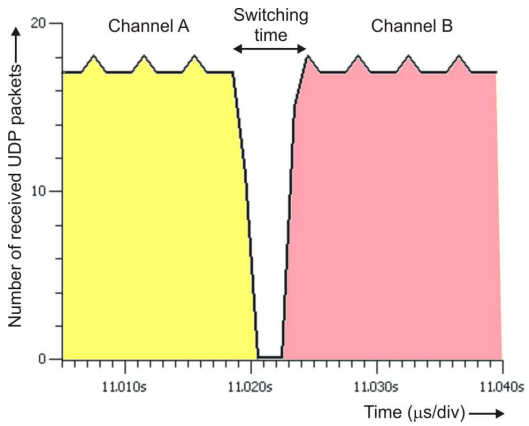

Figure 4.18: Switching time measurement [107].

time passes through the OADM, which is controlled by PC2. Media-converters are used for opto/electrical conversion. The switching time, denoted as the time to achieve maximum throughput again when a micro-ring resonator has to be tuned from channel A to channel B spaced at a distance of 50 GHz, is measured by PC3 at 200 Mbit/s using user datagram protocol (UDP) packets of 1470 bytes. The switching time is determined to be approximately 6 ms, which will inherently lead to packet loss, fig. 4.18. However, when considering a time critical service like voice communication, it will not disturb or disconnect the conversation. The obtained packet loss consists of maximum 20 ms of voice data, which will not be notified by the user. For other applications, retransmission of the packets will take place after time-out.

Chapter 5

Transmission and network impairments in the access network

There are several possible network and transmission impairments which need to be considered in the access network. The estimated power penalties (PP) induced by such distortions are crucial for the link power budget and, thus, the reach of the network.

A number of possible transmission and network impairments that may occur in a hybrid WDM/TDM access network are discussed in Sections 5.1-5.5. In Section 5.6 all PPs induced by the different impairments in the BBPhotonics network are given.

5.1 Limited extinction ratio

In a system with signal-independent noise[1] a limited extinction ratio of a transmitted signal causes PP according to the eq. 5.1, which is plotted in fig. 5.1, [108]:

$$PP_{ER} = -10 \log \left[\frac{r-1}{r+1} \right] \tag{5.1}$$

where r is the linear extinction ratio defined as the ratio of average power for a logic "1" to the average power for a logic "0". The above relation is depicted in fig. 5.1. For extinction ratio equal to 9.5 dB and higher the PP is lower than 1 dB. The penalty is higher when the system is limited by signal-dependent noise, which is typically the case in amplified systems. This is due to the increased amount of noise present at "0" level [108].

[1] E. g. An unamplified system with direct detection PIN receivers.

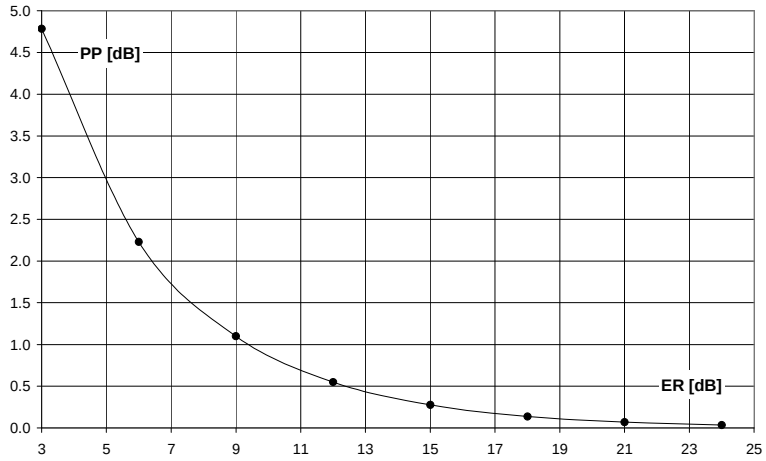

Figure 5.1: Power penalty induced by a limited extinction ratio of a transmitter.

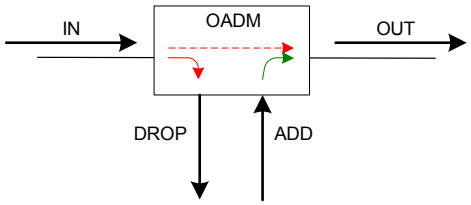

Figure 5.2: Intrachannel crosstalk scenario in an OADM.

5.2 Intrachannel crosstalk

The intrachannel crosstalk arises when the frequency difference between the desired signal and the interferer is within the electrical bandwidth of the receiver.

In a WDM system this type of crosstalk may happen in case of four-wave mixing (FWM) where some of the FWM products may arise close to a wavelength channel or in a system where, for instance, an OADM with low drop ratio is applied. In the latter case if a wavelength channel is only partially dropped and some power leaks to the through-port of the OADM it will interfere with the added signal on the same wavelength. This is the case only if the interfering signals propagate in the same direction through the OADM as explained in fig. 5.2.

In a bidirectional system where DS and US transmission is performed on the same optical carrier (e. g. remotely seeded ONU) over a single fiber, components with low RL contribute to the crosstalk power by reflecting substantial part of the signal power (a. k. a. discrete reflections). This reflected power interferes with the counter-propagating signal. Furthermore, the counter-propagating signals influence each other due to RBS. The maximum accumulated RBS power is achieved

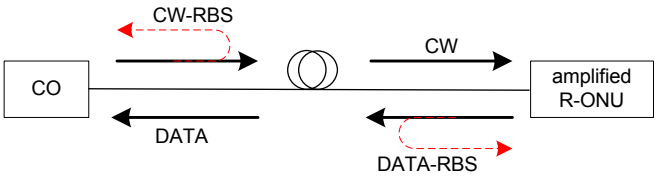

Figure 5.3: Backscattering in the access network link based on amplified colorless ONU.

for around 30 km fiber length, when the input power to RBS (returned) power ratio reaches $\alpha_{RBS} = 34$ dB [63]. Although RBS-induced intrachannel crosstalk is an issue in the single-fiber bidirectional systems it may not result in as high PP as the crosstalk caused by discrete reflections. The discrete reflections may fall in explicit phase interaction with the desired signal resulting in larger amplitude variations than in case of inherently incoherent RBS.

Although, Brillouin backscattering (BBS) products are shifted around 10 GHz apart from the nominal wavelength and reveal lower power than RBS power, for 10 Gbit/s (and higher) amplitude modulated carriers they are still considered as a source of intrachannel crosstalk noise since the BBS power remains within the optical data bandwidth. RBS brings higher return power than BBS and it is at the same nominal wavelength as the desired signal, which makes it more critical for the error-free transmission.

The intrachannel crosstalk noise can be decreased if components with high RL are used in the setup. Also utilizing sources with short coherence length results in weaker interferometric interaction between the desired signal and the interferer. In the systems which are not sensitive to high chromatic dispersion (e. g. short range), external phase modulation can be applied in order to disrupt the coherence. In the access systems employing ONUs equipped with optical amplifiers, proper gain adjustment may improve the SCR.

The situation considered here is depicted in fig. 5.3. The CO provides a single unmodulated (CW) wavelength channel, which is transmitted over 30 km fiber length ($\alpha_f = 0.2dB/km \cdot 30km$). The R-ONU is equipped with an optical amplifier and an amplitude modulator which transmits the US modulated signal on the same nominal wavelength as the input CW carrier over the same fiber.

To distinguish between the SCR_{RBS} at the CO site and ONU site two new ratios are introduced. The $SCR_{RBS,CO}$ is the ratio of the US modulated signal power ($P_{DATA,CO}$) to the power of backscattered CW carrier ($P_{RBS,CO}$) at CO input as given in eq. 5.2. The $SCR_{RBS,ONU}$ is the ratio of the CW power ($P_{CW,ONU}$) to the power of backscattered upstream modulated signal ($P_{RBS,ONU}$) at ONU input as given in eq. 5.3 [63].

$$SCR_{RBS,CO} = P_{DATA,CO} - P_{RBS,CO} \tag{5.2}$$

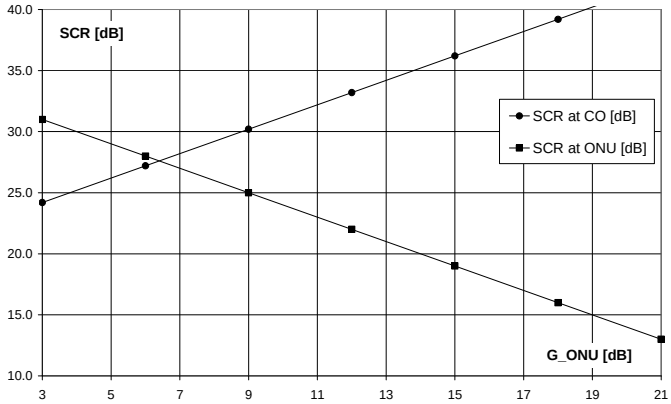

Figure 5.4: RBS-degraded SCR ratios at CO and ONU in function of gain at ONU.

$$SCR_{RBS,ONU} = P_{CW,ONU} - P_{RBS,ONU} \tag{5.3}$$

where $P_{DATA,CO}$, $P_{RBS,CO}$, $P_{CW,ONU}$ and $P_{RBS,ONU}$ are given by eq. 5.4-5.7, respectively.

$$P_{DATA,CO} = P_{CW,CO} - 2\alpha_f + G_{ONU} \tag{5.4}$$

$$P_{RBS,CO} = P_{CW,CO} - \alpha_{RBS} \tag{5.5}$$

$$P_{CW,ONU} = P_{CW,CO} - \alpha_f \tag{5.6}$$

$$P_{RBS,ONU} = P_{CW,CO} - \alpha_f + G_{ONU} - \alpha_{RBS} \tag{5.7}$$

where $P_{CW,CO}$ (dB) is the CW signal power transmitted from the CO, α_f (dB) is the attenuation of 30 km SSMF, and G_{ONU} (dB) is the gain of ONU. After applying eq. 5.4-5.7 into eq. 5.2 and eq. 5.3, one obtains the following formulas:

$$SCR_{RBS,CO} = G_{ONU} - 2\alpha_f + \alpha_{RBS} \tag{5.8}$$

$$SCR_{RBS,ONU} = \alpha_{RBS} - G_{ONU} \tag{5.9}$$

The above relations are shown in fig. 5.4. It can be noticed that there is an optimum value for the gain of ONU, where the SCRs are equal. In this case the optimum corresponds to the total CO-ONU fiber loss.

For the purpose of further analysis the worst-case of intrachannel crosstalk is assumed. This means that the signal and the interferer are out of phase and are co-polarized, which results in the highest amplitude distortion. In a real situation, the phase relation as well as polarization states may fluctuate over long time-scale due to e. g. temperature variations. Assuming an infinite extinction ratio in an optically amplified system, the PP due to intrachannel crosstalk is described with the following formula [108]:

$$PP_{intra} = -5\log(1 - 2\sqrt{\varepsilon_{intra}}) \tag{5.10}$$

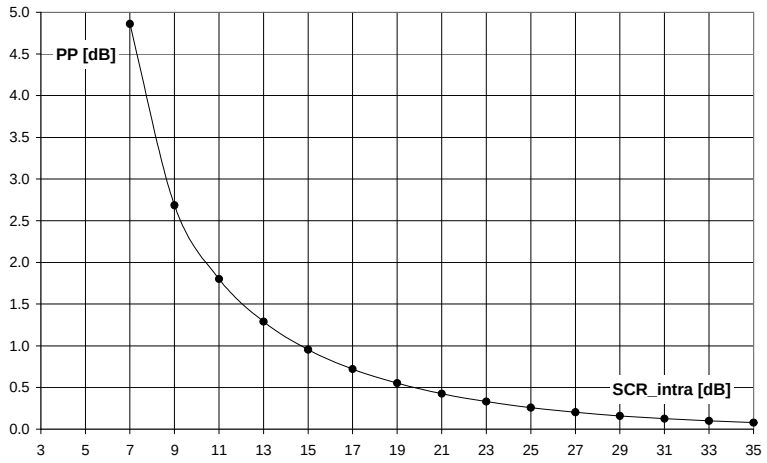

Figure 5.5: Power penalty caused by intrachannel crosstalk.

where ε_{intra} is the linear factor describing the crosstalk power with respect to the signal power (inverse of signal to crosstalk ratio).

The above relation is depicted in fig. 5.5, where it can be seen that SCR_{intra} equal to 20 dB is a minimum requirement for 0.5 dB PP.

5.3 Interchannel crosstalk

The interchannel crosstalk noise is a result of the interaction between the neighboring wavelength channels. It may also happen in the system affected by FWM phenomenon, where some of the FWM products may fall into the optical passband at the receiver. It is an important issue in high bit-rate (D)WDM systems, where FWM products can degrade several wavelength channels.

A practical formula to describe PP due to interchannel crosstalk in an optically amplified system (assuming an infinite extinction ratio) is given as follows [108]:

$$PP_{inter} = -5\log(1 - \varepsilon_{inter}) \tag{5.11}$$

where ε_{inter} is the factor describing the crosstalk power with respect to the signal power. The relation is depicted in fig. 5.6. The interchannel crosstalk induces lower penalty with respect to the intrachannel crosstalk for the same value of SCR. In case of the danger of interchannel crosstalk the requirements for optical filters focus on sharp and relatively narrow passband response with high adjacent channel suppression ratio.

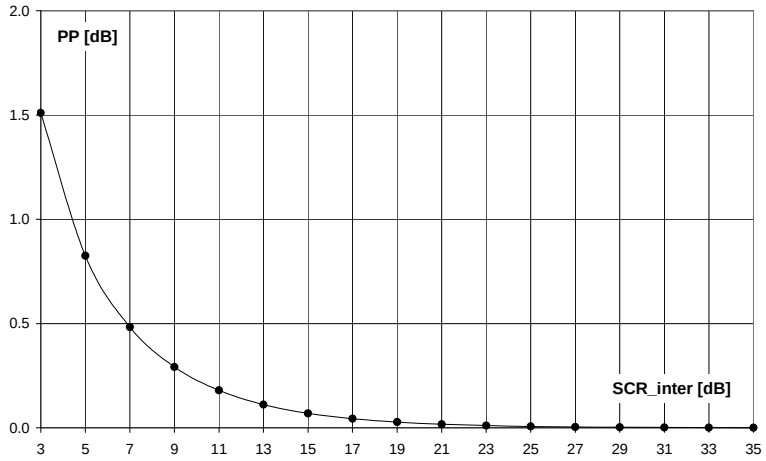

Figure 5.6: Power penalty caused by interchannel crosstalk.

5.4 Accumulation of ASE noise

In case of a system employing several optical amplifiers the accumulated ASE noise becomes an important limiting factor. Adding ASE noise power to the signal power results in electrical beat noise products of the signal and the ASE as well as beat noise products of the ASE against itself during the square-law detection of the photodiode. These limit the maximum obtainable receiver sensitivity [81]. The cascaded amplifiers may build up a high total noise figure (NF) in the system. Although narrow-band optical filters may improve the performance of the system in terms of ASE-ASE beat noise significantly, still signal-ASE beat noise will go through to the receiver resulting in degraded Q-factor and BER of the received signal.

In access systems based on amplified reflective ONU, as discussed in this dissertation, the heaviest ASE accumulation is at the US receiver at the CO, since the CW encounters a cascade of optical amplifiers and then the modulated US encounters the same number of amplifiers. Besides in-field optical amplifiers also SOA in the ONU adds some noise. Total NF becomes difficult to calculate for the complete DS-US transmission for the remotely modulated CW carrier. This is due to the fact that the input signal to the reflective ONU is amplitude-modulated with its primary ASE noise accumulated over DS propagation, fig. 5.7.

Due to the complexity of the designed network a simulation tool is used [89], where the schemes shown in fig. 5.8 are applied. Based on that the influence of accumulated ASE noise on the Q-factor at the ONU and CO receivers can be easily checked for different noise figures of the applied amplifiers. To eliminate potential impairments other than the ASE accumulation, all network elements are substituted with attenuators. The reflective modulator at ONU consists of two

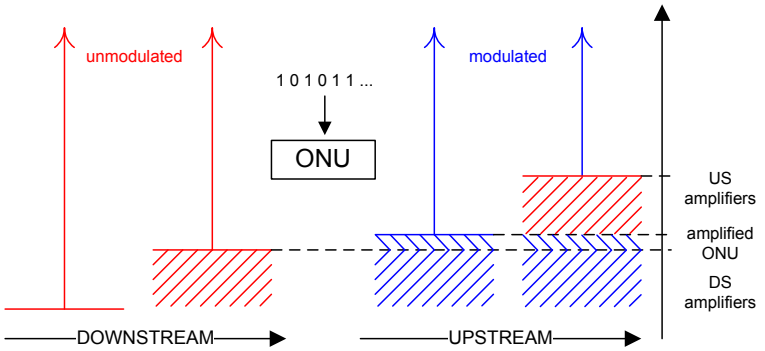

Figure 5.7: ASE noise accumulation in an optically amplified access system.

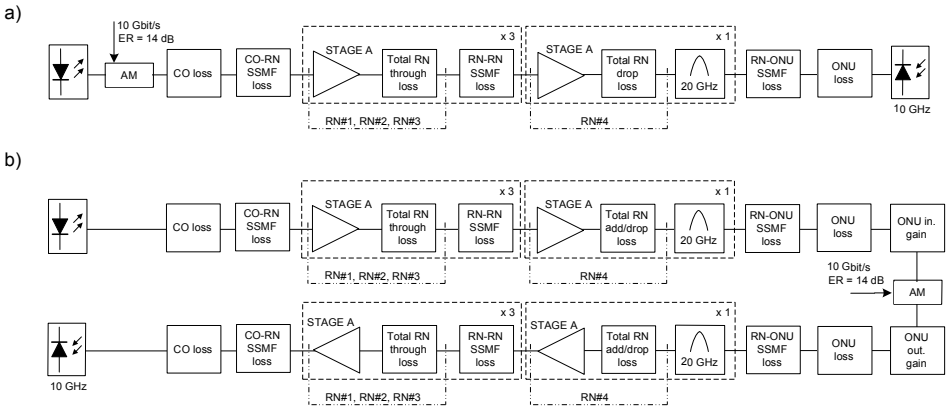

Figure 5.8: Simulation schemes used to estimate the influence of ASE noise on the performance of the BBPhotonics access network a) downstream and b) upstream link.

amplifiers with an ideal amplitude modulator in between. It is important to say that the ASE noise added to the CW input signal while passing the SOA towards the amplitude modulator is also modulated, whereas the ASE noise added to the output signal from the amplitude modulator remains unmodulated. The loss and gain parameters are set according to the power budget given in Chapter 2 (the longest lightpath, uniform capacity distribution). As it was discussed in Chapter 2, regardless which capacity distribution case is applied four out of eight in-line downstream (upstream) amplifiers provide enough gain. The remaining amplifiers are used in case of traffic rerouting.

As it can be noticed in fig. 5.9, the increase of the ASE noise accumulated in the downstream data signal should not cause PP higher than 0.5 dB as long as the

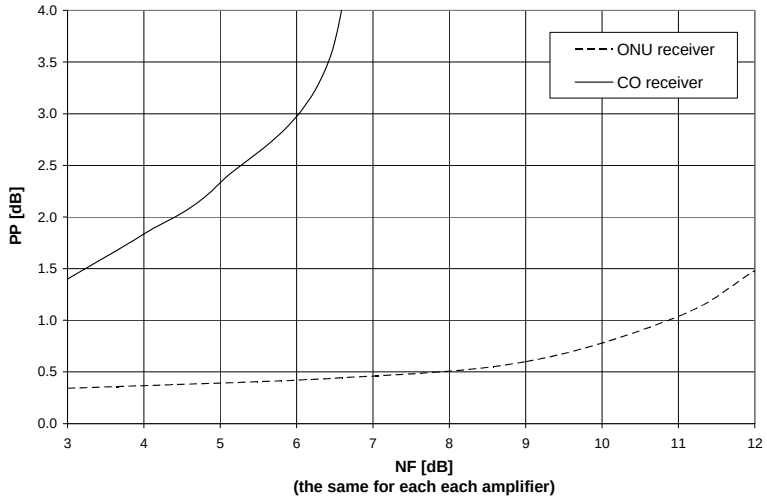

Figure 5.9: Simulation results of the accumulated ASE noise-induced power penalty in the BBPhotonics access network with a cascade of 4 in-field amplifiers and an amplified reflective ONU.

NF of each of 4 amplifiers is kept below 8 dB (dash line). The same amount of ASE power is accumulated in the CW signal used for upstream data modulation. During this modulation more ASE is added as the signal passes twice an SOA in the ONU. Next, the signal propagates through a cascade of 4 upstream amplifiers. Due to a large total number of amplifiers experienced by a wavelength channel propagating from CO to ONU and back to CO and the resulting significant accumulation of ASE noise, the upstream receiver at the CO receives a severely amplitude-distorted signal. As a consequence, power penalty arises at the CO receiver, e. g. 3.0 dB power penalty in case of NF equal to 6 dB (solid line, fig. 5.9).

5.5 Other sources of power penalties

Below, the remaining factors causing PP are discussed.

5.5.1 Dispersion

Dispersion is an effect where different components of the transmitted signal travel at different velocities in the fiber [108]. As a result they arrive at different times at the receiver. A short pulse signal is spread over the transmission link which leads to intersymbol interference (ISI) and PP at the receiver. There are several kinds of dispersion: intermodal dispersion, polarization-mode dispersion (PMD) and chromatic dispersion (CD).

The intermodal dispersion occurs in a system where multimode transmission takes place and, therefore, is out of scope of this discussion.

The PMD is a consequence of difference between group velocities of different polarization states due to the elliptical nature of the fiber cross-section or stress-induced birefringence. In order to keep the PMD-induced PP below 1 dB the following formula needs to be fulfilled [31]:

$$BD_{PMD}\sqrt{L} < 0.14 \tag{5.12}$$

where B is the bit-rate, L is the complete fiber length and D_{PMD} is the PMD parameter with a typical value of 0.5 $\frac{ps}{\sqrt{km}}$. In case of a relatively short-range (30 km) access network even for high bit-rate signals (10 Gbit/s) this condition is well-satisfied ($BD_{PMD}\sqrt{L} = 0.027$).

CD arises because different frequency components of a pulse propagate with different group velocities in the fiber. One reason for chromatic dispersion is that the refractive index is frequency dependent (material dispersion). The second reason is the energy distribution of the signal which partly travels in the core of the fiber and partly in the cladding, which has a different refractive index (waveguide dispersion). In order to maintain the CD-induced PP below 1 dB the following condition is given [108]:

$$BD_{CD}L\Delta\lambda < 0.306 \tag{5.13}$$

where D_{CD} is the dispersion parameter (for C-band transmission over SSMF $D_{CD} = 16$ $\frac{ps}{nm \cdot km}$), and $\Delta\lambda$ is the optical source linewidth ($\Delta\lambda = 130$ kHz). Again, for an access network (30 km, 10 Gbit/s) this condition is well-satisfied ($BD_{CD}L\Delta\lambda = 0.051$). The expression for the chromatic dispersion-induced PP is given as follows:

$$PP_{CD} = -5\log[1 - (4BLD_{CD}\Delta\lambda)^2] \tag{5.14}$$

5.5.2 Frequency chirping in the transmitter

Frequency chirping in the transmitter is the result of direct modulation of a laser (and an RSOA as it is discussed in Chapter 6). The intensity modulation is coupled with the phase modulation in semiconductor material because of the change in refractive index due to carrier density change induced by varying bias current [109]. Because of the spectral shift, the power contained in the chirped portion of the pulse moves out of the bit time-slot when propagating in a dispersive media. PP caused by chirping is included in the PP induced by the chromatic dispersion, eq. 5.14, through $\Delta\lambda$ parameter.

5.5.3 Narrow effective passband

WDM systems tend to have a number of optical filters (e. g. multiplexers). If they are connected in a cascade the overall passband is much narrower than in case of a single filter. Depending on the filter spectral response, wavelength channel spacing

and chirping it may lead to substantial PP. Narrowing the bandpass may also affect the signal modulation spectrum in case of high bit-rate signals, e. g. 10 Gbit/s. It is impractical to describe such power penalty with a single formula. In such systems high wavelength stability and accuracy is required [108].

5.5.4 Nonlinearities

Nonlinear effects arise when high-power signals are transmitted over a fiber or are injected into some network components. Here, only a few different nonlinear effects potentially affecting the performance of the designed network are mentioned:

- fiber nonlinearities (depending on fiber length and effective core area)
  - scattering effects: stimulated Brillouin scattering (SBS) and stimulated Raman scattering (SRS)
  - effects related to power-dependent changes of refractive index: four-wave mixing (FWM), self-phase modulation (SPM) and cross-phase modulation (XPM)
- device nonlinearities: gain saturation and cross-gain modulation (XGM)

The intensity of light scattered in SBS and SRS grows exponentially once the incident power exceeds a specific threshold value [109]. SBS occurs only in the backward direction and the scattered light is shifted by about 10 GHz. The Brillouin gain bandwidth is very narrow (<100 MHz). SRS can occur in both directions and the scattered light is shifted by 13 THz. The Raman-gain bandwidth extends over 20 THz.

Phase modulation in the fiber is the consequence of intensity-dependent refractive index changes. The optical phase of a given wavelength channel changes in time exactly in the same fashion as optical signal power in case of SPM. In case of XPM the nonlinear phase shift of a certain wavelength channel depends on the intensity of a neighboring channel. Both effects lead to the broadening of an optical pulse (chirp) and results in higher dispersion sensitivity.

If the co-propagating wavelength channels happen to fall in a phase-match, additional optical carriers may arise due to annihilation of two photons and a birth of two new photons at a different frequency. This may introduce PP to the received signal if the products of FWM fall into the optical bandwidth of the desired signals. The FWM may be suppressed by proper wavelength spacing, low power transmission and proper dispersion management [109].

The last two effects are related to the performance characteristics of the optical amplifiers. If the optical signals injected to an amplifier have much different intensities, the one with higher power can saturate the amplifier and significantly influence the gain experienced by the channel with lower power. This happens for the co-propagating and counter-propagating signals in the SOAs. As a result the extinction ratio and Q-factor of the weaker signal is strongly suppressed which

leads to PP. The effect can be reduced if optical amplifiers with high output saturation power are applied or, for instance, power equalizers are used at the input of the amplifiers.

In general, nonlinear effects can be minimized when lower power levels are transmitted and shorter fiber lengths are utilized. Ignoring dispersion issues, utilization of large effective area fibers in the access systems may also improve as they allow for higher input power [108]. Since in the designed access network the launched power per channel does not exceed 0 dBm and the utilized fiber lengths are short, the nonlinear fiber effects are assumed not to introduce any significant PP at the receiver side.

5.5.5 PDL, component aging and power margin

The polarization dependence of the transmission properties of optical components has many sources. Some of the most common effects are birefringence, fiber bending and angled optical interfaces [110]. Since the polarization state may vary in time the PDL also changes in time resulting in different performance of transmission link components (e. g. modulators). Usually a 3 dB penalty is accounted for PDL. For component aging-related issues (e. g. wavelength instability in the

Table 5.1: Estimated power penalties in the BBPhotonics network.

	Impairment	DS [dB]	US [dB]	Note
(1)	Intrach. crosstalk	0.0	1.5	RBS and BBS, Sec. 5.2
(2)	Interch. crosstalk	0.3	0.3	broad bandw. in OADM, Ch. 4
(3)	ASE noise accum.	1.0	3.5	more ampl. in US, Sec. 5.4
(4)	Disp. (incl. OADM)	0.0	0.0	short fibers, Sec. 5.5.1, Ch. 4
(5)	Nonlinearities	0.0	0.0	short fibers, low powers, Sec. 5.5.4
(6)	Extinction ratio	0.5	2.0	limited ER at ONU, Ch. 3
(7)	PDL	3.0	3.0	OADM, ONU, Ch. 3 and 4
	Total PP due to impairments only [(1)+(2)+...+(7)]	**4.8**	**10.3**	
(8)	Component aging	3.0	3.0	
(9)	Margin	3.0	3.0	
	Total PP [(1)+(2)+...+(9)]	**10.8**	**16.3**	

transmitter) another 3 dB is assigned. Furthermore, 3 dB of power margin is saved, which may be used for maintenance activities in the transmission link over its lifetime (e. g. extra splicings) [108].

5.6 Power penalties in the BBPhotonics network

In table 5.1 PPs assigned in the BBPhotonics access network design are given for the longest lightpath as explained in Chapter 2. They are extracted from [108] or based on the calculations in this Chapter and the network description in Chapter 2 as well as component descriptions in Chapter 3 and Chapter 4.

After analyzing the power budget of the system, the overall rise-time of the system should be analyzed in order to ensure the data-rate requirement. The system rise-time is a square-root of the sum of the squares of the rise-times of individual components. These components are [111] the rise-time of the transmitter and the receiver as well as the dispersion-related delay. In addition, in BBPhotonics access network one need to account for the impact of the SOAs performance and bandwidth narrowing due to cascaded optical filters. The calculation of the system rise-time is rather a complex task and depends on the frequency characteristics of the pulses generated on the relevant particular linecards (e. g. 1GbE and 10GbE).

Chapter 6

Interferometric crosstalk in the access network with an RSOA

In this Chapter interferometric crosstalk-induced power penalties (PP) and methods to suppress this phenomenon in the RSOA-based access network are investigated. The problem is introduced in Section 6.1. Section 6.2 contains mathematical considerations of the crosstalk scenario and solutions towards limitation of the interferometric noise and Section 6.3 provides appropriate measurement results proving the described methods. A comparison of the methods and discussion on their advantages and disadvantages followed by recommendations is given in Section 6.4.

The work included in this Chapter has been published in [112–115].

6.1 Crosstalk scenario

A wavelength-agile ONU equipped with an RSOA is highly sensitive to backscattered or reflected power coming from e. g. a fiber splice, connector or a neighboring device with low RL. This power interferes with the original CW signal seeding the RSOA and power instabilities arise. This so called in-band (interferometric) crosstalk causes the degradation of SNR and PPs in the system's BER performance [116]. Since coherent and incoherent optical sources can be used in a WDM-PON system, e. g. distributed feedback (DFB) lasers or a spectrally sliced broadband source [30], the phase-induced amplitude variations and resultant PPs at the receiver are larger if the interference takes place within the coherence length of the source (coherent crosstalk) and are smaller if it happens beyond this length or an incoherent source is applied (incoherent crosstalk). However, an incoherent source

causes higher sensitivity to dispersion. Moreover, the incoherent crosstalk can still cause high PPs as its contributions may remain coherent with each other [117].

An access network with an RSOA has already been considered in terms of in-band crosstalk in e. g. [118–120]. However, in those studies, due to the partly reflected or backscattered signal simultaneously propagating in the direction of remotely fed RSOA and the receiver, the investigated crosstalk was a sum of two phenomena, namely, the interference of DS signal with return US and US with return DS signal. In [121] the influence of back-reflected signal on the performance of a saturated RSOA has been experimentally checked for the link architecture involving DS data signal remodulated with US data. There, it has been also proved that the RSOA is very sensitive to backreflections. However, besides different modulation formats and proper RSOA gain adjustment, none of the known publications provided a practical solution for as effective in-band crosstalk mitigation as the techniques described in the following of this Chapter.

There are some solutions to decrease the in-band crosstalk, such as additional phase modulation at the laser, polarization scrambling, low coherence source deployment [122], and time diversity between the desired and the interfering signals [123]. A novel powerful technique based on phase modulation by dithering of the RSOA bias current was proposed to fight with coherent [112, 114] and incoherent [113] crosstalk.

RSOA bias dithering is a novel method, which utilizes the amplitude-to-phase coupling in the active material of the RSOA [124], and phase modulation at the laser is a well-known method, which has been widely published [125–129].

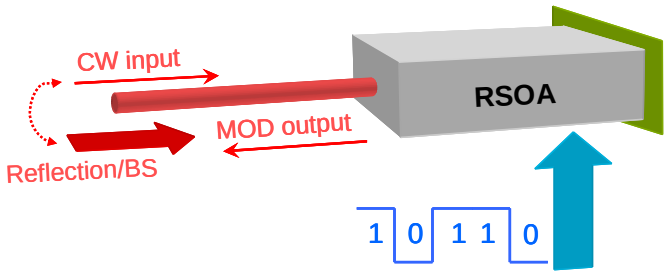

Figure 6.1: RSOA-based drop link with crosstalk.

The optical link investigated here contains an RSOA and a single drop fiber which provides DS CW transmission and US data transmission, fig. 6.1. The CW signal is amplified and intensity modulated (OOK) in the RSOA with 1.25 Gbit/s NRZ PRBS. It is reflected at the end facet of the RSOA and sent back to the CO with US data. The problem may arise in such a drop link, if e. g. the WDM RN to which it is connected has low RL. It may also happen due to the RBS power accumulated over the complete CO-ONU link (e. g. 20-30 km). Since reflected/backscattered signal (interferer) and CW travel along the same fiber in the

same direction and have the same nominal wavelength, they cannot be optically filtered and they interfere with each other. The phase relation between interfering beams remains stable within the coherence length of the source in case of a reflected interferer, and for an RBS-induced interferer such relation has a random nature. Therefore, the former case causes coherent crosstalk and the latter one incoherent crosstalk.

6.2 Analytical models

In order to reduce the interferometric crosstalk we apply methods which are based on spectral broadening. Optical power of a spectrally broadened signal is spread over a larger optical bandwidth, which means that the coherence length (or coherence time) of the light is reduced. The relation of coherence length and spectral width is described by eq. 6.1.

$$L_c = \frac{c}{n}\frac{1}{\pi\Delta\lambda} \tag{6.1}$$

where c is the speed of light in vacuum, n is the refractive index and $\Delta\lambda$ is the spectral linewidth. The spectrum is broadened by phase modulation, which can be introduced by chirping in the RSOA, further denoted as RSOA bias dithering, or by phase modulation at the laser.

6.2.1 Coherent crosstalk and RSOA bias dithering

We investigate the conditions for RSOA bias dithering, which have to be satisfied in order to suppress the crosstalk caused by a reflected power feeding back into the RSOA.

The electric field at the output of the laser is given by eq. 6.2.

$$E(t) = \sqrt{P(t)}e^{j[\Omega_0 t+\varphi(t)]} \tag{6.2}$$

where $P(t)$ is the output laser power, Ω_0 is the optical carrier frequency and $\varphi(t)$ is the laser phase noise. The laser phase noise is much smaller than the phase changes induced by modulation and, therefore, it can be neglected. Therefore, if we assume an output power constant in time the above equation can be written as follows

$$E(t) = \sqrt{P_0}e^{j\Omega_0 t} \tag{6.3}$$

where P_0 is the constant laser output power as shown in fig. 6.2a.

Assuming negligible nonlinear interaction in the fiber, the field which propagates from the laser towards the RSOA at the output of the fiber is described by eq. 6.4.

$$E_{in}(t) = \sqrt{\Psi_0\Psi_1 P_0}e^{j\Omega_0 t} \tag{6.4}$$

where Ψ_0 indicates the fraction of the power remaining after the attenuation of the link between laser output and the point of reflection (including the attenuation at

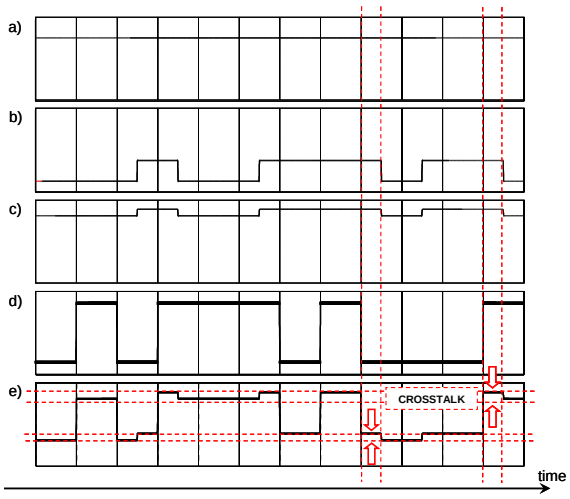

Figure 6.2: Mathematical model of crosstalk in an RSOA link: photocurrent (acc. to eq. 6.10) of (a) the CW input signal, (b) the interferer, (c) the total input signal, (d) the PRBS generator output current, (e) the photocurrent (acc. to eq. 6.10) of RSOA output signal.

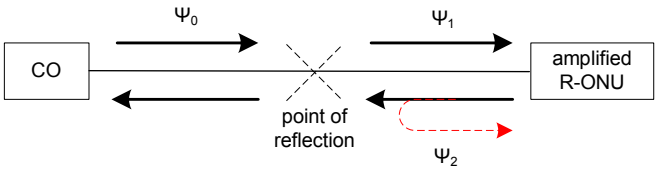

Figure 6.3: Loss parameters in the RSOA-based drop link with crosstalk.

the point of reflection) and Ψ_1 denotes fraction of the power remaining after the attenuation of the fiber on the distance between the point of reflection and the RSOA as indicated in fig. 6.3.

The light is amplitude modulated in the RSOA. Due to the swing of the current, which induces the amplitude modulation, the carrier density changes accordingly. This causes the variations of the refractive index of the active material in the RSOA. Consequently, the phase of the light is also changed (modulated). As a result, the output field is described by the following equation:

$$E(t) = \sqrt{\Psi_0 \Psi_1 G(t) P_0} e^{j[\Omega_0 t + \phi_r(t)]} \tag{6.5}$$

where $G(t)$ is the modulated linear gain of the amplifier. $\phi_r(t)$ represents the changes in optical phase induced by amplitude-to-phase coupling in the RSOA (chirp).

Due to e. g. very low RL of a connector (point of reflection) part of the output signal returns to the RSOA. At the input of the RSOA such reflected beam is represented by eq. 6.6 and plotted in fig. 6.2b.

$$E_{feedback}(t) = \sqrt{\Psi_0\Psi_1\Psi_2 G(t) P_0} e^{j[\Omega_0(t)+\phi_r(t)]} \tag{6.6}$$

where Ψ_2 represents the fraction of the power remaining after the total RL, which includes fiber attenuation in the link from the RSOA to the point of reflection, RL at the point of reflection and the fiber attenuation on the distance from the point of reflection to the RSOA. The two signals represented by eq. 6.4 (delayed) and eq. 6.6 are coupled together at the RSOA input, eq. 6.7, and the complete input light is described by eq. 6.8, fig. 6.2c.

$$E_{total,in}(t) = E_{in}(t-\tau) + E_{feedback}(t) \tag{6.7}$$

$$E_{total,in}(t) = \sqrt{\Psi_0\Psi_1 P_0} e^{j\Omega_0(t-\tau)} + \sqrt{\Psi_0\Psi_1\Psi_2 G(t) P_0} e^{j[\Omega_0(t)+\phi_r(t)]} \tag{6.8}$$

where τ is the time difference (delay) between the unmodulated signal and the interferer. This equation is valid only when the polarization states of the signal and the interferer are aligned (worst-case).

Because the two signals have the same nominal wavelength and propagate in the same direction they will interfere. Subsequently, such disturbed signal is amplitude modulated by a PRBS signal (fig. 6.2d) and its phase is also changed due to the same phenomenon as before. The final output electric field is schematically shown in fig. 6.2e and it is described by eq. 6.9.

$$\begin{aligned} E_{out}(t) = &\sqrt{\Psi_0\Psi_1 G(t-\tau) P_0} e^{j[\Omega_0(t-\tau)+\phi_r(t-\tau)]} \\ &+\sqrt{\Psi_0\Psi_1\Psi_2 G(t) G(t-\tau) P_0} e^{j[\Omega_0(t)+\phi_r(t)+\phi_r(t-\tau)]} \end{aligned} \tag{6.9}$$

In general, the photocurrent generated at the photodetector after neglecting shot noise and thermal noise can be written as follows:

$$I = R[|E(t)|]^2 \tag{6.10}$$

where R is the photodetector responsivity given in A/W. The photocurrent generated after photodetection of the signal represented by eq. 6.9 is therefore given by eq. 6.11.

$$i_s(t) + i_n(t) = R[|E_{out}(t)|]^2 \tag{6.11}$$

The term $i_s(t)$ represents the amplitude-modulated desired signal, whereas the noise term $i_n(t)$ is the result of interferometric crosstalk indicated by arrows in fig. 6.2e. After the introduction of the right side of the eq. 6.9 into eq. 6.11 we obtain the expressions for the signal (assuming $\Psi_2 \ll \Psi_1$) and noise current.

$$i_s(t) = R\Psi_0\Psi_1 G(t-\tau) P_0 [1 + \Psi_2 G(t)] \cong \Psi_0\Psi_1 G(t-\tau) P_0 \tag{6.12}$$

$$i_n(t) = 2R\Psi_0\Psi_1 G(t-\tau) P_0 \sqrt{\Psi_2 G(t)} \cos[-\Omega_0\tau - \phi_r(t)] \tag{6.13}$$

A common figure of merit used for analysing the chirp performance is the alpha parameter (a. k. a. linewidth enhancement factor, LEF) given by the following equation, [130]:

$$\alpha_{eff} = -2\frac{\Delta\phi_r}{ln(\Delta G)} \tag{6.14}$$

We use here the effective α-factor, which is defined as the phase to gain changes coupling factor measured at the output of the RSOA. The phase deviation $\Delta\phi_r$ can be obtained from the eq. 6.14:

$$\Delta\phi_r = \frac{-\alpha_{eff}}{2} ln(\Delta G) \tag{6.15}$$

If the phase deviation $\Delta\phi_r$ caused by gain change ΔG is equal to or higher than π the term on the right side of eq. 6.13 ($i_n(t)$) fully oscillates around 0 [127].

$$|\Delta\phi_r| \geq \pi \tag{6.16}$$

After combining eq. 6.15 and eq. 6.16 we obtain the following:

$$|\frac{-\alpha_{eff}}{2} ln(\Delta G)| \geq \pi \tag{6.17}$$

If the term on the right side of the eq. 6.13 oscillates at a frequency which is out of the receiver bandwidth it is averaged out in the stopband by the low-pass filter of the receiver. That way the interferometric noise is mitigated by superposition of high frequency modulation [131]. To satisfy these two conditions we need to induce large enough amplitude-to-phase coupling at a frequency higher than the data rate, which can be achieved by applying an additional current (dither) to the RSOA with appropriate amplitude and frequency.

Fig. 6.4 shows the relation of the gain swing ΔG versus LEF based on eq. 6.17. The gain swing has to be higher for the materials with lower LEF in order to produce sufficient phase deviation. For the case of high values of LEF the phase is strongly modulated by the data current. However, in such situation the phase modulation is done at the frequency which is within the electrical bandwidth of the data signal and cannot be filtered out by the low-pass filter at the receiver. It may cause chromatic dispersion-induced PP.

For commercially available devices LEF varies from 2-3 to 4-8 for MQW- and bulk material-based RSOAs, respectively [109]. At the same time, the electrical bandwidth is lower for the RSOA with bulk material. Therefore, the required dithering amplitude has to be considered based on the type of RSOA material (value of LEF), its maximum electrical bandwidth, the bit-rate and the dithering frequency. In general, if the modulation bandwidth is low and LEF is high, the amplitude and the frequency of dithering signal should be lower than in the case of a device with a larger bandwidth and lower LEF.

The relevant measurement results are given in Section 6.3.1.

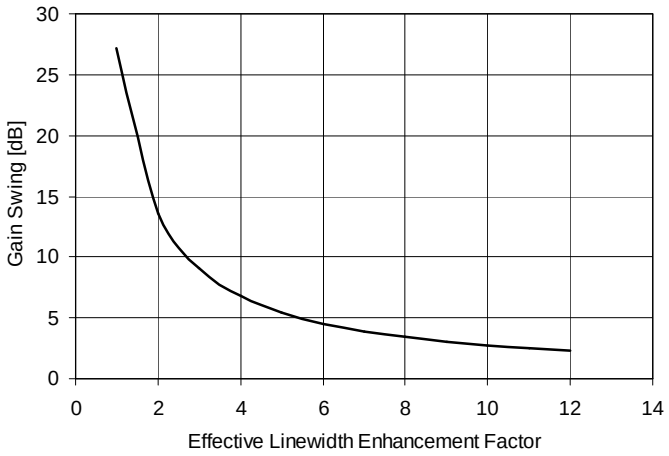

Figure 6.4: Gain swing required for π phase shift in function of linewidth enhancement factor.

6.2.2 Incoherent crosstalk and RSOA bias dithering

A single reflection in the link as described in the previous Section produces coherent crosstalk under the condition that the light beams interact within the coherence length. However, if the interferer arises as a result of multiple discrete reflections, like RBS, or when the beams interact outside the coherence length the relation between the crosstalk signal and the useful signal is incoherent. One can expect that the PP in such situation is smaller than when both beams are highly coherent.

In the coherent crosstalk the phase of the reflected beam is very important. It can happen that the interfering beams meet in phase and produce large amplitude deviation, thus, the phase shift required to mitigate the crosstalk is higher. On the other hand, it can also happen that the beams meet out of phase and no amplitude-to-phase coupling is needed, since there is no crosstalk-induced amplitude variation. In the case of incoherent crosstalk it is impossible to describe exactly the phase relation and the interference between the beams is completely random. Hence, for the mathematical model the worst case condition is taken, which means that the co-polarized beams (polarization mismatch will cause weaker influence of the interferer on the desired signal) meet in phase and interfere constructively. The same assumption was taken for the model with coherent crosstalk to find the largest phase shift needed. Therefore, the relation of the gain swing versus LEF (Section 6.2.1) remains valid for the case of incoherent crosstalk.

The appropriate measurements are provided in Section 6.3.2.

6.2.3 Coherent crosstalk and external phase modulation

Another method to introduce phase modulation is to apply an external phase modulator at the laser. Here, we mathematically define the conditions for such phase modulation, which have to be satisfied in order to suppress the crosstalk.

The electric field at the output of the laser is given by eq. 6.3. Next, this signal enters the phase modulator which is introduced here as an ideal device (no insertion loss). The output of the modulator is described by the following equation (after neglecting laser phase noise).

$$E(t) = \sqrt{P_0} e^{j[\Omega_0 t + \phi_p(t)]} \tag{6.18}$$

where ϕ_p represents the modulated phase of the optical carrier. If we apply the same procedure as in eq. 6.4-6.11 to the signal given by the above formula, we obtain an expression for the interferometric noise component of the photocurrent.

$$i_n(t) = 2R\Psi_0\Psi_1 G(t-\tau) P_0 \sqrt{\Psi_2 G(t)} f(t)$$

$$f(t) = \cos[-\Omega_0\tau + \phi_p(t-\tau) - \phi_p(t) - \phi_r(t)] \tag{6.19}$$

If a sine-shape signal is applied to modulate the phase at the source, the expression describing phase deviation at the phase modulator is given as follows:

$$\phi_p(t) = M \sin(2\pi f_p t) \tag{6.20}$$

where M is the modulation index and f_p is the frequency of the phase modulating signal. When the above is taken into account together with the assumption that the phase changes induced in the RSOA are negligible with respect to the external phase modulation, we can modify the eq. 6.19 to the following:

$$i_n(t) = 2R\Psi_0\Psi_1 G(t-\tau) P_0 \sqrt{\Psi_2 G(t)} f(t)$$

$$f(t) = \cos\{-\Omega_0\tau - 2M \sin(\pi f_p \tau) \cos[\pi f_p (2t-\tau)]\} \tag{6.21}$$

Applying the same condition as in eq. 6.16 to the phase deviation induced by the phase modulator gives the formula below.

$$|-2M \sin(\pi f_p \tau)| \geq \pi \tag{6.22}$$

The result after solving eq. 6.22 shows the relation of modulation index to the frequency of phase modulating signal, fig. 6.5 (RSOA LEF = 0). This curve shows the minimum phase modulation index to be applied in order to have phase deviation equal to or higher than π. The results show strong periodic dependence, and the interval between the peaks on the graph corresponds to the delay time between the interfering beams, eq. 6.23.

$$\Delta f = \frac{1}{\tau} \tag{6.23}$$

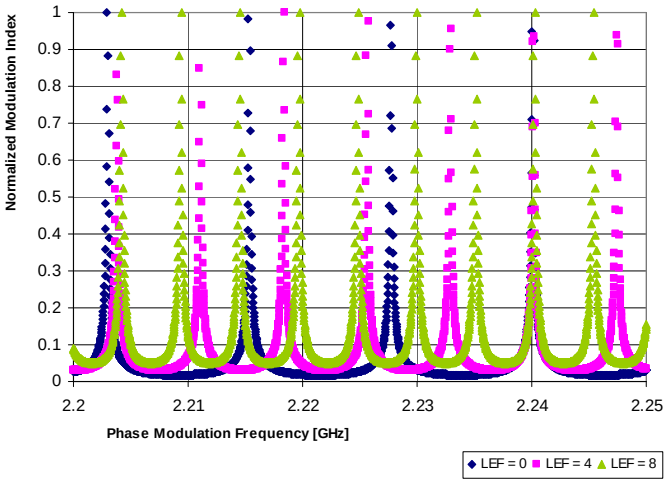

Figure 6.5: Required phase modulation index as a function of the frequency of phase modulation.

In eq. 6.21 amplitude-to-phase coupling in the RSOA was neglected, as there was no bias dithering applied. However, the data current itself which is applied to the RSOA causes some amplitude-to-phase coupling (LEF $\neq 0$). Putting this phenomenon back into consideration results in a modification of eq. 6.22 as follows:

$$| - 2M \sin(\pi f_p \tau) - \frac{\alpha_{eff}}{2} ln|\Delta G|| \geq \pi \tag{6.24}$$

The results for some example LEF values are given in fig. 6.5. The interval between the peaks changes with respect to the case when LEF is equal to 0 (no amplitude-to-phase coupling), which is due to the fact that the phase delay between the interfering beams is different for each case because of the phase shifting in the RSOA.

In practice the relation depicted in fig. 6.5 will be applicable only within the coherence length of the laser and it implies additional restriction for the phase modulation frequency with respect to the first condition given in eq. 6.16.

Beyond the coherence length this phase relation is unpredictable and the beams interfere randomly causing less interferometric noise than within the coherence length and, therefore, only condition given by eq. 6.16 remains applicable.

This theory has been verified experimentally in Section 6.3.3.

6.2.4 Incoherent crosstalk and external phase modulation

Here, the mathematical model is the same as for the coherent crosstalk with external modulation (Section 6.2.3). However, since the light coming back to the RSOA

is incoherent and the beams interfere randomly, the delay included in the model for coherent crosstalk cannot be defined with an exact value. Due to that, the periodic relation presented in fig. 6.5 is not applicable here and the exact quantitative requirement for phase modulation index M cannot be given.

The relevant measurement results are provided in Section 6.3.4.

6.3 Experimental results

The setup which is used for measurements is shown in fig. 6.6. A CW carrier is transmitted from the external cavity laser (linewidth < 15 MHz[1]) through the variable attenuator, the circulator, the polarization controller (polarization state adjusted for the highest output power) and the 3 dB coupler into the MQW-based RSOA. The 3 dB coupler enables power monitoring. It also enables the addition of reflected or backscattered light only in the direction of the RSOA.

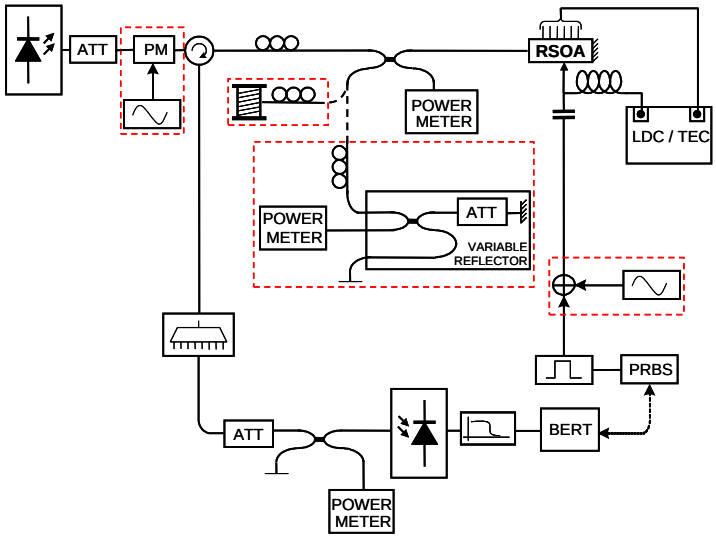

Figure 6.6: Experimental setup: ATT - variable attenuator, PM - phase modulator, LDC - laser diode controller, TEC - temperature controller, PRBS - pseudo-random bit sequence, BERT - bit error-rate tester.

The RSOA is temperature controlled and it is biased with around 27 mA. The transparency current is 9 mA and the RF current swing used for data modulation is set to 20 mA ($2^{31} - 1$ PRBS at 1.25 Gbit/s).

The output power is divided in a 3 dB coupler and part of it goes through the polarization controller either into the variable reflector, where the RL can be

[1]Coherence length > 15 m, according to eq. 6.1 for $c = 299792458$ m/s and $n = 1.46$.

adjusted, or into the 25 km SSMF to induce the RBS. The reflected/backscattered power passes again through the 3 dB coupler into the same fiber where the original CW light is transmitted towards the RSOA. The CW light and the reflected light interfere introducing interferometric noise. This interference is coherent when variable reflector is used and incoherent when the SSMF is used instead. The final modulated signal passes the circulator where it is directed to the AWG to filter out the ASE noise (0.8 nm bandwidth). Next, in order to measure the BER versus ROP, the ROP is adjusted with a variable attenuator and monitored by a power meter attached to one of the outputs of the 3 dB coupler. The other output sends light into a 1.25 Gbit/s receiver with limiting amplifier followed by a BER measurement testset. The eye diagrams are recorded with an O-E lightwave converter with 800 MHz low-pass filter which clearly shows the influence of coherent crosstalk with and without additional modulation.

The utilization of a circulator prevents the modulated output signal of the RSOA to be influenced by the reflected or backscattered power of the CW seed.

The RSOA input power is kept at -20 dBm and the linear fiber-to-fiber gain of the RSOA is 20 dB [132]. The 1.25 Gbit/s receiver sensitivity is -22 dBm (BER = 10^{-9}). However, in the following experiments the reference curve represents the results of the measurement taken in the setup as given in fig. 6.6 without any feedback, RSOA bias dithering or external phase modulation. The reference signal is modulated in the RSOA and, therefore, the receiver sensitivity is decreased to -21.5 dBm at BER = 10^{-9} (around -20.5 dBm at BER = 10^{-12}). The direct reason for this 1.5 dB reduction is the performance of the RSOA as a modulator (extinction ratio is < 8 dB, residual ASE noise after 0.8 nm filter)[2].

As described in Section 6.2 two methods are used to mitigate the interferometric crosstalk, namely RSOA bias dithering and external phase modulation at the CW laser. The first technique requires an extra RF signal generator used to dither the bias of the RSOA. This signal is combined with the RF signal used for data modulation and goes through the bias tee into the RSOA. For the second technique an extra phase modulator at the output of the laser is used. In this case the output of the dithering signal generator is connected to the phase modulator.

In both methods the frequency (around 2.5 GHz) of the phase modulating signal is situated out of the receiver bandwidth so the low-pass filter at the receiver suppresses the superposed interferometric noise products at higher frequencies.

6.3.1 Coherent crosstalk and RSOA bias dithering

First, we induce coherent crosstalk by applying a variable reflector and bias dithering by adding a sine-wave signal to the bias of the RSOA, fig. 6.6. The RL is adjusted in the variable reflector, and the total RL which is used to calculate signal-to-crosstalk ratio (SCR) includes 3 dB coupler and loss of all connectors.

The dithering frequency (2.5 GHz) is equal to twice of the bit-rate. This yields

[2]This device has been intensively examined in Chapter 3.

a shift of the crosstalk products sufficiently far above the baseband data spectrum. It allows the suppression of the interferometric crosstalk in the stopband of the low-pass filter in the receiver. The required amplitude of the dithering is high due to the low value of the linewidth enhancement factor (around 2-3 for the applied MQW-RSOA).

The spectrum of the output signal of the RSOA, fig. 6.7, is broader when dithering is applied on the bias. According to eq. 6.1 the coherence length of such light becomes shorter and, thus, the phase relation between the interfering beams is weaker. The receiver sensitivity penalty caused by RSOA bias dithering (measured in the absence of interferometric crosstalk) is lower than 0.2 dB at BER = 10^{-9} and, therefore, it is neglected further in this work.

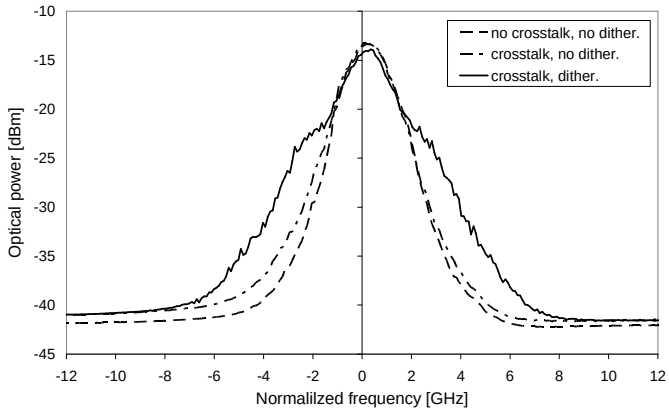

Figure 6.7: RSOA output spectra.

Fig. 6.8 shows the degradation of the eye diagram for the SCR equal to 11 dB. The standard deviation of the "1"-level is significantly reduced after applying the dithering on the RSOA bias. At the same time the eye-opening improves, although the signal amplitude decreases. This, in general, improves the signal-to-noise ratio and thus lowers the BER.

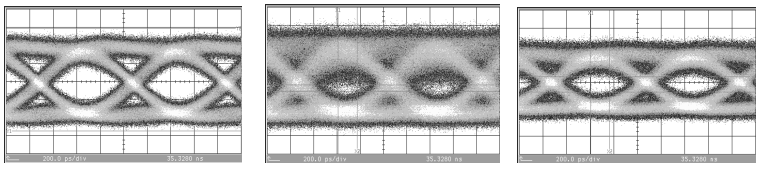

Figure 6.8: Example eye diagrams for $SCR = 11$ dB.

PP at BER equal to 10^{-9} is measured for different values of SCR, fig. 6.9. It

can be seen that with this technique the PP is remarkably reduced even for very low values of SCR (6 dB improvement for SCR equal to 18.5 dB). The error floor is eliminated which shows that even better BER values can be achieved.

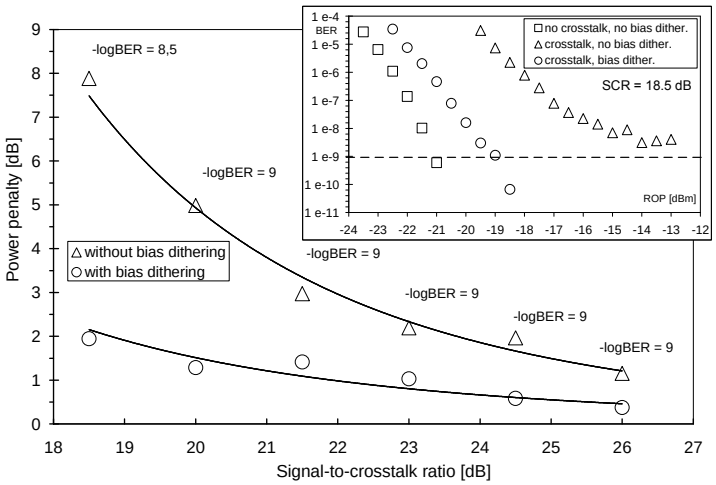

Figure 6.9: Coherent crosstalk-induced PPs with and without RSOA bias dithering.

6.3.2 Incoherent crosstalk and RSOA bias dithering

The incoherent crosstalk is a result of interference between the CW beam and the RBS power accumulated over 25 km SSMF. In our setup it results in a SCR equal to 18.5 dB and it introduces around 5 dB PP and an error floor (at BER= $3 \cdot 10^{-9}$), fig. 6.10.

The spectrum of the reference signal at the output of the RSOA, where no dithering is applied and no RBS is present, is shown in fig. 6.11 together with the spectrum of the RBS-distorted signal. As it can be seen besides the RBS there is also Brillouin backscattering. However, the latter has much lower power than the former and, thus, it does not influence the useful signal. After applying the bias dithering at the RSOA the spectrum of the output signal broadens, fig. 6.11, and the PP is reduced with around 3 dB.

6.3.3 Coherent crosstalk and external phase modulation

The second method, spectral broadening at the CW source, is realized by applying external phase modulator at a CW laser which can be shared among number of users in a PON. It enables much larger linewidth enhancement than the RSOA bias dithering. The same modulation frequency (2.5 GHz) is applied as in the previous experiment. The difference in the experimental setup with respect to the setup

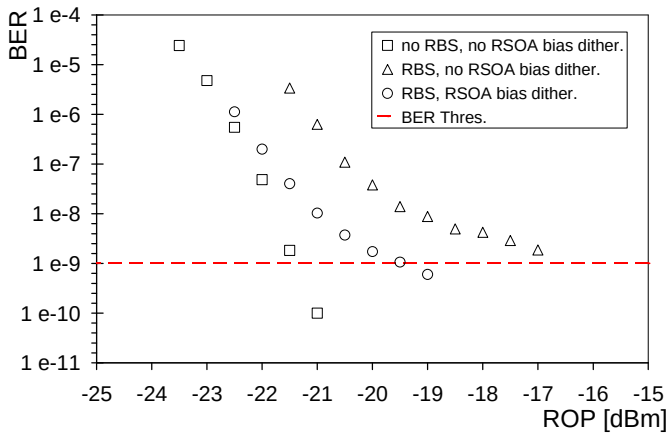

Figure 6.10: BER results with and without RSOA bias dithering in case of incoherent crosstalk.

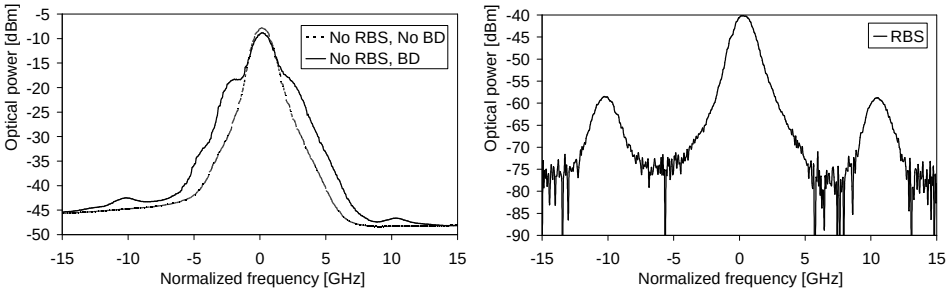

Figure 6.11: Optical spectrum of the original CW, backscattered signal and spectrally broadened signal in case of RSOA bias dithering (BD).

for RSOA bias dithering is that instead of adding the phase modulation signal to the bias of the RSOA it is provided to the phase modulator inserted between the attenuator and the circulator, fig. 6.6. Therefore, in this setup additional insertion loss introduced by the phase modulator has to be taken into account in the power budget of the link. This power loss is compensated by increasing the laser output power.

The phase shift in the phase modulator depends on the RF peak-to-peak voltage applied to the modulator. In the experiment we applied around 0.5 V, 2.5 V and 4.5 V which corresponds to around $\frac{\pi}{4}$, $\frac{2\pi}{4}$ and $\frac{3\pi}{4}$ phase shift, respectively, fig. 6.12. For 2-4 V driving voltage up to 7 dB improvement in PP is achieved, fig. 6.13.

In order to verify the relation between the phase modulation index and the modulator frequency as depicted in fig. 6.5 and prove the applicability of the

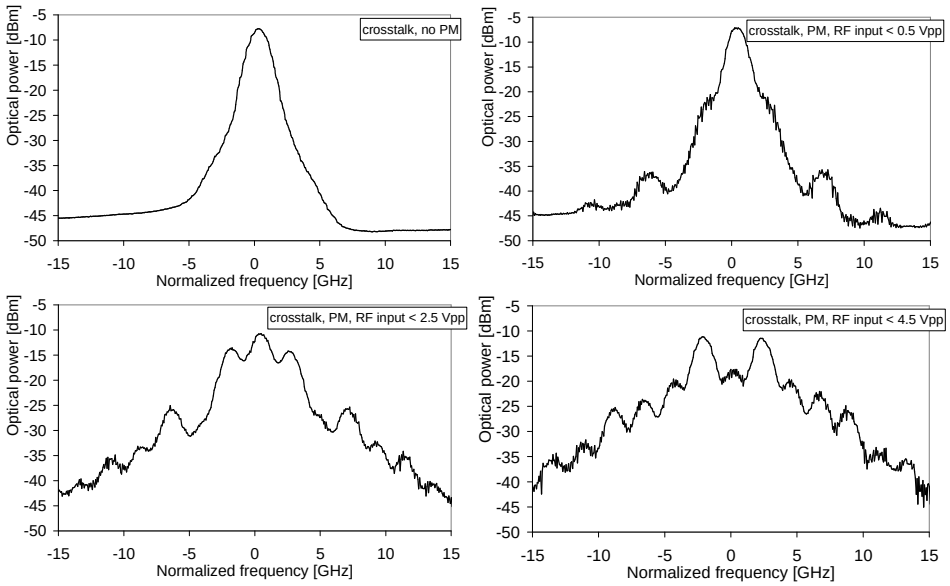

Figure 6.12: Optical spectrum of the signals broadened by external phase modulation in case of coherent crosstalk.

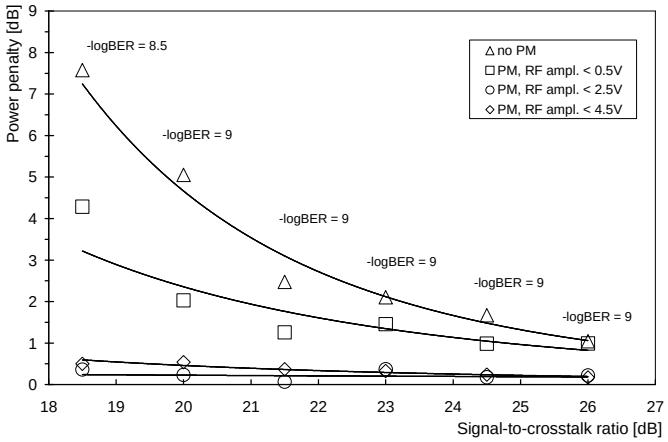

Figure 6.13: Coherent crosstalk-induced PP with and without external phase modulation.

condition given in eq. 6.22 an additional measurement is performed. The SNR of the received signal is measured at a constant SCR and constant phase modulation index for two cases: with and without 2.3 m of extra fiber between RSOA and the

point of reflection, which changes the phase delay between the interfering signals, fig. 6.14.

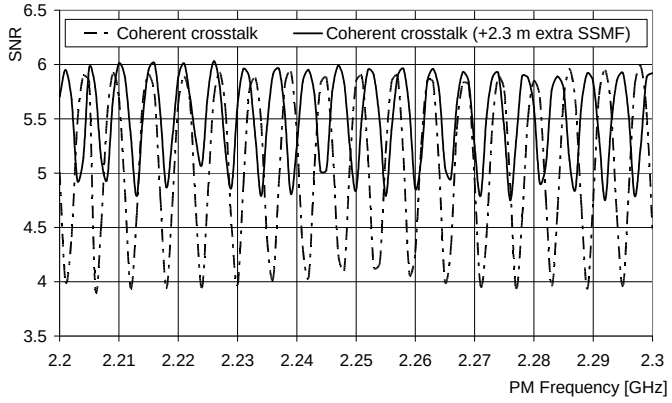

Figure 6.14: SNR of the received signal in function of phase modulation frequency.

The minimum SNR when no extra fiber is applied is lower than the minimum SNR for the other case. This is because of two reasons: first, better SCR is achieved in the latter case, since the RL is around 1 dB higher (mainly due to additional connectors) and, second, the phase relation is different. Phase difference can be lower and the CW light is slightly less coherent after a longer distance which means that the phase-induced power variations are smaller.

Both results in fig. 6.14 show periodic behavior, and the period (or frequency interval) is different in each case. This agrees with the mathematical model, which showed that the required amplitude of the RF signal provided to the external phase modulator is related to its frequency, eq. 6.22. There, the calculation showed that for some specific frequencies (separated by an interval related to the optical phase delay) a higher RF amplitude is required, fig. 6.5.

The frequency interval for the case without extra fiber is 5.9 MHz, which gives the delay time (τ) of around 169.5 ns. The refractive index of the applied fiber (n) is equal to 1.474. Taking these values into account the total distance ($2d$), where the reflected beam experiences the delay with respect to the CW input beam, can be calculated according to the following equation:

$$2d = \tau \frac{c}{n} \tag{6.25}$$

where $c = 299792458$ m/s is the speed of light in vacuum and d is the length of the fiber. After putting the values into the equation one obtains the fiber length equal to 17.24 m, which with respect to the roughly measured fiber (17.50 m) gives a reasonable result.

In the case with the longer fiber the frequency interval in fig. 6.14 is 5.1 MHz, which gives the optical delay time of 196.1 ns and the fiber length of 19.94 m

(roughly measured value is 19.80 m).

The difference between the calculated values (for a shorter and a longer fiber) is 2.70 m, which corresponds to value of 2.30 m of the extra fiber. This small discrepancy is due to the inaccuracy in estimating the delay based on the fig. 6.14. However, this is enough to deduce that for some frequencies of phase modulation a higher phase modulation index is required and that if the optical delay between the interfering beam changes (due to e. g. optical routing) either amplitude or frequency of phase modulation has to be adjusted.

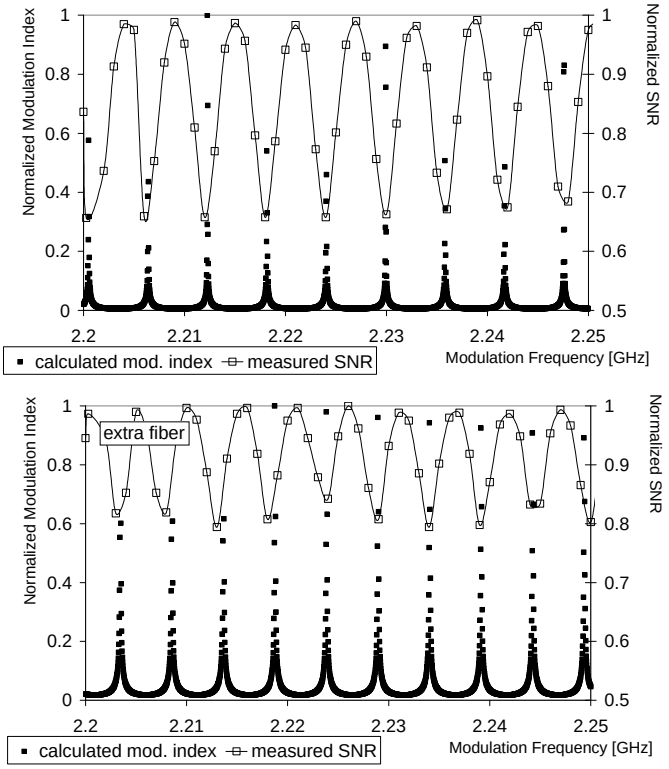

Figure 6.15: Matching the mathematical model to the measurement results.

The dips in fig. 6.14 correspond to the peaks in fig. 6.5 after matching the mathematical model. The matching was achieved for the length of 17.28 m (shorter fiber, top graph in fig. 6.15) and 19.94 m (longer fiber, bottom graph in fig. 6.15) which respectively gives 0.22 m and 0.14 m difference from the values derived from fig. 6.14. The difference is caused by the fact that in the calculation the phase changes in the RSOA are neglected due to the unknown value of LEF.

6.3.4 Incoherent crosstalk and external phase modulation

A similar situation is under consideration here as in Section 6.3.2. In this case the interferer originates from the 25 km long SSMF, where the RBS accumulates. To combat the destructive influence on the useful signal external phase modulation at the laser is applied as in Section 6.3.3. The spectrum of the backscattered signal changes for different phase modulation indexes, fig. 6.16.

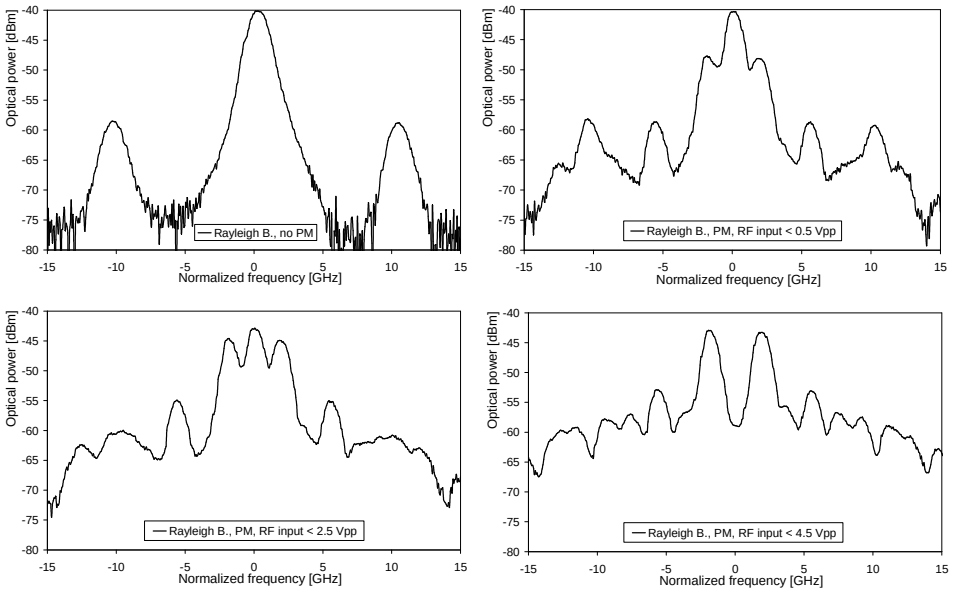

Figure 6.16: Optical spectrum of the signals broadened by external phase modulation in case of incoherent crosstalk.

The BER testing is performed for a single value of SCR equal to 18.5 dB. The phase modulation frequency is around 2.5 GHz and the bit-rate is 1.25 Gbit/s. The results in fig. 6.17 show that external phase modulation can effectively mitigate the incoherent crosstalk and reduce the PP from around 5 dB down to 0.5 dB.

The SNR of the received signal is independent from phase modulation frequency, fig. 6.18, which is in agreement with the predictions in Section 6.2.4.

6.4 Discussion

RSOA bias dithering and external phase modulation at the CW laser in the CO, show great potential in interferometric crosstalk mitigation by spectral linewidth broadening. They are compared in fig. 6.19 for example value of SCR equal to 18.5 dB (coherent crosstalk).

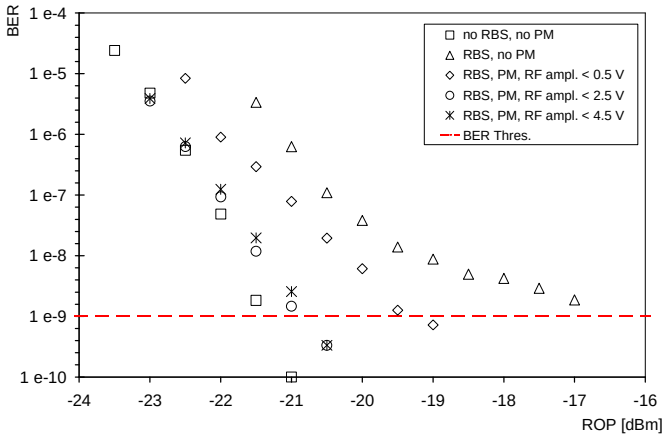

Figure 6.17: BER results with and without external phase modulation in case of incoherent crosstalk.

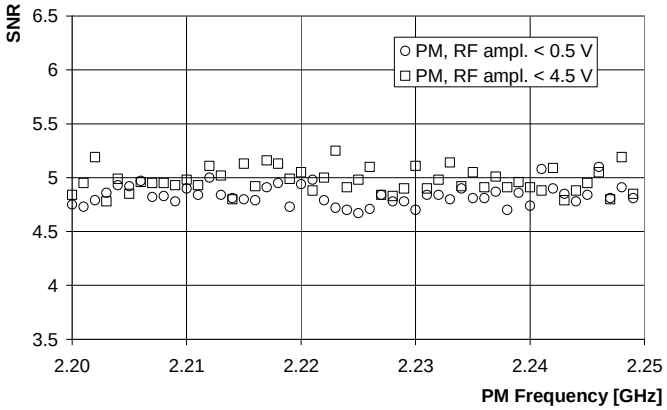

Figure 6.18: SNR of the received signal in function of phase modulation frequency.

A common disadvantage for both methods is that by occupying a larger optical bandwidth the adjacent channels are a subject to interchannel crosstalk in a WDM system. A further drawback is the increased sensitivity to dispersion. This is especially critical for large phase-modulated signals, which experience phase-to-amplitude conversion while propagating in dispersive media. Thus, the adjustment of phase modulation parameters has to be done in a deliberate manner taking into account channel spacing, fiber length and dispersion properties.

Coherent and incoherent types of crosstalk can be reduced by any of the mentioned techniques. The phase modulator is more efficient in spectral broadening than bias dithering in terms of required voltage. In the discussed system applying

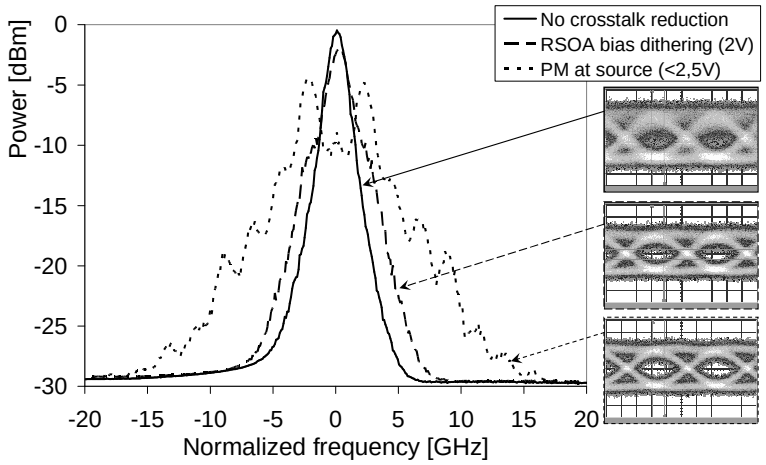

Figure 6.19: Comparison of the two techniques in terms of spectral broadening and eye diagram improvement for coherent crosstalk.

2 V of dithering amplitude to the RSOA does not bring as good results as around 2 V amplitude of driving voltage applied to the phase modulator. The difference between methods in terms of PP reduction is a 1.0 dB at 18.5 dB SCR for coherent crosstalk, when comparing fig. 6.9 and fig. 6.13, and 1.5 dB at the same SCR for incoherent crosstalk, when comparing fig. 6.10 and fig. 6.17. However, two kinds of penalty have to be paid when phase modulation is applied at the laser. The first is the requirement for extra hardware (a phase modulator, RF signal generator) or the deployment of directly modulated laser at a frequency higher than the bit rate, and the second is the decrease in the power budget of the optical link if a phase modulator is applied. The latter one may reduce split ratio in the passive optical network or require additional optical amplifier in the CO.

From the point of view of WDM-PON architecture external phase modulation at a source side is a cost-efficient solution, since a single phase modulator with a local oscillator can be used after a WDM multiplexer to provide the spectral broadening to all channels. It has been shown here that in case of coherent crosstalk due to the dependence of modulation index on the frequency of phase modulation this technique is not flexible (fig. 6.14). This is because of the possible changes in optical delay between the interfering beams (due to e. g. optical switching), which after each such change forces the readjustment of phase modulation frequency. Therefore, for the real network situation where the distances between CO and ONU may differ on a case by case basis, RSOA bias dithering is more advantageous but possibly more costly due to ONU complexity. For this method there are no extra restrictions for phase modulation frequency apart from the requirement to set it out of the receiver bandwidth and within (or close to) the electrical bandwidth of

the RSOA. The dithering amplitude boundaries are set by the maximum RSOA RF amplitude value, the electrical bandwidth of the RSOA (the dithering frequency has to be increased if it is out of 3-dB bandwidth of the RSOA) and the value of LEF which is depicted in 6.4.

By improving the tolerance to higher return power levels both methods can extend the reach of the optical link. Nevertheless, bias dithering seems to have some basic advantages over phase modulation at a source. It is an easy-to-implement sufficiently effective technique to mitigate interferometric crosstalk.

As a conclusion it is recommended that RSOA bias dithering technique is applied in the links where a danger of coherent crosstalk is high, e. g. short links between the RSOA and the adjacent network element. In case of RBS or any other incoherent-type of crosstalk, phase modulation at the laser is recommended because of the capability of large phase modulation and possibility to share the additional hardware at the CO among all PON subscribers.

Chapter 7

Reconfigurable WDM/TDM access network - experiments

In this Chapter, which is based on [50, 133–137], the transmission experiments of the BBPhotonics access network are presented. A successful transmission of two 1.25 Gbit/s wavelength channels over the 26 km SSMF carrying data to and from the user proves the feasibility of the basic concept of the designed solution. As a step further four wavelength channels of 10 Gbit/s each are transmitted over 27 km network link in an upgraded testbed with a different architecture of ONU. In each case DS and US signals were received error-free and all power penalties were identified. A full-scale 10 Gbit/s network was tested using VPI [89].

The Chapter is organized as follows. In Sections 7.1 and 7.2 the architecture of the ONU operating at 1.25 Gbit/s per wavelength channel and 10 Gbit/s per wavelength channel are recalled from Chapter 2, respectively, which sketches the basic difference between the experimental systems. In Sections 7.1.1 and 7.2.1 the corresponding measurement setups used in the 1.25 Gbit/s and 10 Gbit/s transmission experiments are explained in detail. Sections 7.1.2 and 7.2.2 contain a discussion on the obtained experimental results. Simulations of the full-scale network with 10 Gbit/s per wavelength channel are discussed in Section 7.3 including the simulation model in Section 7.3.1 and the results in Section 7.3.2. The Chapter is summarized in Section 7.4.

7.1 1.25 Gbit/s transmission

The features of the BBPhotonics access network together with different solutions for ONU have been described in the Chapter 2 of this work. The network testbed examined in this Section provides 1.25 Gbit/s amplitude-modulated signals for DS and US communication. For this purpose, colorless operation of a reflective ONU is achieved by utilization of the MQW-RSOA, earlier discussed in Chapter 3, fig. 7.1.

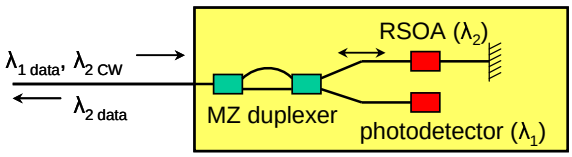

Figure 7.1: Schematic of the RSOA-based ONU for 1.25 Gbit/s network.

7.1.1 Testbed structure

The testbed contains a transmission link from CO via RN to ONU and backwards over a single SSMF as shown in fig. 7.2.

The CO consists of two lasers generating optical carriers for 1.25 Gbit/s DS data (λ) and DS CW ($\lambda + FSR_{OADM}$) transmission. Optionally, (not included in fig. 7.2) the channels are phase-modulated in the CO, which will be discussed later. The receiver part of the CO consists of an AWG, an attenuator for BER versus ROP measurement, power tap to measure ROP and a commercial 1.25 Gbit/s receiver.

The RN is composed with the OADM providing 4 add/drop ports (0.15 nm 3-dB bandwidth) and it is driven by a personal computer (PC) by which the micro-ring resonators are tuned. Due to the fact that this OADM is a prototype device some parameters do not match the desired values. There is an FSR_{OADM} mismatch of around 30 GHz, which allows only one channel from the wavelength pair to be set to an ITU-T standard wavelength (US) and as a result only filters applied to that channel are fixed. The OADM reveals substantial IL of around 15 dB and low RL of 17 dB. The last parameter significantly limits the performance of the system due to low SCR at the receivers. To block the reflected power two identical OADMs were applied together with two circulators to provide adding and dropping operations separately. To compensate for the excess loss in the RN SOAs are applied.

The ONU consists of a splitter, a tunable optical bandpass filter, an attenuator, a power tap, a commercial 1.25 Gbit/s receiver, a fixed bandpass filter and an MQW-RSOA [132].

The power budget presented in table 7.1 leaves around 1.8 dB and 1.3 dB margin for DS and US direction, respectively. The applied total fiber span of 26 km comes close to the distance at which accumulated RBS power is the highest and severely influences the SNR in the bidirectional systems (typically 25-30 km). However, there are cost-effective solutions to mitigate the backreflection by optical signal linewidth enhancement as discussed in Chapter 6 of this dissertation. Here, we use external phase modulation, which enhances the spectral width of the channel and, therefore, reduces coherence length. This leads to lower interferometric noise in the receiver. The second method proposed in Chapter 6 employing RSOA

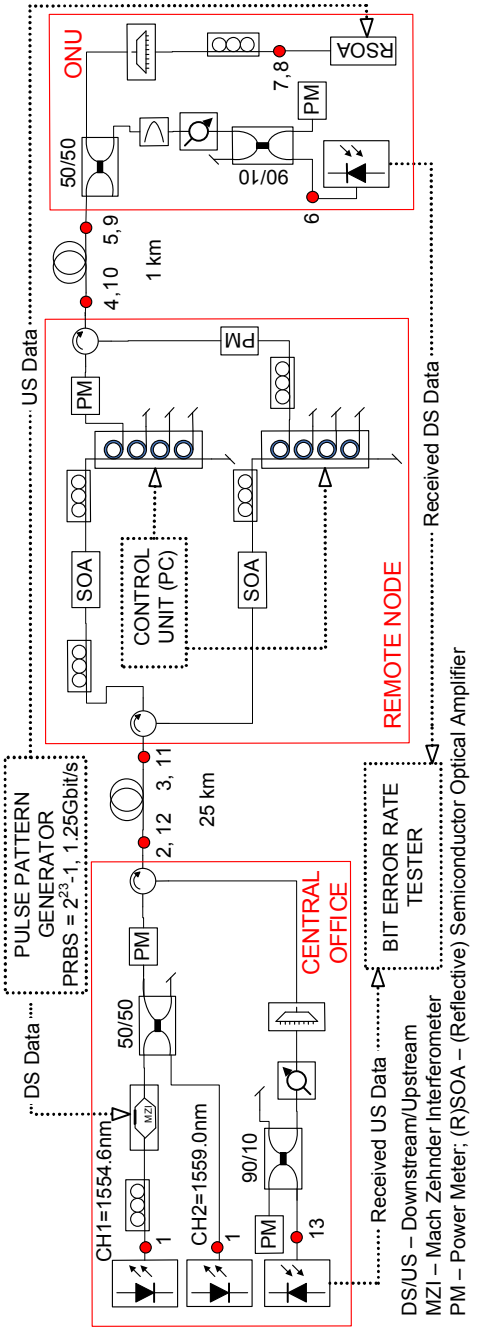

Figure 7.2: Testbed for symmetrical bidirectional 1.25 Gbit/s transmission.

Table 7.1: Power budget for 1.25 Gbit/s setup.

	Parameter	data ch. [dBm]	CW ch. [dBm]
(1)	CO laser output power	5.5	2.5
(2)	CO transmitted power	-4.5	-3.5
(3)	RN input power	-9.5	-8.5
(4)	RN output power	-16.0	-15.0
(5)	ONU input power	-16.2	-15.2
(6)	**ONU ROP**	**-21.7**	n. a.
	ONU RX sensitivity	**-23.5**	n. a.
(7)	ONU RSOA input power	n. a.	-20.2
(8)	ONU RSOA output power	n. a.	0.0
(9)	ONU transmitted power	n. a.	-5.0
(10)	RN input power	n. a.	-5.2
(11)	RN output power	n. a.	-12.7
(12)	CO input power	n. a.	-17.7
(13)	**CO ROP**	n. a.	**-22.2**
	CO RX sensitivity	n. a.	**-23.5**

bias dithering limits the extinction ratio of the output signal of the RSOA[1], which, as it will be discussed in the next Section, is an important parameter for upstream transmission.

7.1.2 Measurement and simulation results

The BtB DS measurement (no fiber span, black squares) shows around 0.3 dB ROP difference with respect to the reference curve (bold curve, the same for DS and US measurement), which is within the accuracy of the measurement, fig. 7.3. After inserting 25 km of the feeder fiber and 1 km of the distribution fiber (black triangles) the ROP did not change.

The US received signal reveals around 2.5 dB PP for a BtB (black rhombus). This is justified by two factors. The first one is the difference in the performance of the RSOA as a modulator and the MZ modulator, which was used in the reference measurement. The former has much lower electrical bandwidth (1.5 GHz) than the latter one (10 GHz). The low electrical bandwidth of the RSOA is a result of carrier

[1]The required dithering amplitude is twice as the amplitude of the data modulation signal. Due to limited RF amplitude which can be provided to the RSOA this yields the decrease in the data amplitude and as a result lower extinction ratio.

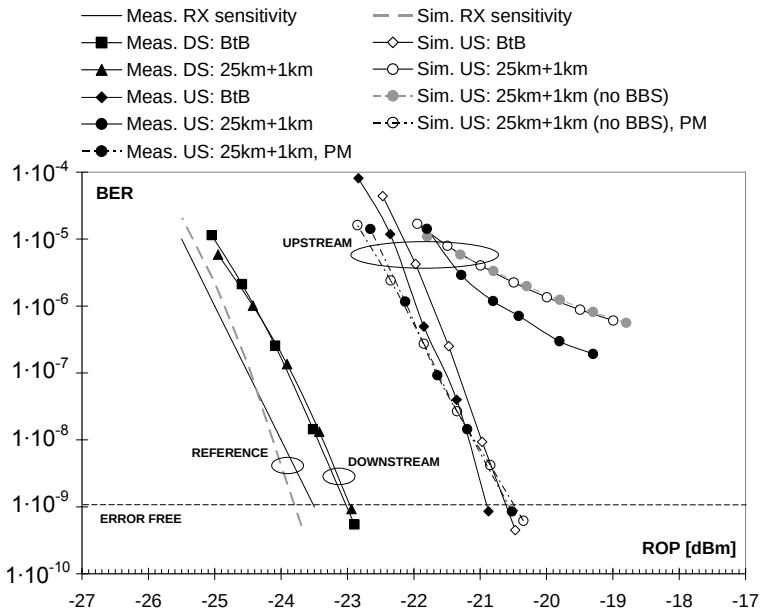

Figure 7.3: Results of transmission experiments on 1.25 Gbit/s testbed.

lifetime, which causes a longer falling edge of the eye diagram and consequently eye symmetry and extinction ratio degradation. The second factor is the ASE noise coming from the three cascaded SOAs which the signal experiences while passing the RN, ONU and RN again. This is not the case for the DS data channel as it encounters ASE source only once. The presence of the DS does not influence the received US, as they are over 500 GHz apart from each other. Inserting the fiber span causes error-floor and the required BER cannot be achieved (black circles) in the US transmission. This is due to the RBS and BBS power propagating in both directions: towards ONU and towards CO.

To define the main distortion in the setup we used the advantage of simulation tool [89], where the corresponding setup was implemented and the RBS and BBS could be switched on/off. The rate-equation-based model of the RSOA with parameter values set accordingly to the data and the performance of the real device was used [132]. The RSOA model is summarized in Appendix B and its parameters match the real device used in the experiments as described in Chapter 3.

Only CW DS/data US channel was simulated as it was said before the adjacent DS data channel does not play a role in the received US signal. The PP in the simulations follow the same trend as in the measurements. It can be clearly seen that the error-floor is caused mainly by the RBS (white circles with solid line) since the exclusion of BBS (grey circles with dashed line) did not improve the BER performance.

To reduce the influence of RBS the linewidth of the signal was enhanced by means of phase modulation ($f_{PM} = 2.5\ GHz$, $\Delta\lambda_{3dB} = 50\ pm$). It is introduced by an external phase modulator after 50/50 coupler in the CO. The phase modulation does not influence ROP of the DS data channel, whereas for the US channel RBS-induced PP was completely eliminated (black circles with dashed line). Similar results for the same modulation conditions were obtained in the simulations (white circles with dash-dotted line).

Additionally, in the simulations we verified the contributions of ASE noise accumulation and the RSOA properties to the US power penalty. After neglecting the RBS and BBS as well as the ASE noise of two SOAs placed in the RN (the ASE noise of the RSOA could not be switched off due to virtual model restrictions) the 2.5 dB PP reduced with only 0.4 dB. This means that the RSOA causes the major part of the PP. It is due to a combination of low Q-factor and extinction ratio of the output and electrical bandwidth of the device with respect to the reference modulator, which was 6.1 and 8.1, 10 dB and 13.5 dB, and 1.5 GHz and 9 GHz for the RSOA and the MZM, respectively.

There is some minor discrepancy between the measurement and simulation results. The ASE noise was adjusted based on the measured NF of the real device and here some measurement uncertainty of +/-0.5 dB was involved. Also, stronger interferometric interactions between the RBS and the signal power causing larger error-floor in the simulation was noticed which can be assigned to lower chirp.

7.2 10 Gbit/s transmission

The network testbed examined in this Section provides 10 Gbit/s amplitude-modulated signals for DS and US communication. For this purpose, colorless operation of a reflective ONU is achieved by utilization of the REAM, earlier discussed in Chapter 3, fig. 7.4.

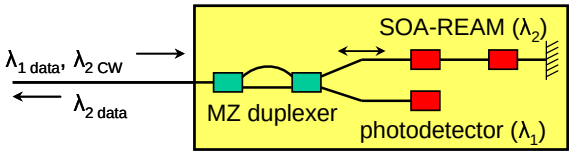

Figure 7.4: Schematic of the REAM-based ONU for 10 Gbit/s network.

7.2.1 Testbed structure

A testbed consists of a transmission link from CO via RN to two ONUs and backwards over a single fiber as shown in fig. 7.5. The photo of the testbed is given in the Appendix C.

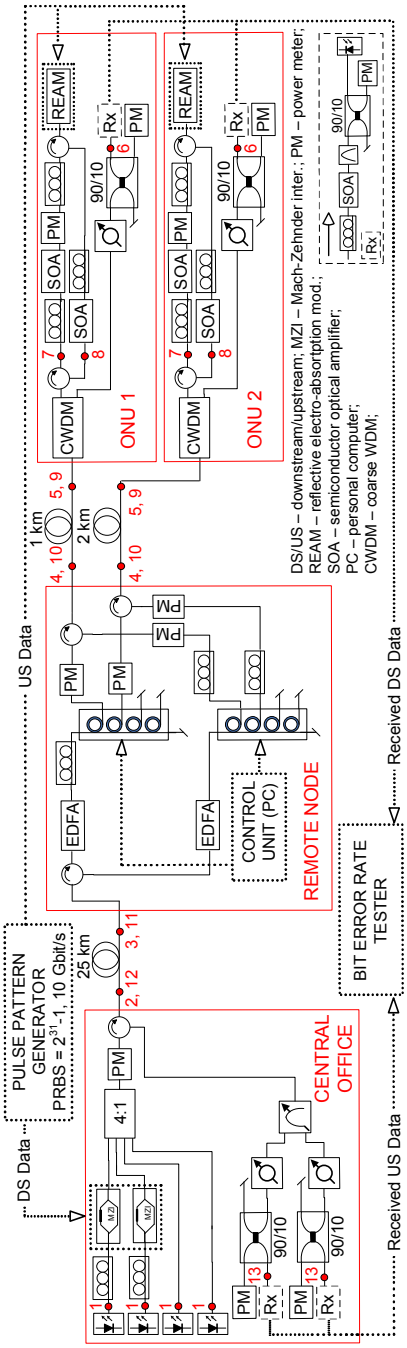

Figure 7.5: Testbed for symmetrical bidirectional 10 Gbit/s transmission.

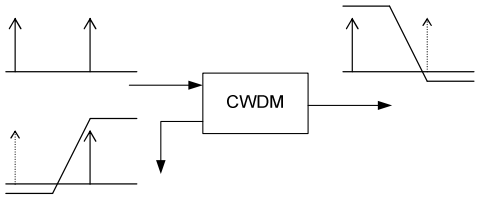

Figure 7.6: CWDM filter applied at the ONU.

The CO contains 4 lasers emitting λ_1, λ_2 (10 Gbit/s DS data) and $\lambda_1 + FSR_{OADM}$, $\lambda_2 + FSR_{OADM}$ (DS CW). All channels are coupled into the feeder fiber by a 4:1 coupler. The receiver part of the CO has a tunable filter (required due to the FSR_{OADM} unintentionally not an integer multiple of the ITU grid interval), step attenuator for BER measurement, 90/10 splitter to measure ROP and an SOA-preamplified commercial 10 Gbit/s receiver.

Table 7.2: Power budget for 10 Gbit/s setup.

	Parameter	data ch. [dBm]	CW ch. [dBm]
(1)	CO laser out. power	9.0	9.0
(2)	CO transm. power	-9.0	0.0
(3)	RN in. power	-14.0	-5.0
(4)	RN out. power	-20.0	-11.0
(5)	ONU in. power	-20.5	-11.5
(6)	**ONU ROP**	**-24.3**	n. a.
	ONU RX sens. av for f_1, f_2	**-26.3**	n. a.
(7)	ONU SOA-REAM in. power	n. a.	-14.0
(8)	ONU SOA-REAM out. power	n. a.	2.5
(9)	ONU transm. power	n. a.	1.0
(10)	RN in. power	n. a.	0.5
(11)	RN out. power	n. a.	-5.5
(12)	CO in. power	n. a.	-10.5
(13)	**CO ROP**	n. a.	**-15.0**
	CO RX sens. $f_{1,2} + FSR_{OADM}$	n. a.	**-26.8**

The RN is similar to the one used in Section 7.1.1, however, here in order to minimize the influence of accumulated ASE noise EDFAs are used instead of SOAs.

Table 7.3: Wavelength allocation schemes applied in 10 Gbit/s testbed.

	ONU♯1	ONU♯2
PtP-A	$(\lambda_1, \lambda_1 + FSR_{OADM})$	$(\lambda_2, \lambda_2 + FSR_{OADM})$
PtP-B	$(\lambda_2, \lambda_2 + FSR_{OADM})$	$(\lambda_1, \lambda_1 + FSR_{OADM})$
PtMP	$(\lambda_1, \lambda_1 + FSR_{OADM})$	$(\lambda_1, \lambda_1 + FSR_{OADM})$

Each ONU contains a CWDM representing the MZI duplexer and its performance is depicted in fig. 7.6. It is followed by a DS part (similar to the CO receiver) and US part with two SOAs and circulators, an REAM [132], and polarization controllers. The US part has the same functionality as an integrated SOA-REAM, as in fig. 7.4, with adjusted polarization states for the optimum performance of each element. The input power of the CW is -15 dBm. The bit sequences provided to the DS and US modulators were decorrelated by means of electrical and optical delay, respectively.

The power budget for the 10 Gbit/s transmission testbed is summarized in table 7.2. The IL of the OADM for ONU♯1 is 1.5 dB lower than for ONU♯2, which is because of the higher waveguide loss at the add/drop communicating with ONU♯2 as explained in Chapter 4. There is also 0.2 dB higher fiber attenuation for ONU♯2. For simplicity the power calculations in table 7.2 show averaged loss which applies to both ONUs.

7.2.2 Measurement results

Fig. 7.7 shows the measurement results for DS and US transmission in various bandwidth configurations as indicated in table 7.3. Two reference measurements were taken for the DS receiver for λ_1 and λ_2.

For the PtP-A and PtP-B case there is 1-1.5 dB PP in a DS BtB (attenuators in place of fiber-spans), which can be assigned to the polarization instability and the misalignment of the optical filters. The polarization instability is considered as polarization changes of the input signal which result in slightly varying device performance i. e. loss at MZMs in the CO, loss at the OADM, extinction ratio of the REAM and gain of the SOAs. After inserting the fiber spans an additional negligible PP of around 0.2-0.4 dB can be noticed. For BtB US measurement (both PtP-A and PtP-B) the main source of PP is the intrachannel crosstalk caused by the imperfect suppression (20 dB) of the adjacent channels of the OADM and a wide bandwidth of the CWDM filter at the ONU. The CW signal which enters the reflective modulator is accompanied by a residual power of the adjacent CW channel. After modulation it travels back to the OADM where it interferes with the data channel from the other ONU, fig. 7.10. This results in the SCR of less than 20 dB (fig. 7.8h and fig. 7.8i) and PP of 2 dB for each ONU. A significant con-

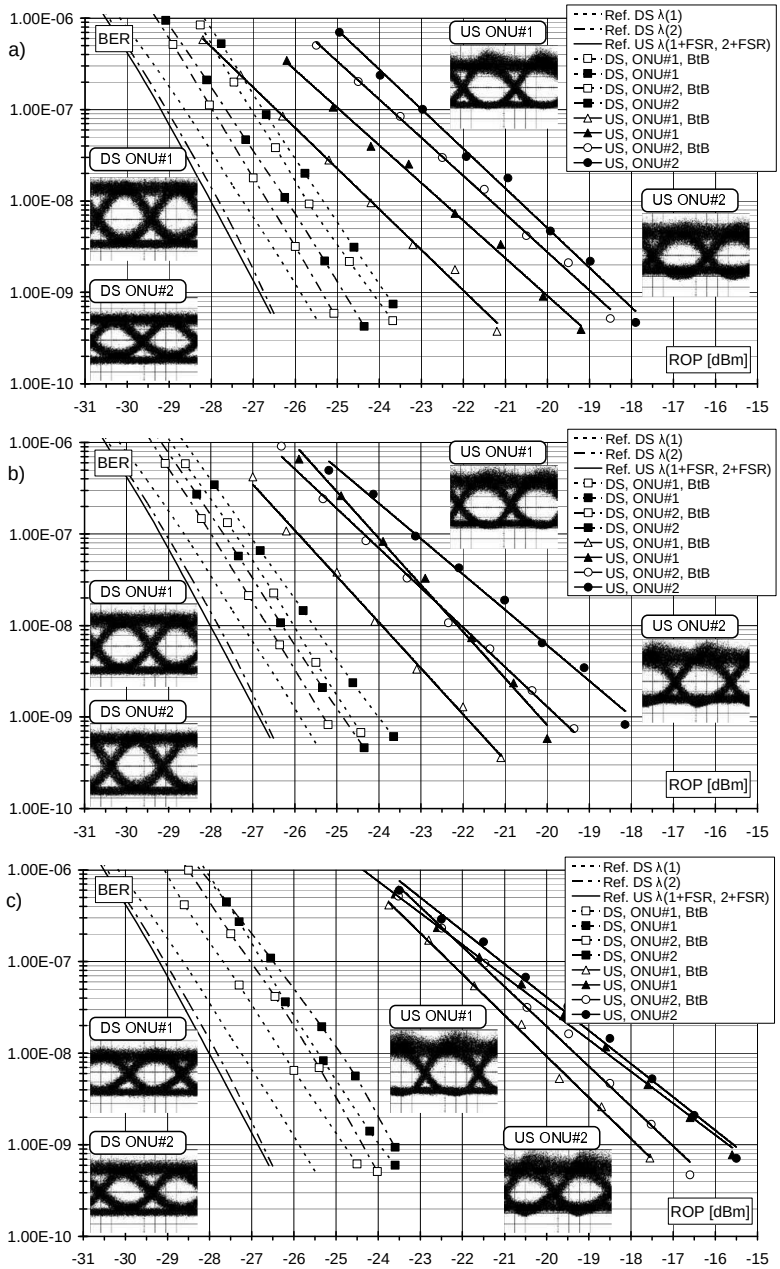

Figure 7.7: Experimental results: a) PtP-A, b) PtP-B and c) PtMP.

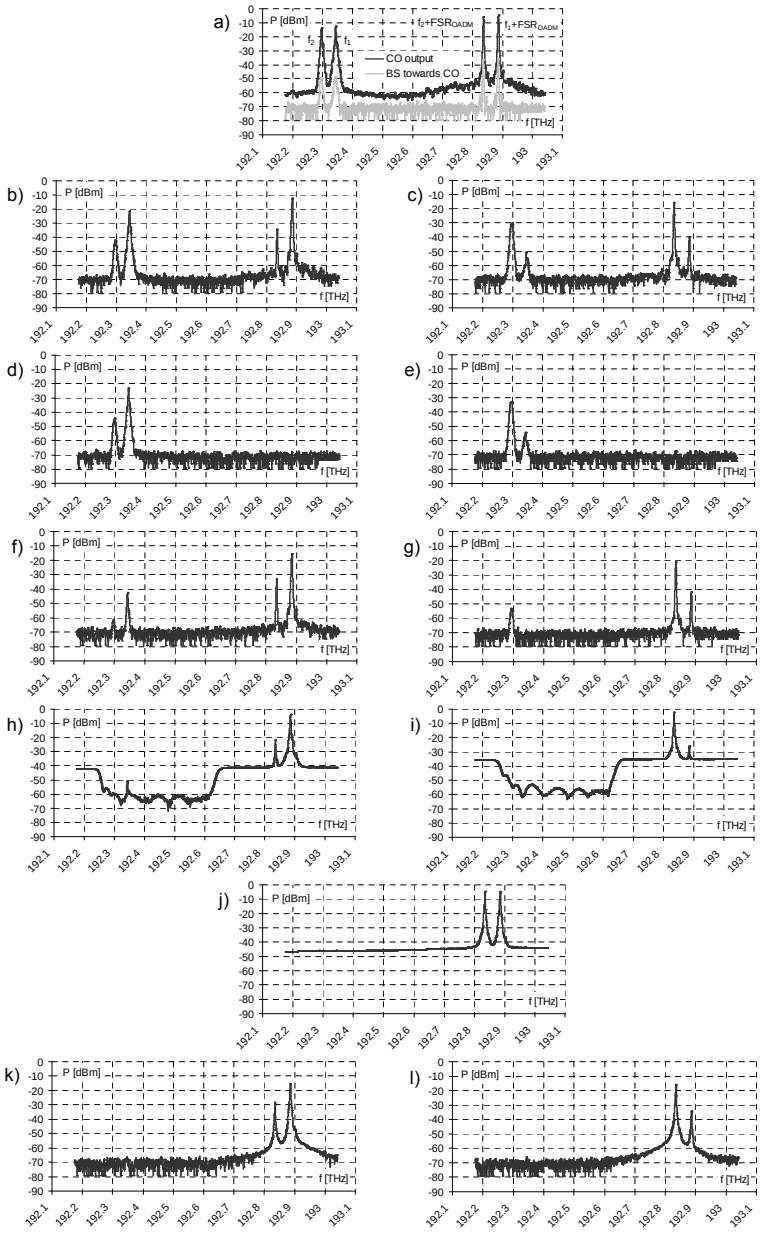

Figure 7.8: Spectrum for PtP-A case: a) CO output and BS towards CO, RN drop port for b) ONU♯1 and c) ONU♯2, received data ch. at d) ONU♯1 and e) ONU♯2, received CW ch. at f) ONU♯1 and g) ONU♯2, RN add port for h) ONU♯1 and i) ONU♯2, j) RN output, CO received data ch. from k) ONU♯1 and l) ONU♯2.

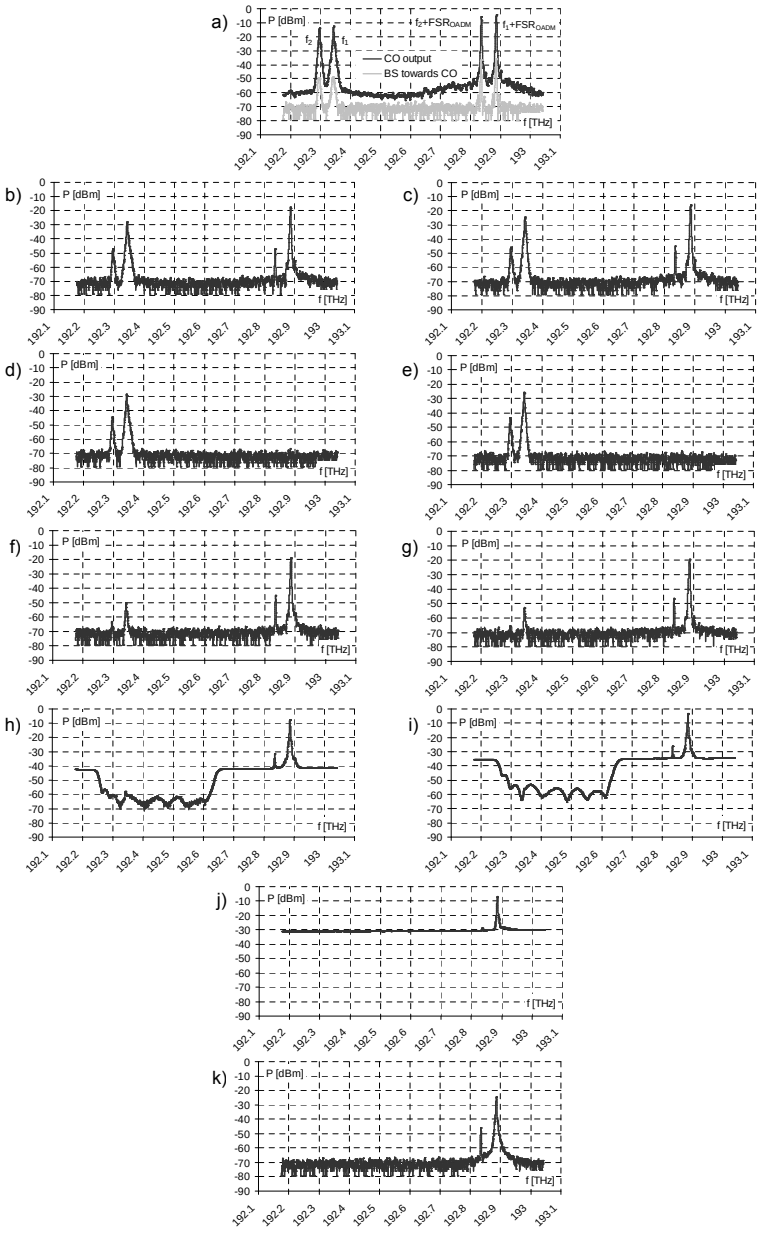

Figure 7.9: Spectrum for PtMP case: a) CO output and BS towards CO, RN drop port for b) ONU♯1 and c) ONU♯2, received data ch. at d) ONU♯1 and e) ONU♯2, received CW ch. at f) ONU♯1 and g) ONU♯2, RN add port for h) ONU♯1 and i) ONU♯2, j) RN output, k) CO received data ch. (the same for ONU♯1 and ONU♯2).

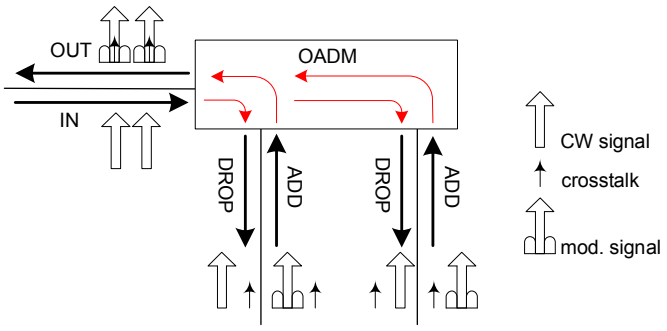

Figure 7.10: Interference at the OADM.

tribution to the total PP brings lower ER of the REAM ($ER_{ONU\sharp1} = 10$ dB and $ER_{ONU\sharp2} = 7.5$ dB) with respect to the reference modulator ($ER_{REF} = 12$ dB), which gives 0.7 dB and 1.2 dB PP for ONU♯1 and ONU♯2, respectively, according to Chapter 5. The other distortions are the ASE noise accumulation in the complete DS CW transmission (EDFA, SOA) and US data transmission (SOA, EDFA, SOA), polarization instability and optical filters misalignment (total 2.0 dB). The inclusion of fiber spans adds 1-1.5 dB (after proper ONU gain adjustment according to Chapter 5) PP due to the RBS resulting in SCR of 20 dB, fig. 7.8a. In case of a larger RBS-induced PP, there are efficient techniques to improve the SCR based on e. g. centralized phase modulation [114].

During the PtMP BER measurement to simulate TDM one ONU was working at a time while the other one had the SOA and REAM biases set to 0 V. For DS transmission the 3 dB multicast loss in the OADM (reached at 13 GHz detuning) was covered with the available power budget and no significant difference in BER was observed. For US measurement lower CW power injected into the ONU caused lower output power which led to a stronger impact of the RBS of the CW carrier ($SCR_{incoh} = 18$ dB) and additional 2-2.5 dB PP. The extinction ratio was decreased (0.8 dB) because of polarization instabilities at the ONU input which also contributed to the PP. No dispersion induced intersymbol interference was noticed.

7.3 Full-scale network transmission model

The complete optical part of the designed network is modeled and examined here using the simulation tool VPI [89]. Special emphasis is put on ASE noise accumulation and interchannel crosstalk due to backscattering, which have been estimated in Chapter 5 as causing the largest distortion of the signal in the complete transmission link.

In Chapter 4, it has been discussed that in order to provide split ratio at the

RN higher than 2 the spectral response of the OADM has to be steeper which is achieved by applying higher order rings. Another way for improvement is to apply larger wavelength channel spacing. Both solutions would result in lower interchannel crosstalk. However, the former would make the OADM a very complex structure, and the issues such as thermal stability and loss would become more critical and difficult to manage. Enlargement of the channel interval, under the condition of preserving the same amount of wavelength channels (the same aggregated bandwidth), would require a change of the FSR_{OADM} and FSR_{MZI}. This yields a fundamental redesign of the network components (OADM, ONU). Alternatively, the remaining wavelength channels can be set in the next FSR_{OADM} periods. However, this would bring the requirement for additional filters at each drop-port of the OADM to enable splitting multiple wavelength pairs transmitted at each port. In this case, the wavelength required at one ONU connected to a given drop-port would determine the wavelengths received by the rest of the ONUs sharing the same drop-port, which inevitably leads to the limitations in bandwidth reconfigurability.

To keep the OADM architecture as described in Chapter 4 and the wavelength set and the resulting aggregated bandwidth unchanged, passive power-splitters are applied at each drop-port. Although this solution can provide the required split-ratio at the RN, it limits the wavelength reconfigurability. As a result each wavelength always serves a PON tree and PtP connectivity is not possible. However, the proposed solution seems to be appropriate, since the OADM-splitter structure can be upgraded to fully reconfigurable OADM at any time without necessity of changing the rest of the network infrastructure. It is further denoted as limited-reconfigurability BBPhotonics architecture (LR-BBPhotonics), fig. 7.11. The comparison with the original BBPhotonics design is given in table 7.4

7.3.1 Model description

If a fiber failure occurs between the CO and one RN, the complete transmission from/to CO is performed via the remaining branch of the ring as indicated in fig. 7.12. The transmission over such distance, further denoted as the longest lightpath, results in the maximum accumulation of the distortions caused by different transmission impairments, which leads to the highest PPs in the system. Such situation is considered in the simulations discussed in this Section. Such fiber break may also occur somewhere else along the ring, e. g. between the RNs. Tuning the variable 1x2 splitter at the CO can handle this by sending an appropriate amount of optical power clockwise and an other amount counter-clockwise along the ring. However, in such case accumulation of distortions is less severe than in case of the transmission over the longest lightpath.

The reconfigurability capabilities (switching time and maximum split-ratio) have been discussed in Chapter 4 and earlier in this Chapter. Based on that, the simulation model concerns a wavelength allocation scheme, where each ONU is assigned symmetrical bandwidth of 1.25 Gbit/s in the LR-BBPhotonics architec-

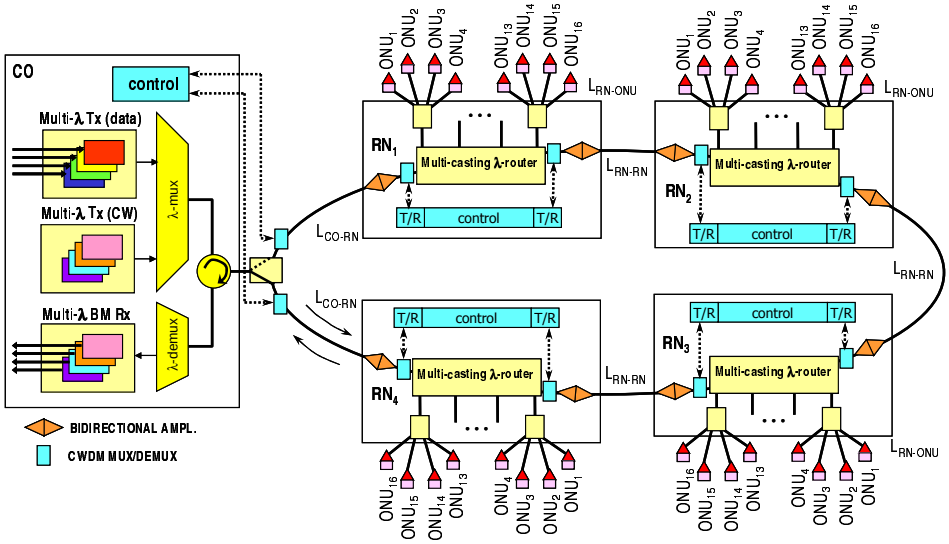

Figure 7.11: LR-BBPhotonics network architecture.

Table 7.4: BBPhotonics vs LR-BBPhotonics.

	BBPhotonics	LR-BBPhotonics
Split-ratio per RN	8 (8 at OADM)	8 (2 at OADM, 4 at a splitter)
Max. bandwidth per user min. split-ratio at OADM	10 Gbit/s	2.5 Gbit/s
Min. bandwidth per user max. split-ratio at OADM	1.25 Gbit/s	1.25 Gbit/s
Aggregated bandwidth, infrastructure (excl. RN), power budget and wavelength set	-	the same as in BBPhotonics
Wav. reconfigurability	high	moderate

ture. This means that each wavelength channel is shared by 8 ONUs (2 splits at the OADM and 4 splits at the splitter) as indicated in fig. 7.12.

For TDM operation in US the same approach is used as in the experiments described in Section 7.2. The time-slotted transmission is achieved by proper settings of the SOA and REAM biases at the ONUs, which enable only one ONU to

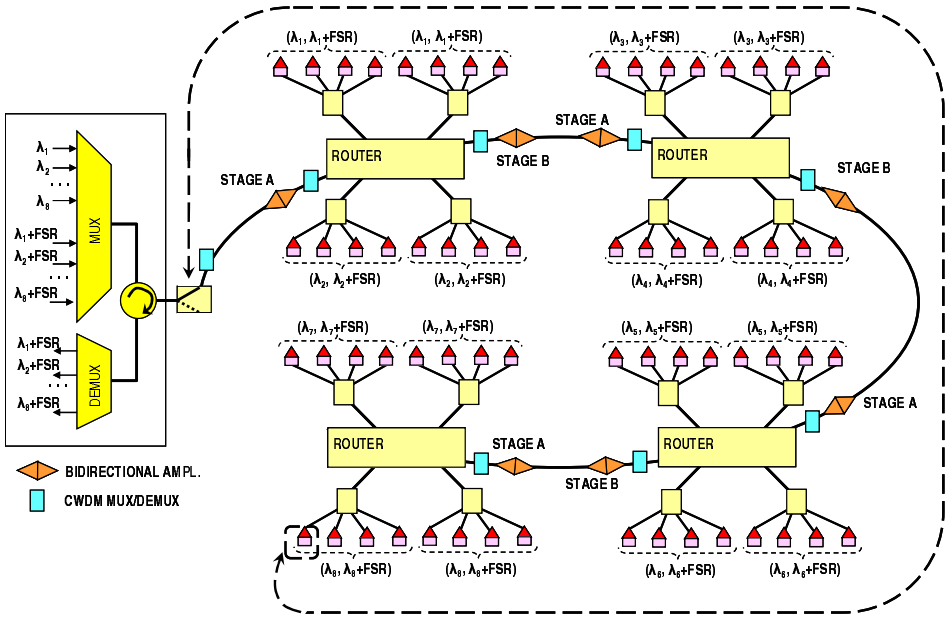

Figure 7.12: The longest lightpath in the LR-BBPhotonics network.

work at a time in a given PON system while the remaining ONUs are off.

To eliminate polarization dependencies only X-polarization is simulated, which also shortens considerably the computation time[2].

Due to the unavailability of micro-ring resonator module in the simulation tool, the OADM is constructed with a set of periodic single add/drop-port sections connected in series, fig. 7.13. The filter parameters of such module are set in correspondence to the parameters of the real device as described in Chapter 4. This yields a Lorentzian profile with 0.43 nm and 1.60 nm of -10 dB and -20 dB passband, respectively.

Also due to the unavailability of the reflective EAM module it is replaced with traveling-wave EAM, an ideal circulator and an attenuator which emulates the return loss at the reflective facet of the real device, fig. 7.14.

The required wavelength-selective gain at the RNs is provided by bidirectional amplification modules as shown in fig. 7.15. The gain of all amplifiers applied in the simulation setup is assumed to be flat over the computed optical bandwidth (around 15 nm). After such amplifier an integrated array of variable optical at-

[2]The time required to achieve reliable (realistic) results also depends on the number of bits transmitted and several other simulation parameters. After time-optimization the calculation period was reduced significantly. Due to numerous bidirectional modules applied in the system and the possible interactions between the counterpropagating signals (e. g. RBS, BBS) each simulation set was run several times in order to achieve repeatable results.

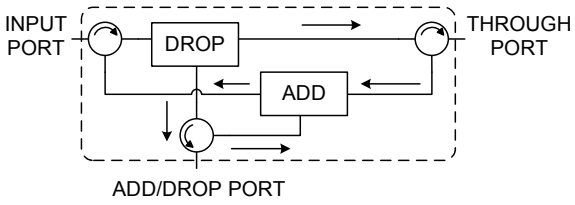

Figure 7.13: The micro-ring resonator model designed in VPI. The complete OADM module consists of several such sections.

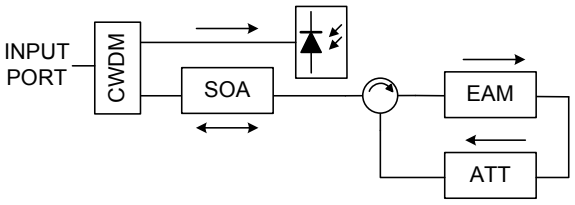

Figure 7.14: The ONU model designed in VPI.

tenuators sandwiched between two multiplexers is applied [138]. This enables the adjustment of the power level per wavelength channel. The switches in the amplification module enables by-passing the amplifier in case of traffic direction change as discussed in Chapter 2.

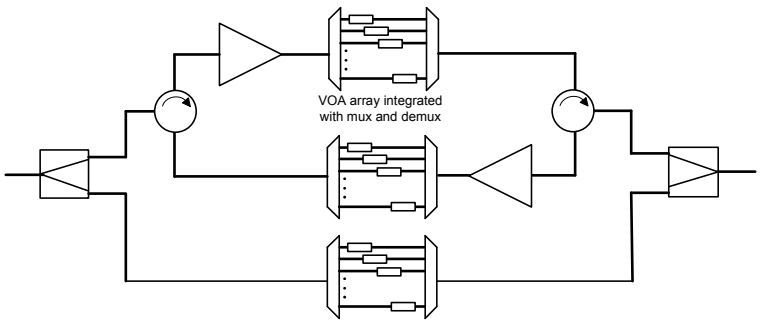

Figure 7.15: Bidirectional amplification module with wavelength-selective gain.

The parameters of the simulation system are given in the table 7.5. The power budget calculation is given in table 7.6 and table 7.7 for downstream and upstream, respectively. It is calculated according to the unity-gain approach (the resultant RN loss is 0 dB at a through port), discussed in Chapter 2, which enables easier network reconfiguration/restoration in case of e. g. protection switching.

The CO loss includes the insertion loss of a WDM DS multiplexer and US

Table 7.5: LR-BBPhotonics network simulation model.

Parameter	Value
CO: DFB laser linewidth	50 kHz
CO: Data TX extinction ratio	17 dB
CO: Channel spacing	50 GHz (0.4 nm)
CO: Number of data channels, CW channels	8, 8
CO: 1st Data channel	193.1 THz (1552.52 nm)
CO: 1st CW channel	193.6 THz (1548.51 nm)
CO: AWG MUX/DEMUX -3 dB passband	30 GHz (0.24 nm)
CO-RN, RN-CO, RN-RN, RN-ONU: Fiber att.	0.2 dB/km
CO-RN, RN-CO, RN-RN, RN-ONU: Fiber disp.	16 ps/nm·km
CO-RN, RN-CO: Fiber length	20 km
RN: OADM drop-port -10 dB passband	54 GHz (0.43 nm)
RN: OADM FSR	500 GHz (4 nm)
RN-RN: Fiber length	1 km
RN-ONU: Fiber length	1 km
ONU: Data TX extinction ratio	13 dB
ONU: CWDM -3 dB passband	50 GHz
DS, US RX bandwidth	8 GHz
DS, US bit-rate	10 Gbit/s

demultiplexer (4.0 dB each), a CWDM coupler (1.0 dB), a circulator (0.8 dB), a switch (1.0 dB) and connectors (0.6 dB in total). The through loss in RN_1, RN_2 and RN_3 each includes OADM insertion loss (6 dB)[3], connectors (0.6 dB in total) and two times insertion loss of a CWDM coupler (1.0 dB) and a switch (1.0 dB)[4]. The drop loss in RN_4 includes OADM insertion loss (6 dB), OADM split loss (9.0 dB), connectors (0.6 dB in total), a CWDM coupler and a switch. For the applied wavelengths, table 7.5 the fiber loss is 0.2 dB/km. The insertion loss in ONU (8.5 dB) includes connector, fiber/chip coupling, MZ duplexer and waveguide losses. The power margin for impairment-induced penalties is 5.0 dB for downstream and 6.0 dB for upstream.

These calculations reveal only minor differences with respect to the calculations in Chapter 2. The differences are caused by different multicast losses in the RN

[3]The insertion loss of the OADM includes fiber/chip coupling and waveguide loss.

[4]As indicated in fig. 7.12 each wavelength channel feeds exactly 8 ONUs connected to one RN. This means that for the longest lightpath the wavelength channels transmitted to the last RN do not experience any split loss in the earlier RNs

Table 7.6: System power budget for downstream path (data and CW channel) in LR-BBPhotonics access network (the longest lightpath).

	Parameter	loss/gain [dB] or power [dBm]
(1)	Transmitted power per wav. channel	6.0
(2)	CO loss	- 7.4
(3)	CO-RN_1 fiber att.	- 4.0
	RN_1 input power	- 5.4
(4)	RN_1 stage A gain/att.	12.7
(5)	RN_1 through loss	- 10.6
(6)	RN_1 stage B gain/att.	- 1.9
(7)	RN_1-RN_2 fiber att.	- 0.2
	RN_2 input power	- 5.4
(8)	RN_2 stage A gain/att.	12.7
(9)	RN_2 through loss	- 10.6
(10)	RN_2 stage B gain/att.	- 1.9
(11)	RN_2-RN_3 fiber att.	- 0.2
	RN_3 input power	- 5.4
(12)	RN_3 stage A gain/att.	12.7
(13)	RN_3 through loss	- 10.6
(14)	RN_3 stage B gain/att.	- 1.9
(15)	RN_3-RN_4 fiber att.	- 0.2
	RN_4 input power	- 5.4
(16)	RN_4 stage A gain/att.	12.7
(17)	RN_4 drop loss	- 17.6
	RN_4 power at drop port	- 10.3
(18)	RN_4-ONU fiber att.	- 0.2
(19)	ONU loss	- 8.5
	Received power	- 19.0
(20)	10 Gbit/s receiver sens./refl. mod. sens.	- 24.0
(21)	Power budget, [(1)-(20)]	30.0
	Remaining power margin [(2)+(3)+...+(19)+(21)]	5.0

Table 7.7: System power budget for upstream path in LR-BBPhotonics access network (the longest lightpath).

	Parameter	loss/gain [dB] or power [dBm]
	Refl. mod gain	22.0
	ONU fiber-to-fiber gain	5.0
(1)	Refl. mod. transmitted power	3.0
(2)	ONU loss	- 8.5
(3)	RN_4-ONU fiber att.	- 0.2
	RN_4 power at add port	- 5.7
(4)	RN_4 add loss	- 17.6
(5)	RN_4 stage A gain/att.	16.7
(6)	RN_4-RN_3 fiber att.	- 0.2
	RN_3 input power	- 6.8
(7)	RN_3 stage B gain/att.	- 5.9
(8)	RN_3 through loss	- 10.6
(9)	RN_3 stage A gain/att.	16.7
(10)	RN_3-RN_2 fiber att.	- 0.2
	RN_2 input power	- 6.8
(11)	RN_2 stage B gain/att.	- 5.9
(12)	RN_2 through loss	- 10.6
(13)	RN_2 stage A gain/att.	16.7
(14)	RN_2-RN_1 fiber att.	- 0.2
	RN_1 input power	- 6.8
(15)	RN_1 stage B gain/att.	- 5.9
(16)	RN_1 through loss	- 10.6
(17)	RN_1 stage A gain/att.	16.7
(18)	RN_1-CO fiber att.	- 4.0
	CO input power	- 10.6
(19)	CO loss	- 7.4
	Received power	- 18.0
(20)	10 Gbit/s receiver sensitivity	- 24.0
(21)	Power budget, [(1)-(20)]	26.0
	Remaining power margin [(2)+(3)+...+(19)+(21)]	6.0

Table 7.8: Settings of amplifiers.

	DS: ampl. tot. output p. [dBm] (required gain 12.7 dB)	US: ampl. tot. output p. [dBm] (required gain 16.7 dB)
RN_1	19.3 (16 wav. ch.)	2.4 (8 wav. ch.)
RN_2	18.1 (12 wav. ch.)	1.2 (6 wav. ch.)
RN_3	16.3 (8 wav. ch.)	-0.6 (4 wav. ch.)
RN_4	13.9 (4 wav. ch.)	-3.7 (2 wav. ch.)

due to different wavelength allocation schemes. In BBPhotonics access network, as discussed in Chapter 2, each wavelength pair feeds two ONUs per RN. In the LR-BBPhotonics, as discussed in this Chapter, each wavelength pair is shared by 8 ONUs at a single RN only.

In table 7.8 the required amplifier settings are summarized. The NF of the amplifiers is set to 3.0 dB (ideal) and 6.2 dB (real). The second value is between commercially available device parameter[5] and research records (5.7 dB) [139]. Although currently available gain-clamped SOAs cannot fully satisfy mentioned requirements, some models of devices with saturation output power beyond 22 dBm ($>$ 15 dBm) are already available [56].

Setup optimization

The setup was optimized with respect to backscattering based on the calculation of gain at ONU similar to the calculation performed in Chapter 5. Here, it is assumed that the largest backscattered power is accumulated over the CO-RN fiber, and the other fiber sections (RN-RN and RN-ONU) have a negligible contribution. This is a reasonable assumption since the CO-RN is the longest fiber section in the network.

To estimate the optimum ONU fiber-to-fiber gain the model in fig. 7.16 is used to calculate the SCRs at the CO and at the ONU, $SCR_{RBS,CO}$ and $SCR_{RBS,ONU}$, respectively. The DS and US losses in the RN_1 to RN_3 including the inter-node fiber sections are balanced by the amplifiers in the RN, and the resultant loss in the RN_4 is 4.9 dB in DS and resultant gain of 0.1 dB in US direction, as deduced from table 7.6 and table 7.7. Based on the discussion in Chapter 5, the following equations for SCRs apply.

$$SCR_{RBS,CO} = \alpha - 2\alpha_{f_1} + \alpha_{RBS} \tag{7.1}$$

$$SCR_{RBS,ONU} = \alpha_{RBS} - \alpha \tag{7.2}$$

[5]CIP, SOA-L-OEC-1550, NF specified as 6.4 dB.

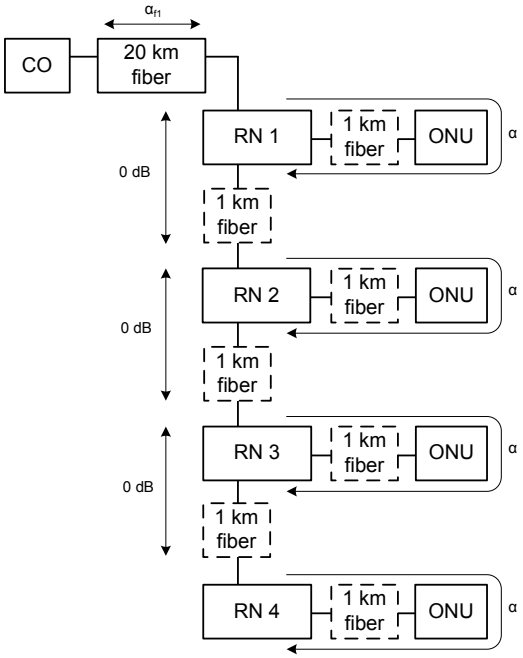

Figure 7.16: Scheme used to calculate the SCRs.

where α_{f_1} is the attenuation of 20 km CO-RN fiber and α_{RBS} is the ratio of the input power to RBS returned power (around 35 dB for 20 km SSMF according to [63]). Parameter α is the net attenuation as indicated in fig. 7.16 and it is given by the following equation.

$$\alpha = \alpha_{RN,DS} + 2\alpha_{f_2} - G_{ONU} + \alpha_{RN,US} \tag{7.3}$$

where $\alpha_{RN,DS}$ is the loss/gain parameter of the last RN in the downstream direction, α_{f_2} is the attenuation of the RN-ONU fiber, G_{ONU} is the ONU fiber-to-fiber gain, and $\alpha_{RN,US}$ is the loss/gain parameter of the RN in the upstream direction.

Eq. 7.1 and eq. 7.2 are depicted in fig. 7.17. It can be noticed that there is an optimum value for the gain of ONU, where the SCRs are equal. In case of the simulated system the maximum achievable fiber-to-fiber gain of ONU is 5 dB. According to graphs in fig. 7.17 this results in $SCR_{RBS,CO} = 27$ dB and $SCR_{RBS,ONU} = 35$ dB. According to the measurement results in [63] this should cause less than 1.0 dB PP.

Because of the unity-gain approach and tunable amplification the power levels transmitted in each fiber-section are constant regardless different multicast loss. Therefore, the above calculation is always valid for the designed network.

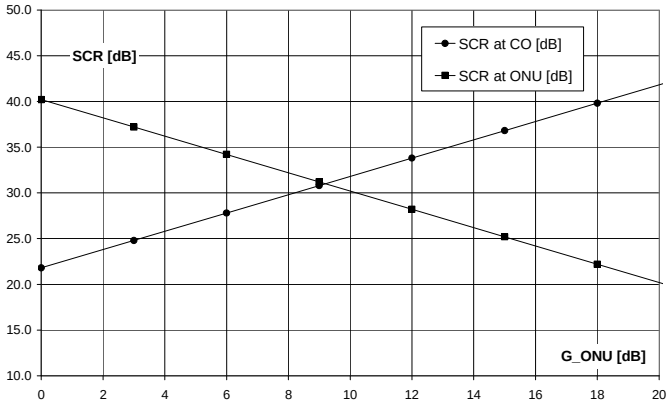

Figure 7.17: RBS-degraded SCR ratios as a function of gain at ONU in the LR-BBPhotonics network.

Table 7.9: LR-BBPhotonics simulation parameters.

Set	indiv. ampl. NF	Dispersion	RBS	BBS
A	3.0	off	off	off
B	6.2	off	off	off
C	6.2	on	off	off
D	6.2	on	on	off
E	6.2	on	on	on (ONU 4.9-4.12)

7.3.2 Simulation results

The simulation results are depicted in fig. 7.18, where PPs for each ONU are given. The denotation ONU $X.Y$ means an Y-ONU connected to an X-node, where X scales up to 4 and Y scales up to 16. The ONUs are grouped in four groups connected to four 1x4 splitters at each RN. A single point on the graph in fig. 7.18 applies to all four ONUs in the group, as all of them receive the same signals. The results show generally clear trends, and the random placement of the points around the trend lines is caused by the limited representation of different received bit sequences due to simulation-time restrictions.

The simulations were performed for four sets of parameters as explained in table 7.9, where the last sets (D and E) correspond to a real situation and all previous sets are applied just to enable the analysis of PPs. Due to the large computing power and long calculation time required to simulate the system with BBS, set E was tested only for the most critical case. This concerns ONU 4.9-4.12

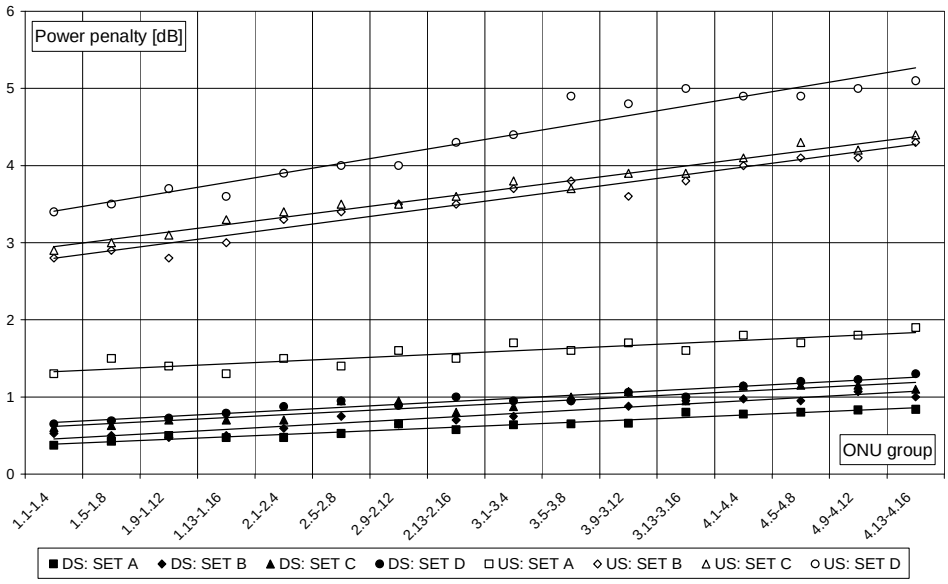

Figure 7.18: Simulation results of the LR-BBPhotonics full-scale network.

which is placed at the maximum fiber distance. Furthermore, the drop port to which it is connected is detuned with 10 GHz towards the BBS product (11 GHz red-shifted from the nominal wavelength of the channel), which may result in the highest PP.

Analysis of the DS transmission

The results for DS transmission for all sets of parameters show 0.4-1.3 dB across all ONUs with the growing tendency towards the last ONU (the longest lightpath). Although, it is difficult to justify such small PP as in case of set A, it is recognized as a result of residual ASE noise from the in-field amplifiers and interchannel crosstalk (around 23 dB) due to large -10 dB bandwidth of the filters at the OADM (0.43 nm) and ONU (0.40 nm).

Increasing the noise figure of each amplifier from 3.0 dB to a realistic value for low-noise SOAs (6.2 dB), set B, shows an increase in PP of only 0.1 to 0.3 dB for the furthest ONU. This can be explained by the high extinction ratio of the DS transmitted signal from the CO (17 dB).

Including the dispersion phenomenon (set C) in all fiber section (16 ps/nm·km) results in 0.1 to 0.2 dB increase of PP. Similar increase is recorded when RBS is included in the simulations (set D, RBS coefficient equal to -82 dB as specified in [140]). The BBS (set E) is not causing any extra PP for downstream transmission, fig. 7.19a.

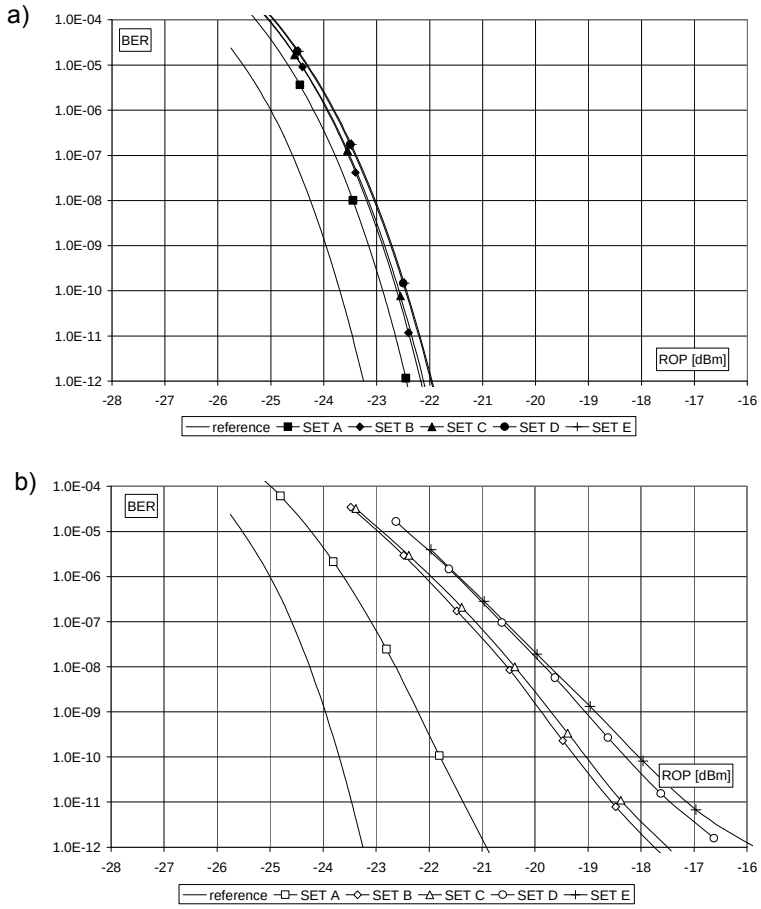

Figure 7.19: Simulation results for ONU 4.9-4.12 including BBS: a) DS and b) US.

Analysis of the US transmission

The results for US transmission show larger PP and also an increasing trend towards the last ONU.

For the simplest case (set A), the PP of 1.4-1.8 dB was mainly caused by the lower extinction ratio of the ONU modulator (11 dB) with respect to the reference modulator (17 dB) and the residual ASE noise after amplification at ONU.

Additional PP of 1.4 to 2.5 dB is recorded for set B, which is caused by the accumulation of the ASE noise over a number of cascaded amplifiers (4 downstream, 4 upstream and 1 in the ONU). This is close to the predictions in Chapter 5, where it was concluded that the ASE noise accumulated in an amplified-ONU system with the noise figure of each amplifier equal to 6 dB may bring 3.0 dB

PP[6].

Although, the influence of the dispersion (set C) is becoming visible (0.1 dB of PP increase for the longest lightpath) it is a negligible distortion in the transmission in this system.

After the ASE noise accumulation, one of the most important transmission impairments is the backscattering (set D), which remarkably increases the PP to 5.2 dB at maximum. This 1 dB difference with respect to set C for the last ONUs is a consequence of lower SCRs at ONU and CO as discussed in Section 7.3.1. It has been also verified that this transmission degradation is caused by RBS, whereas BBS (set E) has a minor contribution (0.1 dB) to the backscattering-induced power penalty as shown in fig. 7.19b.

7.4 Summary

The experiments of the 1.25 Gbit/s and 10 Gbit/s BBPhotonics access network proof the principle of the designed architecture. An error-free transmission of two wavelength channels of 1.25 Gbit/s each over the 26 km SSMF in a basic testbed was achieved and followed by an experiment with four wavelength channels of 10 Gbit/s each over 27 km network link in an upgraded testbed with a different architecture of ONU.

In each case all DS and US power penalties were identified. The extinction ratio is the major source for the power penalty difference between DS and US. The other main contribution to the US signal degradation is caused by the presence of RBS. In case of the 1.25 Gbit/s system it was minimized by spectral broadening and in case of a 10 Gbit/s system by proper gain settings of the ONU.

Using VPI [89] a full-scale 10 Gbit/s network was tested. It concerned a system with limited reconfigurability due split-ratio limitations in the OADM as discussed in Chapter 4.

Based on the measurement and simulation results and assuming improved filter response as well as loss parameters of the OADM, no major restrictions limiting the performance of the complete network are predicted. Although a significant power penalty is recorded for upstream transmission, still all signals could be received error-free (BER=10^{-9}). Enhancement of the network with more RNs will be accompanied by larger noise accumulation and increased power penalty. Therefore, when upscaling the network very low-noise amplifiers need to be applied [139].

[6]The system in Chapter 5 used to evaluate this PP consists of attenuators and amplifiers which correspond to the loss and gain values of the BBPhotonics and LR-BBPhotonics network designs. Since those values do not differ much between the two designs, as discussed earlier in this Section, one can expect similar noise accumulations and resulting power penalties.

Chapter 8

Migration towards WDM/TDM access network

This Chapter discusses the issues related to the implementation of NGA networks.

In Section 8.1 the hardware upgrade required to migrate from currently deployed fiber-optic access networks to WDM/TDM-PON is described based on [50]. It is followed by a discussion on the economics of the next-generation access networks in Section 8.2, which are considered to be the crucial aspect of the FTTx-based solutions.

8.1 Hardware upgrade

There are different intermediate solutions for FTTH enrollment, like: FTTC, FTTP or FTTB. For any of the above there is a variety of connectivity topologies, namely PtP or PtMP (TDM-PON, WDM-PON or WDM/TDM-PON).

The main advantage of PtP (home run) is that, apart from providing a complete channel with fully symmetric bandwidth per user, all maintenance is in two places only (CO, ONU) without any interruption to other subscribers in a given network. However, with respect to PON systems, an extra deployment cost is related to such installation mainly due to investment in the equipment at the CO.

TDM-PON (either in distributed or cascaded splitter configuration) brings some alleviation in the initial investment, as some resources (feeder fiber, CO equipment) are shared among a number of users. Here, the drawback is the reduction of available bandwidth per user due to a high splitting ratio which divides a single wavelength channel into user-dedicated time slots.

WDM-PON provides more transmission channels and so the network stretches to cover larger number of users. Moreover, such network upgrade is not related to significant ODN costs as the fiber plant can be reused, which is discussed later in

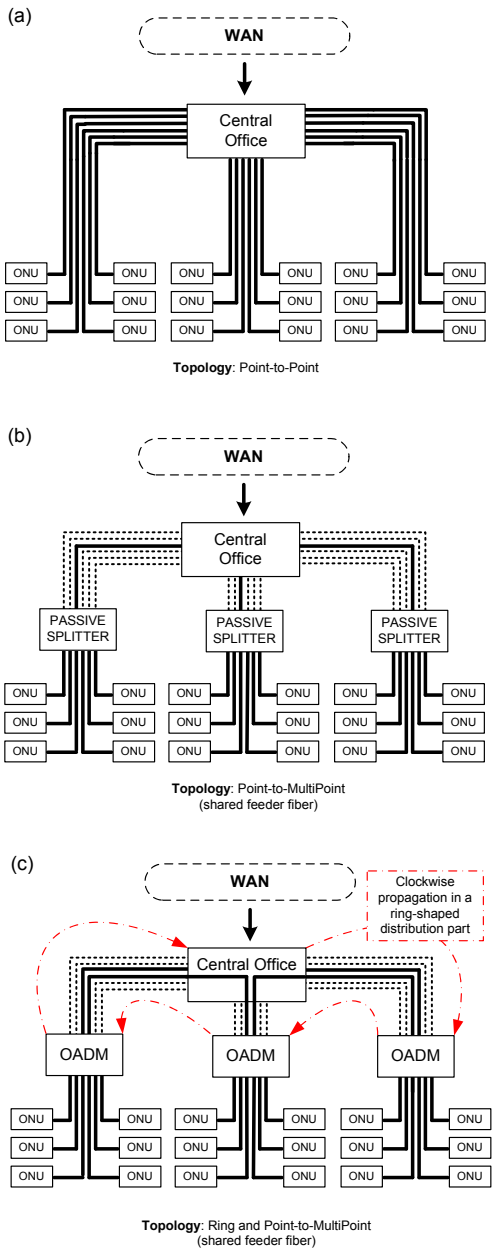

Figure 8.1: Migration scenario from existing a) PtP topology via b) PtMP topology to c) hybrid ring-PtMP topology (e. g. BBPhotonics).

this Section. Although the amount of feeder fibers is reduced in a WDM-PON, the amount of equipment in the CO is still large like in a corresponding fiber-PtP.

When considering an "open access" network model PtP topology enables sharing the infrastructure by a number of service providers simply by assigning a specific physical link or a group of links to one operator within a given access network. Therefore, a PtP topology based on a dedicated fiber or a dedicated wavelength (WDM-PON) is advantageous over PtMP TDM-PON.

Nowadays most of the green-field installations (e. g. in Europe) provide PtP connectivity as depicted in fig. 8.1a. Thus, when considering new services in the network a migration scenario to future-proof network is needed. Such upgrade should be as less noticeable to connected users as possible (short down-time) and should involve only minor investment.

In order to avoid high cost related to the initial upgrade a transition from PtP to several TDM-PON systems is proposed. This means that several passive splitters have to be installed somewhere between the CO and the ONUs. Depending on the topology it may be a cabinet in the street, building etc. For this purpose a single fiber can be reused from the previous PtP installation to connect a splitter to the CO. The PtP links from the splitter to ONUs may reuse the existing fibers and ducts. In the electric domain the upgrade requires installation of all TDM protocol-related resources, which may become a significant investment at this stage. On the other hand, the number of optical sources at the CO is reduced to the number of feeder fibers as shown in fig. 8.1b. Upgrading a fiber-PtP topology with 128 users with 100 Mbit/s bandwidth each to two 10GPON systems with 64 split-ratio each, will result in a similar bandwidth available per user.

The step towards WDM-PON is to exchange the equipment in the splitting points from passive splitters to wavelength (de-)multiplexers [32] and to implement an appropriate set of optical sources at the CO as well as wavelength-agile ONUs. The BBPhotonics Access project upgrades the access network to a hybrid WDM/TDM scheme which enables easy network scaling, and can provide capacity on-demand efficiently by means of flexible wavelength routing [50]. Therefore, passive splitters are changed to reconfigurable OADMs. As explained earlier, each wavelength pair in a WDM/TDM-PON serves a separate PON system (e. g. GPON). This requires as many OLTs as wavelength pairs. To dynamically reallocate the bandwidth over all PONs the MC and LCs have to be implemented at the CO and RNs, respectively, as explained in Chapter 2.

In order to improve the network protection the CO-RN distribution fibers topology is changed to a ring-shaped topology. Together with the variable 1x2 optical power splitter at the CO, it provides a protection path in case of a fiber break in the feeder ring. The connectivity at this stage does not change with respect to the TDM-PON. If some of the feeder fibers pass by the CO as indicated in fig. 8.1c, the existing fiber plant can be reused leading to lower upgrade costs[1].

[1]When OCDM is considered as a solution for TDM release, as suggested in Appendix A, more changes in the network are required. It involves the upgrade of the CO and ONUs, where the

Considering the above, it is clear that the migration towards a high-bandwidth and wavelength-reconfigurable fiber-optic access layer involves a substantial investment. However, this shall be eventually outweighed by the additional functionalities offered and, therefore, a return of investment.

8.2 Economics of WDM-PON

It may seem obvious that while driving down the NGA-related costs, such solutions are becoming more feasible. However, it is not that straightforward to draw a generic cost model for NGA networks as it depends on several factors:

- deployment scenario: greenfield or brownfield (network upgrade)
- available existing passive infrastructure to be reused: dark fiber, ducts, street cabinets etc.
- demographics: customer density, required network range etc.
- expected take rate defined as subscribed customers-to-passed customers ratio
- bandwidth demands (i. e. services) determining the choice of network solution and the resulting CAPEX and OPEX
- network model: open access or exclusive access network
- target group of customers: private, business or mix
- involvement of local authorities and national regulatory issues.

In spite of the proven fact that FTTH services can generate up to 20-30 % higher average revenue per user (ARPU) than DSL [141], the operators are reluctant with FTTH deployment since the economics of rolling out fiber access (500-1000 €) per termination [27]) require high market shares. In general, this is not compatible with an effective competition [142] and can be satisfied usually only by incumbents[2]. The incumbents can rely on the availability of major network elements needed for NGA, whereas alternative operators still have to invest to build their own infrastructure or to rent it. The latter one may generate lump-sum revenues to the incumbent very often owing such infrastructure. Alternative operators usually face a higher CAPEX also due to their size and risk position. Yet,

encoders and decoders have to be added. Additionally, a single high-speed modulator to produce the short pulses may be included in the CO, and that requires another stage of AWGs. The RNs are upgraded with a passive splitter to which all drop ports are connected. The fiber plant does not require any change, as the existing installation may be used again, which limits the cost of network upgrade.

[2]Incumbent - a company with extensive market power who first existed at regulated utilities with exclusive rights (i. e. monopoly) to serve a given area (e. g. country).

they may act as first movers in NGA deployments because their current business model as a whole is under threat.

The open access network model, which enables LLU (in fiber-PtP networks) or SLU[3] (in PtMP networks), is favored by alternative operators as it limits their initial investment considerably. It is also favored by policy makers as it enables the exploration of innovation and competition potential. Although the open access model aims for efficient investment so that the infrastructure is rolled out profitably with minimum risk for the economy and a maximum reach, it does not seem to be favorable to the incumbents who are afraid of return on investment (ROI) decrease after opening newly built infrastructure to their competitors. However, according to [142] the incumbents can reduce their costs by infrastructure sharing, increase the profitability of their NGA roll-out and reach this profitability with a lower level of retail market shares if they provide wholesale services (LLU or SLU). It suggests that the incumbents' investment may be supported rather than undermined through open access requirements and deliver market outcomes that are more compatible with effective competition at the same time.

The incumbents' search for wider revenue sources is the major catalyst for FTTH projects [143]. However, a typical European incumbent does not currently anticipate large-scale deployment of FTTH and most of them prefer a staged transition from ADSL to VDSL with FTTH following a few years after.

Municipal fiber networks offer an alternative to the network of the incumbent [144]. The deployment of those networks is a result of regional initiatives very often funded by municipalities and local authorities. The most important characteristic of municipal networks is open access. Usually, they are based on a layered model consisting of: service layer (e. g. triple play), active layer (e. g. optoelectronics) and passive layer (e. g. ducts). In such model suppliers of network equipment, services management, and services share the revenues. Alternatively to the incumbents' motivation, the principal aims of municipal networks deployment are: the support to the local business and the local economy, the prevention of outward migration of businesses and households, the aid to the local government, health and education, and the provision of a universal high-quality utility service to the local citizens.

Fair opening of the access networks to all operators has to be addressed by telecom regulators by emphasizing the structural limitations of infrastructure-based competition. Taking into account the expectations of the operators, preferred models for NGA deployment need to be identified. These should account for SLU at the metro core locations and LLU at the distribution points.

Passive power splitter architectures rely on complex TDM switching technologies in the active access equipment in order to achieve communications path to individual customers. This means that the full LLU (as possible with todays copper access or with a fiber-PtP architecture) is not feasible with such architectures,

[3]SLU - subloop unbundling, e. g. releasing the drop-fibers (from a splitter to an ONU) to different service providers.

which may be a problem for the service providers' business models. In such cases, an FTTC architecture with SLU in connection with a wholesale bitstream access might be a solution. However, as an SLU is possible only with the collocation at the splitter sites it is expensive especially for the market entrants.

The physical duct and fiber access infrastructure are seen as a natural monopoly by many regulators, i. e. the huge investment required to build the infrastructure means that the first provider to install such infrastructure in an area would typically deter any other entrant and so would end up as an incumbent by default [145]. Additionally, while the fiber infrastructure will be in place for 50 years or more, the active equipment enabling services across the infrastructure will be on a 5 to 10 year technology lifecycle. Therefore, in order to ensure that consumers gain the bandwidth and the advantages of emerging services, LLU should be enabled. This perspective of competition will drive the service providers to explore the bandwidth that the fiber access infrastructure offers today through deployment of successive new generations of active access equipment. Only an infrastructure that allows independent light paths to each customer can enable full LLU. In that respect wavelength-PtP (WDM-PON) is similar to fiber-PtP.

Assuming the availability of relevant passive infrastructure, the expenses for network devices in the central office, distribution point and subscriber site become a major expense. This part of CAPEX is the critical issue in the development of NGA architectures based on WDM-PON. It demands high take rate of at least 60 % to provide the lowest cost per subscriber per Mbit/s [146].

In table 8.1, based on [29], different PON solutions are compared in terms of DS and US bit-rates, split ratios and the ONU link cost relative to the cost of ONU link in a GPON system. There are two basic types of WDM: CWDM which works with cheap interfaces but only supports up to 18 different wavelengths, and DWDM whose interfaces are significantly more expensive, but offer up to 162 wavelengths each providing high bit-rate signals. Thanks to the multiwavelength transmission in a single fiber, deploying WDM equipment helps to overcome fiber scarcity. It is especially economically feasible where the deployment of additional fiber is more expensive and usually requires more time than the installation of a WDM solution, for instance in case of limited amount of lines in a network [142].

The integration of WDM and TDM in one PON system (hybrid WDM/TDM-PON) can increase the splitting ratio dramatically. From the perspective of unbundling WDM/TDM-PON offers optimal solutions, where each operator has its own wavelengths serving independent TDM-PON systems. Also, the optimum costs can be achieved when combinations of (C/D)WDM-PONs TDMA with different per-wavelength bit-rates ranging from 1 to 10 Gbit/s will be used [29].

The wavelength-reconfigurable WDM/TDM-PON (BBPhotonics) introduces the capability of more efficient optical bandwidth utilization. This yields a reduction of the resources at the CO with respect to a pure WDM-PON system. Fewer wavelength channels means fewer transmitters and fewer MUX/DEMUX ports. However, at the same time the cost of each RN rises as it contains tunable filters and electronics which require power supply. This can be provided by a

Table 8.1: Comparison of different PON systems [29].

System	DS/US bit-rate [Gbit/s/λ]	Max. split[I]	Max. power budget [dB]	ONU link cost[II]
GPON	2.5/2.5	64	5 (PIN)	100
EPON	1.25/1.25	32	5 (PIN)	78[III]
Splitter WDM-PON	10/10[IV]	32	8 (APD)	242[V]
AWG WDM-PON	10/10[IV]	40	10 (PIN)	256[V]
Multi-AWG PON	10/10[IV]	40	12 (APD)	300[V]
CWDM-PON	10/10[IV]	8	13 (PIN)	122[V]
CWDM/TDM-PON	1.25/1.25[VI]	64	11 (APD)	132[VII]
DWDM/TDM-PON	1.25/1.25[VIII]	160	11 (APD)	234[VII]
Ampl. DWDM-PON	10/10[IV]	40	$>$ 30 (PIN)	280[IX]
Ampl. DWDM/TDM-PON	1.25/1.25[VI]	320	$>$ 30 (PIN)	198[X]

[I] max. split ratios resulting either from the WDM technology or from the max. losses for the respective PON design;
[II] calculated for a dual-ended link, incl. the respective portion of common components (the sum of all components divided by the number of ONU links);
[III] rel. to GPON ONU link cost;
[IV] dedicated;
[V] rel. to GPON ONU link cost, calc. for 1 Gbit/s/λ;
[VI] 250 Mbit/s/ONU for 1:8 split and 2.5 Gbit/s aggregate bandwidth;
[VII] rel. to GPON ONU link cost, calc. for 2.5 Gbit/s/λ;
[VIII] 500 Mbit/s/ONU for 1:4 split and 2.5 Gbit/s aggregate bandwidth;
[IX] rel. to GPON ONU link cost, calc. for 1 Gbit/s/λ, 1 active node, booster and pre-amp at OLT;
[X] rel. to GPON ONU link cost, calc. for 2.5 Gbit/s/λ, 1 active node, booster and pre-amp at OLT;

dedicated connection to the public electric lines as for existing FTTN and FTTP networks [31]. In the best case, the additional costs of a complete switchable RN should be balanced by the savings gained at the CO[4]. Assuming a sufficient split ratio, the cost of such wavelength-reconfigurable system will be close to the cost of an amplified DWDM/TDM-PON as indicated in table 8.1.

[4]Alternatively, one may use a broadcast-and-select scheme where all wavelengths are sent to all ONUs, and at each ONU the desired wavelength is selected [23]. Due to wavelength-independent power splitting this approach requires a larger power budget and/or intermediate optical amplification and wavelength-selective ONUs.

Chapter 9

Conclusions and further work

In this Chapter, the conclusions from the research described in the thesis are given, Section 9.1. It is followed by set of possible future research directions based on the achieved results in Section 9.2.

9.1 Conclusions

The general conclusion is that the WDM-PON-based solutions, and in particular wavelength-reconfigurable access networks, have a great potential in satisfying increasing bandwidth demands. To achieve this in a cost-efficient way the emphasis has to be put on the optical integration, which enables relatively cheap mass production. As a result, significantly decreased network hardware costs contribute to quicker large-scale deployments of NGA solutions and enable access to novel network services for larger communities.

In this thesis, from technical point of view the concept of a dynamically reconfigurable WDM/TDM-PON architecture has been proved. This included development and testing of novel solutions for a high bit-rate wavelength-agile transceiver based on different reflective modulation mechanisms and an integrated micro-ring resonators structure for dynamic wavelength reconfiguration in the RN. The reflective ONU as well as the ROADM have been applied in the transmission testbed where a set of proof-of-principle experiments have been performed with bidirectional multiwavelength transmission of high bit-rate wavelength channels. Backscattering and backreflections have been extensively examined as one of the most critical transmission impairments in a single-fiber bidirectional link incorporating reflective ONU and solutions towards improvement have been proposed, realized and tested. The full-scale network model has been implemented in the simulation software and verified in terms of error-free transmission. Furthermore,

a migration scenario to a wavelength reconfigurable access network and the economical aspects of such network have been discussed.

The detailed results are given below per Chapter.

Chapter 1

- The subscriber needs large and symmetric bandwidth which is a result of emerging video-related services and P2P traffic.
- The location of the traffic congestion changes on a specific time-scale basis and the bandwidth needs to be adapted accordingly.
- Current access network installations are a bottle neck in the whole internet communication and a migration from copper-based to fiber-based NGA networks is required.
- Solutions based on WDM-PON (fixed or reconfigurable TDM/WDM-PON) are capable of addressing all NGA requirements from service providers and subscribers' viewpoint since they combine the advantages of PtP communication and PtMP infrastructure.
- Wavelength reconfigurability in the access domain improves the efficiency of the CO resources in a WDM-PON system and enables larger system loads.
- Network operators understand the need for fiber-optic access and an increase in FFTx deployment projects is noticed.

Chapter 2

- The BBPhotonics access network architecture aims to provide the end-users with high bandwidth available on-demand thanks to a dynamic wavelength reallocation.
- The wavelength reconfigurability requires wavelength-flexible nodes and colorless ONUs supported by a proper choice of wavelength set.
- The BBPhotonics access network is a stack of coloured TDM-PON systems where any ONU can be assigned to any OLT by proper network control and management protocol.

Chapter 3

- WDM-PON-based systems demand wavelength-independent ONUs among which laser-free reflective transceivers in combination with centralized light generation are the most promising ones in terms of cost-efficiency.
- OOK is the most favorable modulation scheme in the access domain as it works with only simple direct receivers.

- Due to fundamental limitations an RSOA is capable of modulation speeds up to a few Gbit/s, and for modulation speeds reaching 10 Gbit/s different approaches for reflective ONUs are proposed: REAM and MIM.

Chapter 4

- The examined ROADM is capable of providing unicast and multicast (incl. dynamic reconfiguration) operation with an uninterrupted service provisioning for a vast range of high bit-rate wavelength channels.

- Although it is obvious that such critical parameters as loss, filter response and temperature stability of the ROADM need to be improved, the micro-ring resonators reveal a great potential as cost-efficient wavelength-switching devices.

Chapter 5

- In terms of potential impairments, the most critical communication in the BBPhotonics network is in the US path.

- The accumulated ASE noise coming from a cascade of optical amplifiers in the DS CW and US data transmission adds a substantial power penalty at the CO receiver and is considered as the main impairment in the designed network.

- Since an access network concerns fiber-distances of max. 20-30 km, a significant power penalty is caused by interferometric crosstalk as a result of backscattering, which is a characteristic impairment in a system with centralized light generation, reflective ONUs and bidirectional transmission over a single-fiber.

- Another factor which may degrade the US receiver performance is the limited extinction ratio of the US transceiver.

Chapter 6

- The interferometric crosstalk which results in phase-induced amplitude variations arises from backscattering and/or backreflections and it is especially critical in links deploying RSOA.

- The interferometric crosstalk can be reduced by coherence disruption due to additional high frequency phase modulation of the optical carrier which in electrical domain results in shifting the noise out of data bandwidth.

- With respect to phase modulation at the laser a novel, cost-efficient and easy to implement method based on RSOA bias dithering shows a greater

potential in interferometric noise reduction in an RSOA-based WDM-PON system.

- The RSOA bias dithering technique is especially efficient in links where the danger of coherent crosstalk is high (e. g. discrete reflections), and in case of incoherent-type of crosstalk (e. g. RBS) phase modulation at the laser is more favorable.

Chapter 7

- The proof-of-concept transmission experiments have been successfully performed on the BBPhotonics access network testbed showing error-free US and DS bidirectional WDM transmission 1.25-10 Gbit/s wavelength channels over 27 km SSMF in different wavelength allocation schemes.

- The analysis of the obtained results confirmed the interferometric crosstalk, the extinction ratio and the ASE noise to be the key contributors to the overall power penalty in the US path, whereas the DS path does not suffer much from any such impairments.

- In the 1.25 Gbit/s system the influence of BS was effectively reduced by proper phase modulation, and in the 10 Gbit/s system similar improvement was achieved by proper gain settings at the ONU.

- The simulation results of the BBPhotonics architecture with reduced reconfiguration capabilities (LR-BBPhotonics) suggest error-free DS and US communication with all ONUs in the network.

- Assuming improved characteristics of the ROADM, no major restrictions limiting the performance of the complete network have been predicted.

Chapter 8

- Yet still not cost-competitive to current solutions, WDM-PON systems constitute next step in the migration towards high bandwidth access networks and, therefore, a clear upgrade scenario is needed.

- Flexible WDM/TDM-PON systems introduce efficient OLT resources utilization through dynamic wavelength allocation and, therefore, cost-efficiency with respect to wavelength-fixed WDM systems.

- With respect to network components the emphasis has to be put on the cost-reduction of the equipment in the CO, RN and especially ONU where the largest cost-savings can be achieved by optical integration.

9.2 Further work

In course of the work on the BBPhotonics access architecture concept, few research aspects were left unexplored or respective improvement directions were indicated. These are:

- The development of an MIM-based transceiver for a reflective ONU
- The implementation of higher order micro-ring resonators structure in the ROADM with improved filter response (improved multicast capability)
- The investigation of the influence of backscattering on the performance of the link with REAM and R-SOA-EAM
- The implementation of OCDMA in the BBPhotonics network, as suggested in Appendix A, and related enhancement of the BBPhotonics testbed.

Appendix A

Optical code division multiple access-extended BBPhotonics network architecture

The constraints originating from the time-slotting of the data from/to different users operating in TDM mode on the same wavelength (WDM/TDM) still requires a complex control and management layer. Optical code division multiplexing (OCDM) may alleviate this issue. Optical codes enable users to asynchronously access the network via optical orthogonal codes. This reduces the complexity because, for instance, strict time-scheduling is not needed in the network anymore. Moreover, it facilitates network scalability because OCDMA has soft capacity properties, i.e. no hard user limit is present at the expense of multiple user interference.

Let us consider the traffic handling in the BBPhotonics network, where DS traffic is centrally controlled at the CO while medium access has to be provided in case of US traffic. Shared access in BBPhotonics is enabled via TDMA on WDM. Instead, optical codes are proposed which rely on communication via a unique and (pseudo-)orthogonal code. In an optical code (OC) transmission system, the unique OC signs a logical one or both data bits depending on the modulation scheme. The orthogonality of the code allows the carrier to be asynchronously shared with other users on the network. OCDMA has its primary application in the access network because it offers cost-effective network deployment and management combined with physical layer security [147]. In this case, deploying OCDMA on BBPhotonics enables broadcasting the data in the DS direction. Moreover, on top of WDM it allows code re-usage per wavelength channel. It is clear that

OCDMA offers potential benefits to the reconfigurable BBPhotonics architecture as it alleviates the network from complex time-management schemes while offering dynamic networking behavior, inherently introducing transmission security and enabling fully symmetric communication channels, that is, bandwidth is equally available for US and DS traffic. A dynamical assignment of different codes may be used to obtain a variable quality of service (QoS) level per user.

A.1 Two-dimensional incoherent optical coding

Many different OCDMA systems have been demonstrated which may be classified by their coding principle, coding domain, optical sources, and en/decoder (E/D) implementation [148]. Taking a migration scenario into account, the aim in this work is to implement an optical coding technique which has the least impact on the BBPhotonics architecture while providing a solid performance. As a result a 2-D time-wavelength incoherent OCDMA system is considered with fully integratable E/Ds [149]. A four-user scenario has been experimentally demonstrated for such a system with a 2.5 Gbit/s channel per user employing multi-wavelength optical pulses which are matched to the 50 GHz ITU grid. It has been shown that for similar systems the number of simultaneous users can be significantly increased by using a number of different techniques [150]. From hereon the implementation of [149] in BBPhotonics is discussed because the bandwidth of active components in the network only allows for 2-D codes constructed by four wavelengths.

Essentially, the 2-D time-wavelength optical codes are constructed by short pulses which are arranged in time at four different wavelengths according to a hopping sequence. At the transmitter-side (TX) the binary source data is modulated via OOK thus a 2-D optical code is transmitted to represent a logical one and no information is sent in case of a logical zero. At the receiver-side (RX) the opposite time-delay configuration is used to reconstruct a high-intensity data signal via the incoherent summation of the pulses.

On the physical level, a multi-wavelength source produces a short-pulse train, which is modulated by an external modulator. The pulses are then encoded, via the method described above, after which they are denoted chips. During the encoding process, firstly the pulses are de-multiplexed by a wavelength demultiplexer (DEMUX) and most of them are given a defined time delay greater than zero. Then, the time-shifted pulses are combined by a wavelength multiplexer (MUX). This three-step operation is performed in a single device denoted encoder. The receiver subsequently decodes the received data stream by re-arranging the optical pulses with the opposite time-delays. Since the photodetector is wavelength agnostic, the incoherent summation of pulses at different wavelengths results in a high-intensity output (autocorrelation peak, ACP). Note that this only occurs for matched delays, and, of course, amplification is required at various stages of the setup in order to compensate for losses in the system. The codes have been designed in such a way that a non-matched set of delays results in a low-intensity

output (crosscorrelation peak, CCP). In other words, if encoded data is received from other users, only the CCP is detected. The CCP should therefore be as close to zero as possible through rigorous code design and accurately tuned encoders and decoders. An optical thresholder can be used in combination with optical time gating before detection in the receiver to virtually eliminate the detrimental effect of other users and as such improving the performance. Optical thresholding is preferred in such systems over optical time gating because the latter requires synchronization on a chip level and, therefore, effectively removes the advantage OCDMA has over TDMA [151].

A.2 Implementation of two-dimensional OCDMA in BBPhotonics network architecture

The system in [149] employs a mode-locked supercontinuum (SC) and spectral slicing to generate the multi-wavelength pulses. Four 50 GHz thin film filters (TFFs) are used to slice the SC spectrum according to the ITU grid. The pulses have a width of 9.5 ps before they are launched into the encoder. The encoder operates with a maximum pulse width of 9.8 ps in order to fit 41 chips in a 400 ps bit slot of a single carrier-hopping prime code according to [152]. A fiber-based encoder is employed using components such as passive splitters and fiber delay lines (FDLs), and only a DS scenario is evaluated by the authors.

According to the system in [149] four wavelengths (a quadruple) are required to construct 2-D codes per US and DS band in BBPhotonics. As a result, a total optical bandwidth of $2 \times 4 \times FSR_{OADM} = 4$ THz is required for deployment. Well-known pre- or post-dispersion compensation schemes may be required in order to compensate relative wavelength drifts because of the large total optical bandwidth. If we consider at least one shared pair of quadruples per RN, then a minimum of $4(\text{RNs}) \times 8(2 \times 4) = 32$ wavelengths need to be continuously available. This number increases if dynamic bandwidth provisioning is enabled in the OCDMA/WDM network such that more than one pair of quadruples is provided per RN.

Central office

In the BBPhotonics design, the CO is readily equipped with an array of multi-wavelength sources as shown in Chapter 2 for the US and DS traffic hence these available optical resources should be reused in order to meet the system requirements of [149]. As mentioned before, additional optical sources may be required depending on the demands in the network. A revised architecture of the CO is shown in fig. A.1 in which communication via 2-D optical codes is enabled.

Basically, all sources are operated in CW mode after which a single external modulator produces the pulse train at all wavelengths simultaneously with pulses smaller than 10 ps. The MUX and DEMUX operations are done by using AWGs with a matching channel spacing. For sake of simplicity, the upper half of the

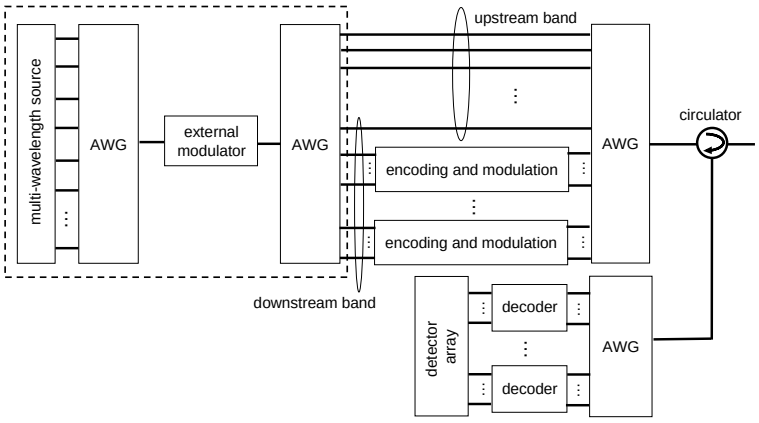

Figure A.1: Central office enabling 2-D OCDMA in BBPhotonics.

pulsed wavelength channels are directly multiplexed toward the single output of the CO. Therefore, these channels constitute the un-modulated and non-coded US bands. The lower half of the channels are encoded and modulated for DS data transmission. Alternatively, the multi-wavelength array in fig. A.1 can be replaced by SC sources or individual mode-locked laser diodes (MLLDs) which would replace all components in the dashed box. The SC sources used in [149] provide pulses with a relatively flat spectrum of about 12 nm which are spectrally sliced. As such only several SC sources are required with respect to the total optical bandwidth of the system. Another option may be the recently shown ultra-fast integrated MLLDs fabricated in InP/InGaAsP [153]. These stable, compact and small footprint pulse sources introduce a cost-reduction regarding the required optical hardware at the transmitter.

Additionally, compared with the system in [149], the encoder and decoder in fig. A.1 may be equipped with AWGs as (DE-)MUX components instead of passive splitters and TFFs. Large-port AWGs are well-known devices and can be easily combined with tunable delay lines on a single photonic chip with other optical functions and may provide lower device losses.

Remote node

The OADM in the RN operates in a similar way as in the basic BBPhotonics design given in Chapter 2, so the periodicity of the OADM is used to drop all 8 equally-spaced wavelengths. The wavelengths constituting the US and DS band are alternatively positioned in the optical spectrum and spaced by FSR_{OADM}. The use of optical codes in the network prohibits an US wavelength band to be dropped at multiple ports of one or more OADMs because user data is asynchronously multiplexed in the US direction. In other words, modulated US data arriving at

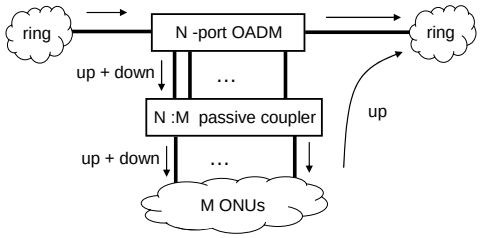

Figure A.2: Remote node enabling 2-D OCDMA in BBPhotonics.

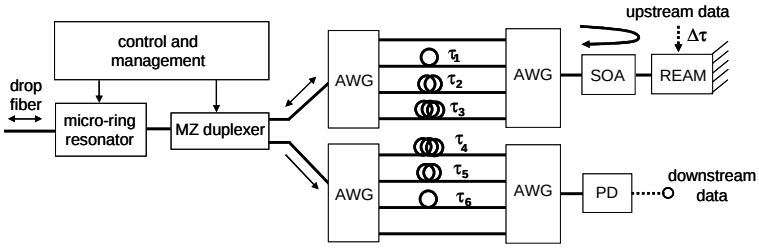

Figure A.3: Architecture of the optical networking unit enabling 2-D OCDMA in BBPhotonics.

a first port may not be partly dropped at a second port because it would cause significant interference. In case of the original TDMA this was allowed because the use of access control via time management schemes. As a result of this restriction, an $N : M$ passive coupler is added to the RN in order to broadcast all dropped wavelengths to the M connected ONUs as shown in fig. A.2 for the revised RN architecture.

As shown, all N outputs of the OADM are connected to the passive coupler to enable dynamic bandwidth-on-demand provisioning by dropping multiple US wavelength bands. If only one port is operated, all M ONUs can asynchronously access the network via the single broadcasted four-wavelength US band. If two or more ports are operated, multiple wavelength bands are dropped which can be accessed by all ONUs using their optical code. The multiplexed encoded data streams in the US direction are automatically blocked by all ports not tuned to the correct wavelength band.

Optical networking unit

As mentioned in Chapter 3 the ONU is equipped with a reflecting modulator. A reflective 2-D OCDMA ONU is shown in fig. A.3, which enables the system to be used in a reflecting configuration on top of a reconfigurable WDM scheme. The filter pattern layout of the architecture is shown in fig. A.4.

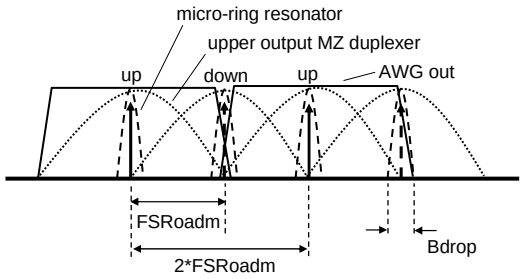

Figure A.4: Filter scheme applied in the the optical networking unit enabling 2-D OCDMA in BBPhotonics.

The principle of operation is as follows. The micro-ring resonator has the same FSR and drop band as the OADM, therefore, it can tune to the same wavelength band. The periodicity of the tunable MZ duplexer equals to $2 \times FSR_{OADM}$ and it is used to de-multiplex the US and DS channels at its two outputs. Both are controlled by a control and management block. The modulated and encoded DS data is processed by a decoder while the un-modulated and non-coded pulse train is processed by the reflective encoder. The reader should note that the time-delays in the reflective encoder are half of the required time shifts at a regular encoder because after amplification by the SOA and modulation by the REAM the pulses pass the encoder for the second time. As a result, the reflective encoder is half the size of a regular encoder. The AWGs with a channel spacing of $2 \times FSR_{OADM}$ ensure the correct de-multiplexing of the pulses at the encoder. Note that the data signal that drives the REAM needs to be adequately timed in order to provide a correct "gating" of the incoming unmodulated pulse train. This only needs to be once since the time delay between CO and ONU may be considered as fixed.

Appendix B

RSOA simulation model

In the simulation software a transmission-line laser model (TLLM) is used to describe the behavior of an SOA [89]. The idea of a TLLM is based on the algorithm design methods introduced by Johns and Beurle in their transmission-line matrix method of simulating microwave cavities in the time-domain by using meshes of transmission-lines [154, 155]. In a transmission line model, a device is separated in longitudinal sections which are simulated separately [156]. In each section, gain, loss and noise are calculated, after which the results are passed on to the next section via a transmission-line, representing the waveguide propagation delay. In the sections, a laser model is used to calculate the influence of this section on the optical signals, taking all other parameters constant. Of course the internal reflections in these sections are ignored. The number of sections a SOA is divided in depends on the sampling frequency. Each section is regarded as a spot, which reduces calculation time drastically. The most important assumption taken in the TLLM is that the generated carrier-density by drive current is homogeneous over the entire device length.

The parameters of the model are given in table B.1.

Table B.1: RSOA model parameters [62].

Parameter	Value
laser chip length	$505.56 \cdot 10^{-6}$ m
active region width	$1.2 \cdot 10^{-6}$ m
active region thickness	$0.056 \cdot 10^{-6}$ m
MQW confinement factor	0.045
group effective index	3.0
left facet reflectivity	10^{-7}
right facet reflectivity	0.3
optical coupling efficiency	0.5
fixed internal loss	1000 m^{-1}
MQW material linewidth enhancement factor	3.0
MQW differential refractive index	$-1.11 \cdot 10^{-26}$ m^3
chirp reference carrier density	$2.0 \cdot 10^{24}$ m^{-3}
current injection efficiency	1.0
bimolecular recombination coefficient	$2.0 \cdot 10^{-18}$ $\mathrm{m}^3\mathrm{s}^{-1}$
Auger recombination coefficient	$1.3 \cdot 10^{-41}$ $\mathrm{m}^6\mathrm{s}^{-1}$
linear material gain coefficient	$6.7 \cdot 10^{-20}$ m^2
transparency carrier density	$2.0 \cdot 10^{24}$ m^{-3}
nonlinear gain coefficient	$1.0 \cdot 10^{-22}$ m^3
nonlinear gain time-constant	$200 \cdot 10^{-15}$ s
gain coefficient spectral width	$1.0 \cdot 10^{13}$ Hz
population inversion parameter	2.0
spontaneous emission spectral width	$4.7 \cdot 10^{12}$
initial carrier density	$1.0 \cdot 10^{24}$ m^{-3}
carrier capture time-constant	$70 \cdot 10^{-12}$ s
carrier escape time-constant	$140 \cdot 10^{-12}$ s

Appendix C

The BBPhotonics testbed

Figure C.1: The BBPhotonics testbed in the Network Laboratory, COBRA Research Institute, Eindhoven University of Technology, The Netherlands, April 2009.

References

[1] J. Hecht. *City of light: the story of fiber optics*. Oxford University Press, 2004.

[2] D. R. Goff. *Fiber optic reference guide, A practical guide to communications technology*. Focal Press Woburn, Massachusetts, 2002.

[3] Sandvine. Global broadband phenomena, Executive report. 2008.

[4] FierceIPTV - The IPTV weekly monitor. So many streamers, so little bandwidth. *http://www.fierceiptv.com*, 2007.

[5] P. J. Urban. Bliski koniec DSL (*Nearing the end of DSL*). *IDG Computerworld Poland*, (34), 2008.

[6] M. J. O'Mahony, C. Politi, D. Klonidis, R. Nejabati, and D. Simeonidou. Future optical networks. *IEEE J. Lightw. Technol.*, 24(12):4684–4696, 2006.

[7] Y. Xiao, X. Du, J. Zhang, F. Hu, and S. Guizani. Internet protocol television (IPTV): the killer application for the next-generation internet. *IEEE Commun. Mag.*, 45(11):126–134, 2007.

[8] R. W. Heron, T. Pfeiffer, D. T. van Veen, J. Smith, and S. S. Patel. Technology innovation and architecture solutions for the next-generation optical access network. *Bell Labs Technical J.*, 13(1):163–182, 2008.

[9] K. Cho, K. Fukuda, H. Esaki, and A. Kato. The impact and implications of the growth in residential user-to-user traffic. In *Proc. SIGCOMM 2006*, pages 207–218.

[10] M&I Partners. Fiber speed demonstration version 1.2. November 2003.

[11] C.-H. Lee, W. V. Sorin, and B. Y. Kim. Fiber to the home using a PON infrastructure. *IEEE J. Lightw. Technol.*, 24(12):4568–4583, 2006.

[12] A. M. J. Koonen. Flexible wavelength multiplexing techniques for broadband fibre access networks. *Telektronikk*, 95(2/3):119–128, 1999.

[13] A. M. J. Koonen. Fiber to the home/fiber to the premises: what, where, and when? *IEEE Proceedings*, 94(5):911–934, 2006.

[14] ITU-T. *G.993.2 Recommendations*. 2006.

[15] ITU-T. *G.983 Recommendations*. 2002.

[16] IEEE. *802.3ah Standard*. 2004.

[17] ITU-T. *G.984 Recommendations*. 2005.

[18] S. Wilkinson. Next-generation PON options promise greater bandwdith. *Lightwave*, July 2008.

[19] P. J. Urban. Swiatłowodem do klienta (*Fiber to the customer*). *IDG NetWorld Poland*, (1), 2009.

[20] Z. Belfqih, F. Saliou, P. Chanclou, T. Soret, and N. Genay. Bidirectional amplifier for standard PON architecture in burst mode configuration with class B+ attenuation range. In *Proc. OFC 2007*, paper OWS1.

[21] Keymile International GmbH. AON vs PON - A comparison of two optical access network technologies and the different impact on operations. *www.keymile.com (white paper)*, pages 1–14, 2008.

[22] J. Baliga, R. Ayre, W. V. Sorin, K. Hinton, and R. S. Tucker. Energy consumption in access networks. In *Proc. OFC 2008*, paper OThT6.

[23] A. M. J. Koonen, T. Muys, C. van der Plaats, S. M. Heemstra de Groot, H. J. H. N. Kenter, I. G. M. M. Niemegeers, and F. N. C. Slothouber. TOBASCO: An innovative approach for upgrading CATV fiber-coax networks for broadband interactive services. *IEEE Commun. Mag.*, 35(4):76–81, 1997.

[24] A. M. J. Koonen, K. Steenbergen, F. Janssen, and J. Wellen. Flexibly reconfigurable fiber-wireless network using wavelength routing techniques: the ACTS project AC349 PRISMA. *Photonic Network Communications*, 3(3):297–306, 2001.

[25] E. Yetginer and E. Karasan. Dynamic wavelength allocation in IP/WDM metro access networks. *IEEE J. Sel. Areas in Commun.*, 26(3):13–27, 2008.

[26] R. Rubenstein. Optical integration moves back onto the agenda. *Fibre Systems Europe*, pages 14–17, May 2006.

[27] E. Iannone. Passive optical networks must evolve to survive. *Fibre Systems Europe*, pages 26–27, January 2008.

[28] P. W. Shumate. Fiber-to-the-home: 1977-2007. *IEEE J. Lightw. Technol.*, 26(9):1093–1103, 2008.

[29] K. Grobe and J.-P. Elbers. PON in adolescence: from TDMA to WDM-PON. *IEEE Commun. Mag.*, 46(1):26–34, 2008.

[30] A. Banerjee, Y. Park, F. Clarke, H. Song, S. Yang, G. Kramer, K. Kim, and B. Mukherjee. Wavelength-division-multiplexed passive optical network (WDM-PON) technologies for broadband access: a review. *OSA J. Opt. Netw.*, 4(11):737–757, 2005.

[31] G. Keiser. *FTTX concepts and applications*. New Jersey: John Wiley & Sons, Inc., 2006.

[32] F.-T. An, D. Gutierrez, K. S. Kim, J. W. Lee, and L. G. Kazovsky. SUCCESS-HPON: a next-generation optical access architecture for smooth migration from TDM-PON to WDM-PON. *IEEE Commun. Mag.*, 43(11):40–47, 2005.

[33] J. Prat, P. E. Balaguer, J. M. Gené, and O. Diaz. *Fiber-to-the-home technologies*. Kluwer Academic Publishers, 2002.

[34] G. Talli, C. W. Chow, P. Townsend, R. Davey, T. de Ridder, X.-Z. Qui, P. Ossieur, H.-G. Krimmel, D. Smith, I. Lealman, A. Poustie, S. Randel, and H. Rohde. Integrated metro and access network PIEMAN. In *Proc. NOC 2007*, pages 493–500.

[35] J. A. Lazaro, J. Prat, P. Chanclou, G. M. Tosi Beleffi, A. Teixeira, I. Tomkos, R. Soila, and V. Koratzinos. Scalable extended reach PON. In *Proc. OFC 2008*, paper OThL2.

[36] I. van de Voorde, C. M. Martin, and J. Vandewege. The SuperPON demonstrator: an exploration of possible evolution paths for optical access networks. *IEEE Commun. Mag.*, 38(2):74–82, 2000.

[37] S. A. Jabar. Alternative architectures for bidirectional single mode fiber SuperPON 512 ONU, 100 km. In *Proc. IEEE TENCON 2005*, pages 1–5.

[38] A. M. J. Koonen, A. Ng'oma, G.-J. Rijckenberg, M. Garcia Larrode, P. J. Urban, H. de Waardt, J. Yang, H. Yang, and H. P. A. van den Boom. How deep should fiber go into the access network? In *Proc. ECOC 2007*, paper M.1.1.4.

[39] C. Paquet. The current and future access networks: an equipment provider's viewpoint. In *e-Photon ONe Summer School 2007*.

[40] R. Montagne. The market's evolution to very high-speed. *IDATE Consulting & Research*, 2006.

[41] Yano Research Institute Ltd. Fiber-optic telecommunication market in Japan: FTTH, a key driver to bring NGN. (paper C48112900), 2006.

[42] G. Finnie. FTTH in Europe: forecast & prognosis, 2006-2011. *Heavy Reading, www.ftthcouncil.eu.*

[43] P. J. Urban. Optyczna rewolucja (*Optical revolution*). *IDG Computerworld Poland*, (47), 2007.

[44] Tariff Consultancy Ltd. FTTH pricing in Europe 2009.

[45] The European Broadband Portal. Regulated access to next generation networks NGA. *Broadband flash*, (2), 2008.

[46] R. Rubenstein. WDM-PON blurs the boundary between metro and last mile. *FibreSystems Europe*, January 2009.

[47] P. J. Urban. Polski broadband (*The Polish broadband*). *IDG Computerworld Poland*, (28), 2008.

[48] M. Forzati and C. P. Larsen. Broadband access and its impact on the economy, a swedish perspective. In *Proc. IEEE ICTON 2008*, paper Th.A2.3.

[49] A. M. J. Koonen and H. de Waardt. *BBPhotonics - dynamically reconfigurable broadband photonic access networks (project plan).* Eindhoven University of Technology, Eindhoven, The Netherlands, 2004.

[50] P. J. Urban, B. Huiszoon, R. Roy, M. M. de Laat, F. M. Huijskens, G. D. Khoe, A. M. J. Koonen, and H. de Waardt. High bit rate dynamically reconfigurable WDM/TDM access network. *IEEE/OSA J. Opt. Commun. and Netw.*, 1(2):A143–A159, 2009.

[51] C. Roeloffzen, G. Manhoudt, G. van den Hoven, P. Stassar, T. Koonen, and H. de Waardt. BBPhotonics project deliverable 1.1: Service and network requirements. *Freeband*, March 2005.

[52] T. Koonen, P. Urban, E. Pluk, H. de Waardt, and G. van den Hoven. BBPhotonics project deliverable 1.3: First design of reconfigurable access network, first specifications for components and modules. *Freeband*, December 2005.

[53] E. J. Klein, P. J. Urban, G. Sengo, L. T. H. Hilderink, M. Hoekman, R. Pellens, P. van Dijk, and A. Driessen. Densely integrated microring resonator based photonic devices for use in access networks. *OSA Optics Express*, 15(16):10346–10355, 2007.

[54] T. Nakanishi, K.-I. Suzuki, Y. Fukada, N. Yoshimoto, M. Nakamura, K. Kato, K. Nishimura, Y. Ohtomo, and M. Tsubokawa. High sensitivity APD burst-mode receiver for 10 Gbit/s TDM-PON system. *IEICE Electronics Express*, 4(19):588–592, 2007.

[55] P. J. Urban, R. Roy, E. G. C. Pluk, and H. de Waardt. BBPhotonics project deliverable 1.4-1.5: FlexPON network design and MAC protocol description. *Freeband*, June 2006.

[56] VPI TransmissionMaker. Gain-clamped SOA. *http://www.vpiphotonics.com/App_SemLasersPICs_GainCSOA.php*, available on 06/09/2009.

[57] L. Xu. *Monolithic integrated reflective transceiver in indium phosphide*. PhD thesis, Eindhoven University of Technology, Eindhoven, The Netherlands, 2009.

[58] R. Roy, G. Manhoudt, and W. van Etten. Bandwidth re-distribution techniques for extended EPON based multi-wavelength networks. In *Proc. IEEE ICTON 2007*, paper Mo.P.21.

[59] R. Roy, G. Manhoudt, C. Roeloffzen, and W. van Etten. Control and management scheme in a DWDM EPON. In *Proc. IEEE ICTON 2006*, paper Tu.D1.6.

[60] P. J. Urban, E. G. C. Pluk, A. M. J. Koonen, G. D. Khoe, and H. de Waardt. First design of dynamically reconfigurable broadband photonic access networks (BBPhotonics). In *Proc. IEEE LEOS Benelux Symposium 2005*, pages 117–120.

[61] P. J. Urban, E. J. Klein, L. Xu, E. G. C. Pluk, A. M. J. Koonen, G. D. Khoe, and H. de Waardt. 1.25-10 Gbit/s reconfigurable access network architecture. In *Proc. IEEE ICTON 2007*, paper Th.B1.6.

[62] E. G. C. Pluk. M. Sc. Thesis: Dynamic performance analysis of reflective semiconductor optical amplifiers. Master's thesis, Eindhoven University of Technology, Eindhoven, The Netherlands, 2006.

[63] R. L. Duijn. M. Sc. Thesis: Solutions toward high-speed colorless optical network units. Master's thesis, Eindhoven University of Technology, Eindhoven, The Netherlands, 2007.

[64] J. Rong. Internship Report. Master's thesis, Eindhoven University of Technology, Eindhoven, The Netherlands, 2009.

[65] N. J. Frigo, P. P. Iannone, P. D. Magill, T. E. Darcie, M. M. Downs, B. N. Desai, U. Koren, T. L. Koch, C. Dragone, H. M. Presby, and G. E. Bodeep. A wavelength-division multiplexed passive optical network with cost-shared components. *IEEE Photon. Technol. Lett.*, 6(11):1365–1367, 1994.

[66] A. Garreau, J. Decobert, C. Kazmierski, M. C. Cuisin, J. G. Provost, H. Sillard, F. Blache, D. Carpentier, J. Landreau, and P. Chanclou. 10 Gbit/s amplified reflective electroabsorption modulator for colorless access networks. In *Proc. IPRM 2006*, pages 168–170.

[67] E. K. MacHale, G. Talli, and P. D. Townsend. 10 Gbit/s hybrid DWDM-TDM PON for long-reach optical access. In *Proc. IET ICAT 2006*, pages 37–40.

[68] I. Tafur-Monroy, F. Öhman, K. Yvind, R. Kjaer, C. Peucheret, A. M. J. Koonen, and P. Jeppesen. 85 km long-reach PON system using a reflective SOA-EA modulator and distributed Raman fiber amplification. In *Proc. IEEE LEOS Annual Meeting 2006*, pages 705–706.

[69] N. Buldawoo, S. Mottet, H. Dupont, D. Sigogne, and D. Meichenin. Transmission experiment using a laser amplifier-reflector for DWDM access network. In *Proc. ECOC 1998*, 273-274.

[70] P. Healey, P. Townsend, C. Ford, L. Johnston, P. Townley, I. Lealman, L. Rivers, S. Perrin, and R. Moore. Spectral slicing WDM-PON using wavelength-seeded reflective SOAs. *IEE Electronics Lett.*, 37(19):1181–1182, 2001.

[71] W. Lee, M.-Y. Park, S.-H. Cho, J. Lee, C. Kim, G. Jeong, and B.-W. Kim. Bidirectional WDM-PON based on gain-saturated reflective semiconductor optical amplifiers. *IEEE Photon. Technol. Lett.*, 17(11):2460–2462, 2005.

[72] H.-D. Kim, S.-G. Kang, and C.-H. Lee. A low-cost WDM source with an ASE injected Fabry-Perot semiconductor laser. *IEEE Photon. Technol. Lett.*, 12(8):1067–1069, 2000.

[73] Y. J. Wen and C. J. Chae. WDM-PON upstream transmission using Fabry-Perot laser diodes externally injected by polarization-insensitive spectrum-sliced supercontinuum pulses. *Optics Commun.*, 260:691–695, 2006.

[74] D. J. Shin, D. K. Jung, H. S. Shin, J. W. Kwon, S. Hwang, Y. Oh, and C. Shim. Hybrid WDM/TDM-PON with wavelength-selection-free transmitters. *IEEE/OSA J. Lightw. Technol.*, 23(1):187–195, 2005.

[75] H. C. Kwon, W. S. Jang, and S. K. Han. Optimisation of remote seeding optical source in wavelength-locked FP-LD bidirectional WDM access optical link. *IEE Optoelectronics Proc.*, 152(5):247–249, 2005.

[76] L. Xu, X. J. M. Leijtens, M. J. H. Sander-Jochem, T. de Vries, Y. S. Oei, P. J. van Veldhoven, R. Nötzel, and M. K. Smit. InP-based polarization insensitive tunable duplexer and integrated reflective transceiver. In *Proc. ECIO 2007*, pages 1–4.

[77] L. Xu, M. van Heijningen, G. van der Bent, P. J. Urban, X. J. M. Leijtens, E. Smalbrugge, T. de Vries, R. Nötzel, Y. S. Oei, H. de Waardt, and M. K. Smit. Hybrid InP-SiGe photoreceiver for the access network. In *Proc. IEEE LEOS Annual Meeting 2008*, pages 121–122.

[78] L. Xu, M. van Heijningen, G. van der Bent, P. J. Urban, X. J. M. Leijtens, E. Smalbrugge, T. de Vries, R. Nötzel, Y. S. Oei, H. de Waardt, and M. K. Smit. 4 Gbit/s hybrid InP-SiGe photoreceiver for the user access network. In *Proc. IEEE LEOS Benelux Symposium 2008*, pages 83–86.

[79] L. Xu, X. J. M. Leijtens, P. J. Urban, E. Smalbrugge, T. de Vries, R. Nötzel, Y. S. Oei, and M. K. Smit. Novel reflective SOA with MMI-loop mirror based on semi-insulating InP. In *Proc. IEEE LEOS Benelux Symposium 2008*, pages 43–46.

[80] L. Xu, X. J. M. Leijtens, P. J. Urban, E. Smalbrugge, T. de Vries, R. Nötzel, Y. S. Oei, and H. de. Waardt. InP-based monolithic integrated colorless reflective transceiver. In *Proc. ECIO 2008*, pages 13–16.

[81] H. de Waardt. *High capacity 1300 nanometer optical transmission.* PhD thesis, Technische Universiteit Delft, Delft, The Netherlands, 1995.

[82] T. P. Lee. Effect of junction capacitance on the rise time of LED's and on the turn-on delay on injection lasers. *Bell Labs Technical J.*, 54(1):53–68, 1975.

[83] U. Koren, B. I. Miller, M. G. Young, M. Chien, G. Raybon, T. Brenner, R. Ben-Michael, K. Dreyer, and R. J. Capik. Polarization insensitive semiconductor optical amplifier with integrated electroabsorption modulators. *IEE Electronics Lett.*, 32(2):111–112, 1996.

[84] G. Talli and P. D. Townsend. Hybrid DWDM-TDM long-reach PON for next-generation optical access. *IEEE J. Lightw. Technol.*, 24(7):2827–2834, July 2006.

[85] I. Tafur-Monroy, F. Öhman, K. Yvind, L. Jin-Christiansen, J. Mrk, C. Peucheret, and P. Jeppesen. Monolithically integrated reflective SOA-EA carrier re-modulator for broadband access nodes. *OSA Optics Express*, 14(18):8060–8064, 2006.

[86] F. Zernike and J. C. Webster. Amplitude modulators based on the Michelson interferometer. *IEEE Trans. on Sonics and Ultrasonics*, 3:163–167, 1972.

[87] P. J. Duthie, M. J. Wale, I. Bennion, and J. Hankey. Bidirectional fiber-optic link using reflective modulation. *IEE Electronics Lett.*, 22(9):517–518, 1986.

[88] D. Caprioli, J. H. den Besten, E. Smalbrugge, T. J. de Vries, X. J. M. Leijtens, and M. K. Smit. A 10 Gb/s traveling wave MZ-modulator for integration with a laser. In *Proc. ECIO 2003*, pages 145–148.

[89] VPI TransmissionMaker. *http://www.vpiphotonics.com.*

[90] E. J. Klein. *Densely integrated microring-resonator based components for fibe-to-the-home applications*. PhD thesis, University of Twente, Enschede, The Netherlands, 2007.

[91] D. H. Geuzebroek. *Flexible optical network components based on densely integrated microring resonators*. PhD thesis, University of Twente, Enschede, The Netherlands, 2007.

[92] N. Calabretta, P. J. Urban, D. H. Geuzebroek, E. J. Klein, H. de Waardt, and H. J. S. Dorren. Exploiting micro-ring resonators for all-optical label extractor/eraser of inband labels and 160 Gbit/s payload. In *Proc. IEEE LEOS Benelux Symposium 2008*, pages 11–14.

[93] N. Calabretta, P. J. Urban, D. H. Geuzebroek, E. J. Klein, H. de Waardt, and H. J. S. Dorren. All-optical label extractor/eraser for in-band labels and 160 Gbit/s payload based on micro-ring resonators. In *Proc. OFC 2009*, paper OWV4.

[94] N. Calabretta, P. J. Urban, D. H. Geuzebroek, E. J. Klein, H. de Waardt, and H. J. S. Dorren. All-optical label extractor/eraser for in-band labels and 160 Gbit/s payload based on micro-ring resonators. *IEEE Photon. Technol. Lett.*, 21(9):560–562, 2009.

[95] A. M. J. Koonen, S. M. Heemstra de Groot, C. A. M. Steenbergen, and I. G. M. M. Niemegeers. Reconfigurable broadband fibre-wireless network employing dynamic wavelength allocation. In *Proc. IEEE ECOC 1998*, volume 1, pages 577–578.

[96] T. Zami, F. Dorgeuille, L. Niorie, N. L. Sauze, and A. Jourdan. Optical metro-access ring featuring a flexible color management. In *Proc. OFC 2004*, paper WG6.

[97] A. Geha, C. Mas, B. Vermeulen, and J. Wellen. HARMONICS, an IP based service network over hybrid fibre-access network supporting QoS. In *Proc. 10th Intern. Conf. on Telecommunications 2003*, pages 628–633.

[98] Y.-L. Hsueh, M. S. Rogge, W.-T. Shaw, L. G. Kazovsky, and S. Yamamoto. SUCCESS-DWA: A highly scalable and cost-effective optical access network. *IEEE Commun. Mag.*, 42(8):S24–S30, 2004.

[99] C. Bock, J. Prat, and S. D. Walker. Hybrid WDM/TDM PON using the AWG FSR and featuring centralized light generation and dynamic bandwidth allocation. *IEEE/OSA J. Lightw. Technol.*, 23(12):3981–3988, 2005.

[100] D. H. Geuzebroek, E. J. Klein, H. Kelderman, N. Baker, and A. Driessen. Compact wavelength-selective switch for gigabit filtering in access networks. *IEEE Photon. Technol. Lett.*, 17(2):336–338, 2005.

[101] LioniX. TriPleX^{TM} planar waveguide circuits. *www.lionixbv.nl (white paper)*, pages 1–2, 2009.

[102] A. Driessen, D. H. Geuzebroek, E. J. Klein, R. Dekker, R. Stoffer, and C. Bornholdt. Propagation of short lightpulses in microring resonators: ballistic transport versus interference in the frequency domain. *Optics Commun.*, 270:217–224, 2007.

[103] D. H. Geuzebroek, E. J. Klein, H. Kelderman, C. Bornholdt, and A. Driessen. 40 Gbit/s reconfigurable optical add-drop multiplexer based on microring resonators. In *Proc. IEEE ECOC 2005*, volume 4, pages 983–986.

[104] C. K. Madsen and J. H. Zhao. *Optical filter design and analysis: a signal processing approach.* John Willy & Sons, Inc., 1999.

[105] O. Schwelb. Transmission, group delay, and dispersion in single-ring optical resonators and add/drop filters - a tutorial overview. *IEEE/OSA J. Lightw. Technol.*, 22(5):1380–1394, 2004.

[106] D. Geuzebroek. private communcation, February 2009.

[107] M. M. de Laat. M. Sc. Thesis: Wavelength routing enables dynamic bandwidth reconfiguration in flexible passive optical networks. Master's thesis, Eindhoven University of Technology, Eindhoven, The Netherlands, 2008.

[108] R. Ramaswami and K. N. Sivarajan. *Optical networks: A practical perspective.* London: Morgan Kaufmann, 2002.

[109] G. P. Agrawal. *Fiber-optic communication systems.* John Willy & Sons, Inc., 2002.

[110] Agilent Technologies, Inc. Polarization pependent loss: measurement of passive optical components. *www.home.agilent.com (application note)*, pages 1–12, 2002.

[111] J. Powers. *An introduction to fiber optic systems.* McGraw-Hill International Editions, 1996.

[112] P. J. Urban, A. M. J. Koonen, G. D. Khoe, and H. de Waardt. Coherent crosstalk-suppression in WDM access networks employing reflective semiconductor optical amplifiers. In *Proc. IEEE ECOC 2007*, volume 3, pages 91–92.

[113] P. J. Urban, A. M. J. Koonen, G. D. Khoe, and H. de Waardt. Rayleigh backscattering-suppression in a WDM access network employing a reflective semiconductor optical amplifier. In *Proc. IEEE LEOS Benelux Symposium 2007*, pages 147–150.

[114] P. J. Urban, A. M. J. Koonen, G. D. Khoe, and H. de Waardt. Mitigation of reflection-induced crosstalk in a WDM access network. In *Proc. OFC 2008*, paper OThT3.

[115] P. J. Urban, A. M. J. Koonen, G. D. Khoe, and H. de Waardt. Interferometric crosstalk reduction in an RSOA-based WDM passive optical network. *IEEE J. Lightw. Technol.*, 27(22):4943–4953, November 2009.

[116] T. Kamalakis, T. Sphicopoulos, and M. Sagriotis. Accurate estimation of the error probability in the presence of in-band crosstalk noise in WDM networks. *IEEE J. Lightw. Technol.*, 21(10):2172–2181, October 2003.

[117] Y. Shen, K. Lu, and W. Gu. Coherent and incoherent crosstalk in WDM optical networks. *IEEE J. Lightw. Technol.*, 17(5):759–764, May 1999.

[118] H. Kim, H. C. Li, and C. H. Kim. Effects of intraband crosstalk on incoherent light using SOA-based noise suppression technique. *IEEE Photon. Technol. Lett.*, 18(14):1542–1544, July 2006.

[119] M. Fujiwara, J-i. Khani, H. Suzuki, and K. Iwatsuki. Impact of backreflection on upstream transmission in WDM single-fiber loopback access networks. *IEEE J. Lightw. Technol.*, 24(2):740–746, February 2006.

[120] H. W. Hu and H. Anis. Degradation of bidirectional single fiber transmission in WDM-PON due to beat noise. *IEEE J. Lightw. Technol.*, 26(8):870–881, April 2008.

[121] Y. J. Lee, Y. Cho, A. Murakami, A. Agata, Y. Takushima, and Y. C. Chung. Reflection tolerance of RSOA-based WDM PON. In *Proc. OECC/IOOC 2007*, paper 11A1-4.

[122] P. J. Legg, M. Tur, and I. Andonovic. Solution paths to limit interference noise induced performance degradation in ASK/direct detection lightwave networks. *IEEE J. Lightw. Technol.*, 14(9):1943–1954, September 1996.

[123] R. Khosravani, M. I. Hayee, B. Hoanca, and A. E. Willner. Reduction of coherent crosstalk in WDM add/drop multiplexing nodes by bit pattern misalignment. *IEEE Photon. Technol. Lett.*, 11(1):134–136, January 1999.

[124] G. P. Agrawal, and N. A. Olson. Self-phase modulation and spectral broadening of optical pulses in semiconductor laser amplifiers. *IEEE J. Quantum. Electron.*, 25(11):2297–2306, November 1989.

[125] A. Yariv, H. Blauvelt, D. Huff, and H. Zarem. An experimental and theoretical study of the suppression of interferometric noise and distortion in AM optical links by phase dither. *IEEE J. Lightw. Technol.*, 15(3):437–443, March 1997.

[126] M. Sharma, H. Ibe, and T. Ozeki. WDM ring network using a centralized multiwavelength light source and add-drop multiplexing filters. *IEEE J. Lightw. Technol.*, 15(6):917–929, March 1997.

[127] K. Inoue. Suppression of influence of homowavelength crosstalk in an optical add/drop multiplexing system by modulating LD light frequency. *IEEE Photon. Technol. Lett.*, 11(9):1177–1179, September 1999.

[128] E. Tangdiongga, I. T. Monroy, R. Jonker, and H. de Waardt. Experimental evaluation of optical crosstalk mitigation using phase scrambling. *IEEE Photon. Technol. Lett.*, 12(5):567–569, May 2000.

[129] W.-S. Jang, H.-C. Kwon, and S.-K. Han. Sppression of Rayleigh backscattering in a bidirectional WDM optical link using clipped direct modulation. *IEE Proc.-Optoelectron.*, 151(4):219–222, August 2004.

[130] L. Occhi, L. Schares, and G. Guekos. Phase modeling based on the alpha-factor in bulk semiconductor optical amplifiers. *IEEE J. Sel. Topics in Quantum Electronics*, 9(3):788–797, May/June 2003.

[131] P. K. Pepeljugoski, and K. Y. Lau. Interferometric noise reduction in fiber-optic links by superposition of high frequency modulation. *IEEE J. Lightw. Technol.*, 10(7):957–963, July 1992.

[132] CIP Technologies. RSOA 02852 datasheet. *http://www.ciphotonics.com.*

[133] P. J. Urban, E. G. C. Pluk, M. M. de Laat, F. M. Huijskens, G. D. Khoe, A. M. J. Koonen, and H. de Waardt. 1.25 Gbit/s transmission over an access network link with tunable OADM and a reflective SOA. *IEEE Photon. Technol. Lett.*, 21(6):380–382, 2009.

[134] P. J. Urban, E. J. Klein, L. Xu, E. G. C. Pluk, A. M. J. Koonen, G. D. Khoe, and H. de Waardt. 1.25 Gbit/s bidirectional link in an access network employing a reconfigurable optical add/drop multiplexer and a reflective semiconductor optical amplifier. In *Proc. IEEE ICTON 2008*, paper We.B4.5.

[135] P. J. Urban, F. M. Huijskens, G. D. Khoe, A. M. J. Koonen, and H. de Waardt. Transmission of 10 Gbit/s per wavelength in a hybrid WDM/TDM access network providing bandwidth on-demand. In *Proc. IEEE ICTON 2009*, paper Tu.C5.6.

[136] P. J. Urban, F. M. Huijskens, M. M. de Laat, G. D. Khoe, A. M. J. Koonen, and H. de Waardt. Experimental demonstration of a 10 Gbit/s/wavelength 27 km-reach WDM/TDM-pon based on reconfigurable OADM and Colorless ONU. In *Proc. IEEE ECOC 2009*, paper 7.5.2.

[137] P. J. Urban, F. M. Huijskens, G. D. Khoe, A. M. J. Koonen, and H. de Waardt. Reconfigurable WDM/TDM access network providing 10-Gbit/s/λ over 27 km SSMF with colorless ONU. *IEEE Photon. Technol. Lett.*, accepted, 2009.

[138] Q. Fang, J. Song, G. Zhang, M. Yu, Y. Liu, G.-Q. Lo, and D.-L. Kwong. Monolithic integration of a multiplexer/demultiplexer with a thermo-optic VOA array on an SOI platform. *IEEE Photon. Technol. Lett.*, 21(5):319–321, 2009.

[139] M. Ken and T. Shinsuke. Record high saturation power (+22 dbm) and low noise figure (5.7 db) polarization-insensitive SOA module. *IEEE Photon. Technol. Lett.*, 17(6):1298–1300, 2005.

[140] Corning. Corning SMF-28e photonic fiber. *www.corning.com (white paper)*, pages 1–4, 2005.

[141] Yankee Group. FTTH services generate more revenue than DSL. *Lightwave*, February 2009.

[142] D. Elixmann, D. Ilic, K.-H. Neumann, and T. Plückebaum. *The economics of next generation access - final report.* WIK-Consult GmbH, Bad Honnef, Germany, 2008.

[143] G. Finnie. The business case for incumbent telco fiber networks. *Heavy Reading, www.ftthcouncil.eu.*

[144] G. Finnie. The business case for municipal fiber networks. *Heavy Reading, www.ftthcouncil.eu.*

[145] Nortel. Future-proof WDM PON based Ethernet access solution. *www.nortel.com (white paper)*, pages 1–7, 2008.

[146] A. V. Tran, C.-J. Chae, and R. S. Tucker. Ethernet PON or WDM PON: a comparison of cost and reliability. In *Proc. IEEE TENCON 2005*, pages 1–6.

[147] K. Fouli and M. Maier. OCDMA and optical coding: principles, applications, and challenges. *IEEE Commun. Mag.*, 45(8):27–34, 2007.

[148] X. Wang. Keys towards practical OCDMA networks. In *Proc. IEEE PHOTONICS 2004*, paper NET2.2.

[149] V. Baby, I. Glesk, R. J. Runser, R. Fischer, Y. -K. Huang, C. -S. Bres, W. C. Kwong, T. H. Curtis, and P. R. Prucnal. Experimental demonstration and scalability analysis of a four-node 102-Gchip/s fast frequency-hopping time-spreading optical CDMA network. *IEEE Photon. Technol. Lett.*, 17(1):253–255, 2005.

[150] A. E. Wilner, P. Saghari, and V. R. Arbab. Advanced techniques to increase the number of users and bit rate in OCDMA networks. *IEEE J. of Sel. Topics in Q. Electron.*, 13(5):1403–1414, 2007.

[151] K.-I. Kitayama, X. Wang, and N. Wada. OCDMA over WDM PON - solution path to Gigabit-symmetric FTTH. *IEEE/OSA J. Lightw. Technol.*, 24(4):1654–1662, 2006.

[152] G.-C. Yang and W. C. Kwong. *Prime codes with applications to CDMA optical and wireless networks.* Norwoord, MA: Artech House, 2002.

[153] M. J. R. Heck. *Ultrafast integrated semiconductor laser technology at 1.55 μm.* PhD thesis, Eindhoven University of Technology, Eindhoven, The Netherlands, 2008.

[154] P. B. Johns and R. L. Beurle. Numerical modelling of 2-dimensional scattering problems using a transmission line matrix. *IEE Proc.*, 118(9):1203–1208, 1971.

[155] W. J. Hoefer. The transmission-line matrix method - theory and applications. *IEEE Trans. Microw. Theory and Techniques*, 33(10):882–893, 1985.

[156] A. J. Lowery. Transmission-line modelling of semiconductors lasers: the transmission-line laser model. *Intern. J. Numerical Modelling, Electronic Networks, Devices and Fields,*, 2(4):249–265, 1989.

Acronyms

Abbreviation	Description
10GPON	10 Gigabit PON
ACP	Autocorrelation peak
ADSL(2 ,2+)	Asymmetric DSL (2, 2+)
APON	*see ATM-PON*
ARPU	Average revenue per user
ASE	Amplified spontaneous emission
ATM	Asynchronous transfer mode
AWG	Arrayed waveguide grating
BBPhotonics	Freeband Broadband Photonics Project
BBS	Brillouin BS
BER	Bit error rate
BERT	Bit error rate tester
BPF	Band-pass filter
BPON	Broadband PON
BPSK	Binary PSK
BS	Backscaterring
BtB	Back-to-back
CAPEX	Capital expenses
CCP	Crosscorrelation peak
CD	Chromatic dispersion
CO	Central office
CPE	Customer premises equipment
CW	Continuous wavelength
CWDM	Coarse WDM
CW	Continuous wavelength

continued on the next page –

– *continued from previous page*

Abbreviation	Description
DAC	Digital-to-analog converter
DEMUX	Demultiplexer
DFB	Distributed feedback
DPSK	Differential PSK
DS	Downstream
DSL	Digital subscriber line
DUT	Device under test
DWDM	Dense WDM
EAM	Electro-absorption modulator
EDFA	Erbium doped fiber amplifier
ER	Extinction ratio
EPON	Ethernet PON
FBG	Fiber Bragg grating
FDL	Fiber delay line
FP-LD	Fabry-Perot laser diode
FSR	Free spectral range
FTTC/B/H/N/P/X	Fiber-to-the-curb/building/home/node/premises/X
FWA	Fixed-wireless access
FWHM	Full width at half maximum
FWM	Four-wave mixing
GbE	Gigabit ethernet
GPON	Gigabit PON
HDTV	High-definition television
HE	Headend
HFC	Hybrid-fiber coax
HSI	High speed internet
ICT	Information and communication technology
IL	Insertion loss
IM	Intensity modulation
IRZ	Inverted return-to-zero
ISI	Inter-symbol interference
ITU	International Telecommunication Union
LC	Local controller
LD/TE	Lase diode/temperature controller
LEF	Linewidth enhancement factor

continued on the next page –

– continued from previous page

Abbreviation	Description
LLU	Local loop unbundling
LPF	Low-pass filter
LR-BBPhotonics	Limited reconfigurability BBPhotonics network
MAC	Medium access control
MC	Master controller
MEMS	Microelectromechanical switch
MIM	Michelson-interferometer modulator
MLLD	Mode-locked laser diode
MQW	Multiple quantum well
MR	Microring resonator
MUX	Multiplexer
MZ	Mach-Zehnder
MZI	MZ interferometer
MZM	MZ modulator
NF	Noise figure
NGA	Next generation access
NRZ	Not-return-to-zero
OADM	Optical add-drop multiplexer
OC	Optical code
OCDM	Optical code division multiplexing
OCDMA	Optical code division multiple access
ODN	Optical distribution network
OFSK	Optical frequency shift keying
OLT	Optical line termination
ONT	Optical network termination
ONU	Optical networking unit
OOK	On-off keying
OPEX	Operational expenses
OSA	Optical spectrum analyzer
OSNR	Optical signal-to-noise ratio
OSP	Outside plant
P2P	Peer-to-peer
PC	Polarization controller, personal computer
PCB	Printed circuit board
PDL	Polarization dependent loss

continued on the next page –

– *continued from previous page*

Abbreviation	Description
PM	Power meter
PMD	Polarization-mode dispersion
PON	Passive optical network
POTS	Plain old telephone service
PP	Power penalty
PPG	Pulse pattern generator
PRBS	Pseudo-random bit sequence
PSK	Phase shift keying
PtMP	Point-to-multi-point
PtP	Point-to-point
QoS	Quality of service
RBS	Rayleigh BS
REAM	Reflective EAM
RF	Radio frequency
RL	Return loss
RN	Remote node
ROADM	Reconfigurable OADM
ROI	Return on investment
R-ONU	Reflective ONU
ROP	Received optical power
RSOA	Reflective SOA
R-SOA-EAM	Reflective SOA-EAM
RX	Receiver
RZ	Return-to-zero
SBS	Stimulated BBS
SC	Supercontinuum
SCH	Separate confinement heterostructure
SCM	Subcarrier multiplexing
SCR	Signal-to-crosstalk ratio
SDTV	Standard definition television
SLU	Subloop unbundling
SMA	Subminiature version A connector
SNR	Signal-to-noise ratio
SOA	Semiconductor optical amplifier
SP	Service provider

continued on the next page –

– *continued from previous page*

Abbreviation	Description
SPM	Self-phase modulation
SRS	Stimulated Raman scaterring
SSMF	Standard single mode fiber
TDM	Time division multiplexing
TDMA	Time division multiple access
TE	Transverse electric
TFF	Thin-film filter
TLLM	Transmission-line laser model
TM	Transverse magnetic
TW	Traveling-wave
TX	Transmitter
US	Upstream
USB	Universal serial bus
UDP	User datagram protocol
VCSOA	Vertical-cavity SOA
VDSL2	Very high speed DSL 2
VOA	Variable optical attenuator
VoD	Video-on-demand
VoIP	Voice-over-internet protocol
WAN	Wide area network
WDM	Wavelength division multiplexing
XGM	Cross-gain modulation
XPM	Cross-phase modulation

Acknowledgements

I take this opportunity to express my gratitude to all the people who contributed in many ways to this book.

I am very grateful to my promotor, prof. Ton Koonen, who offered me the opportunity to do the research presented in this book. I wish to cordially thank to my direct daily supervisor and the first co-promotor, dr. Huug de Waardt, for fruitful discussions, technical excellence and very supportive attitude. I would like to thank to my second co-promotor, dr. Gerlas van den Hoven, whose presence in the research group added a unique flavor to the project.

I am grateful to the rest of my PhD Committee, prof. Josep Prat, prof. Stuart Walker, prof. Harm Dorren, and prof. Meint Smit, who approved this work.

I also acknowledge the Freeband Consortium for financing my position as a PhD researcher in the BBPhotonics project at the COBRA Institute.

I received a lot of support from office- and group-mates, technicians, secretaries, and all the rest of TU/e colleagues and students, IEEE LEOS Benelux Student-Board members, BBPhotonics project members as well as my friends and my family from Poland and my friends from the Netherlands. It is simply impossible to mention all of You by name here. A great part of You came from different countries from all over the world which made my stay in the Netherlands and work in Eindhoven an unrepeatable experience. Thank You for discussions, collaboration, fun and joy.

I owe direct thank-you to Bas Huiszoon who has supported my existence in the Netherlands throughout the time.

I am especially thankful to Marta, the beloved friend, who never stopped believing in the success of my work and assisted me in every single step.

Curriculum vitae

Patryk Urban was born in Szczecin, Poland, in January 1981. He received the M. Sc. Eng. diploma in Electrical Engineering from the Szczecin University of Technology, Szczecin, Poland, in 2004, where he was also a student assistant in 2003-2005 in the Optical Telecommunication and Photonics Group. In 2004 he graduated from Post-M.Sc. studies in Pedagogy at the University of Szczecin, Szczecin, Poland, and in 2004 he joined doctoral studies at Szczecin University of Technology in the field of nonlinear optics. In 2005 he moved to the COBRA Research Institute at the Eindhoven University of Technology, the Netherlands and started his research in optical access networks.

During the period as a Ph. D. researcher at the COBRA Research Institute he worked on the subject of next-generation broadband access network architectures involving network reconfigurability and bandwidth on-demand provision under the Broadband Photonics project. He also participated in KM3Net project which was focused on a high bitrate data transmission using reflective modulation scheme in submarine system.

He acts as a reviewer for the IEEE Photonics Technology Letters, the IET Electronics Letters and the IET Optoelectronics, and since 2007 he has been a journalist to the Polish Section of IDG ComputerWorld and NetWorld ICT magazines. He authored and co-authored over 30 scientific journal and conference papers as well as 10 popular-science papers on optical access networks. Since 2005 he has been an IEEE Student Member and in years 2006-2008 a member of IEEE/LEOS Benelux Student Chapter Board and a correspondent to IEEE Region 8 News.

List of publications

All publications are ranked chronologically per classification.

Books

1. *Progress in optical devices and materials: Proceedings 2007 Annual Workshop of the IEEE/LEOS Benelux Chapter*, Technische Universiteit Eindhoven, May, 2007. Editors: B. Huiszoon, P. J. Urban, and C. Caucheteur.

Refereed contributions

Journals

2. B. Huiszoon, P. J. Urban, H. de Waardt, J. Aracil, Optical Code Transmission Using Reflective SOA, *Submitted to IEEE Photon. Technol. Lett.*, pp. 1-3, September 2009.

3. P. J. Urban, F. M. Huijskens, G. D. Khoe, A. M. J. Koonen, and H. de Waardt, Reconfigurable WDM/TDM access network providing 10-Gbit/s/λ over 27-km SSMF with colorless ONU, *Accepted for IEEE Photon. Technol. Lett.*, pp. 1-3, May 2009.

4. P. J. Urban, G. D. Khoe, A. M. J. Koonen, and H. de Waardt, Interferometric crosstalk reduction in an RSOA-based passive optical network, *IEEE/OSA J. Lightw. Technol.*, vol. 27, no. 22, pp. 4943-4953, November 2009.

5. P. J. Urban, B. Huiszoon, R. Roy, F. M. Huijskens, E. J. Klein, G. D. Khoe, A. M. J. Koonen, and H. de Waardt, High bitrate reconfigurable WDM ring-shaped access network, *IEEE/OSA J. Opt. Commun. and Netw., Special issue on Optical Networks for the Future Internet*, vol. 1, no. 2, pp. A143-A159, July 2009.

6. N. Calabretta, P. J. Urban, D. H. Geuzebroek, E. J. Klein, H. de Waardt, and H. J. S. Dorren, All-optical label extractor/eraser for in-band labels and

160 Gbit/s payload based on micro-ring resonators, *IEEE Photon. Technol. Lett.*, vol. 21, no. 9, pp. 560-562, May 2009.

7. P. J. Urban, M. M. de Laat, F. M. Huijskens, G. D. Khoe, A. M. J. Koonen, and H. de Waardt, 1.25 Gbit/s Transmission over an access network link with tunable OADM and a reflective SOA, *IEEE Photon. Technol. Lett.*, vol. 21, no. 6, pp. 380-382, March 2009.

8. E. J. Klein, P. J. Urban, G. Sengo, L. T. H. Hilderink, M. Hoekman, R. Pellens, P. van Dijk, and A. Driessen, Densely integrated microring resonator based photonic devices for use in access networks, *Optics Express*, vol. 15, no. 16, pp. 10346-10355, August 2007.

International conferences

9. B. Huiszoon, P. J. Urban, H. de Waardt, and J. Aracil, Simulation results of bidirectional transmission on PON: Optically-encoded WDM channels and RSOA-based ONU, *Submitted to Optical Fiber Communication Conference (OFC) 2010*, March 2010, San Diego, CA, USA.

10. P. J. Urban, F. M. Huijskens, M. M. de Laat, G. D. Khoe, A. M. J. Koonen, and H. de Waardt, Experimental demonstration of a 10 Gbit/s/wavelength 27 km-reach WDM/TDM-PON based on reconfigurable OADM and colorless ONU, *Proc. European Conference and Exhibition on Optical Communication (ECOC) 2009*, paper 7.5.2, September 2009, Vienna, Austria.

11. M. M. de Laat, R. L. Duijn, E. G. C. Pluk, G. N. van den Hoven, P. J. Urban, and H. de Waardt, FlexPON: a hybrid TDM/WDM network enabling dynamic bandwidth reconfiguration using wavelength routing, *Proc. European Conference and Exhibition on Optical Communication (ECOC) 2009*, paper 1.6.3, September 2009, Vienna, Austria.

12. P. J. Urban, F. M. Huijskens, G. D. Khoe, A. M. J. Koonen, and H. de Waardt, Transmission of 10 Gbit/s per wavelength in a hybrid WDM/TDM access network providing bandwidth on-demand, *Proc. International Conference on Transparent Optical Networks (ICTON) 2009*, paper Tu.C5.6, Portugal, San Miguel Island.

13. N. Calabretta, P. J. Urban, D. H. Geuzebroek, E. J. Klein, H. de Waardt, and H. J. S. Dorren, All-optical label extractor/eraser for in-band labels and 160 Gbit/s payload based on micro-ring resonators, *Proc. Optical Fiber Communication Conference (OFC) 2009*, paper OWV4, March 2009, San Diego, CA, USA.

14. P. J. Urban, G. D. Khoe, A. M. J. Koonen, and H. de Waardt, Flexible optical access networks: towards the next generation, *Proc. ICT Connects: Next Generation Access Networks 2008*, November 2008, Lyon, France.

15. L. Xu, M. van Heijningen, G. van der Bent, P. J. Urban, X. J. M. Leijtens, E. Smalbrugge, T. de Vries, R. Nötzel, Y. S. Oei, H. de Waardt, and M. K. Smit, Hybrid InP-SiGe photoreceiver for the access network, *Proc. LEOS Annual 2008*, pp. 121-122, November 2008, Newport Beach, CA, USA.

16. P. J. Urban, M. M. de Laat, E. J. Klein, A. M. J. Koonen, G. D. Khoe, and H. de Waardt, 1.25 Gbit/s bidirectional link in an access network employing a reconfigurable optical add/drop multiplexer and a reflective semiconductor optical amplifier, *Proc. International Conference on Transparent Optical Networks (ICTON) 2008*, vol. 4, pp. 166-169, June 2008, Athens, Greece.

17. L. Xu, X. J. M. Leijtens, P. J. Urban, E. Smalbrugge, T. de Vries, R. Nötzel, Y. S. Oei, and H. de Waardt, InP-based monolithic integrated colorless reflective transceiver (POSTDEADLINE), *Proc. European Conference on Integrated Optics (ECIO) 2008*, pp. 13-16, Eindhoven, The Netherlands.

18. P. J. Urban, A. M. J. Koonen, G. D. Khoe, and H. de Waardt, Mitigation of reflection-induced crosstalk in a WDM access network, *Proc. Optical Fiber Communication Conference (OFC) 2008*, paper OThT3, February 2008, San Diego, CA, USA.

19. A. M. J. Koonen, A. Ng'oma, G.-J. Rijckenberg, M. Garcia Larrode, P. J. Urban, H. de Waardt, J. Yang, H. Yang, and H. P. A. van den Boom, How deep should fibre go into the access network? (INVITED), *Proc. European Conference and Exhibition on Optical Communication (ECOC) 2007*, vol. 1, pp. 27-30, September 2007, Berlin, Germany.

20. P. J. Urban, A. M. J. Koonen, G. D. Khoe, and H. de Waardt, Coherent crosstalk-suppression in WDM access networks employing reflective semiconductor optical amplifier, *Proc. European Conference and Exhibition on Optical Communication (ECOC) 2007*, vol. 3, pp. 91-92, September 2007, Berlin, Germany.

21. A. M. J. Koonen, P. J. Urban, H. Yang, M. Garcia Larrode, and H. de Waardt, Flexible optical access and in-building networks (INVITED), *Proc. Optoelectronics and Communications Conference/International Conference on Integrated Optics and Optical Fiber Communication (OECC/IOOC) 2007*, pp. 312-313, Yokohama, Japan.

22. A. M. J. Koonen, M. Garcia Larrode, J. Yang, P. J. Urban, H. Yang, A. Ng'oma, G. J. Rijckenberg, and H. P. A. van den Boom, Advanced technologies for service-integrated optical in-building networks (INVITED), *Proc. International Conference on Transparent Optical Networks (ICTON) 2007*, vol. 1, pp. 122-125, Rome, Italy.

23. P. J. Urban, E. J. Klein, L. Xu, E. G. C. Pluk, A. M. J. Koonen, G. D. Khoe, and H. de Waardt, 1.25-10 Gbit/s reconfigurable access network architecture, *Proc. International Conference on Transparent Optical Networks (ICTON) 2007*, vol. 1, pp. 293 - 296, Rome, Italy.

24. A. M. J. Koonen, M. Garcia Larrode, J. Yang, A. Ng'oma, G.-J. Rijckenberg, P. J. Urban, H. Yang, H. P. A. van den Boom, and H. de Waardt, Advanced techniques for versatile optical access and in-building networks (INVITED), *in Proc. International Symposium on Next Generation of Lightwave Communications 2007*, June 2007, Hong Kong.

25. A. M. J. Koonen, M. Garcia Larrode, J. Yang, A. Ng'oma, G.-J. Rijckenberg, P. J. Urban, H. Yang, H. P. A. van den Boom, and H. de Waardt, Recent research results on flexible optical access and in-building networks (INVITED), *Proc. European conference on Networks and Optical Communications (NOC) 2007*, pp. 153-160, June 2007, Stockholm, Sweden.

26. P. J. Urban, E. G. C. Pluk, E. J. Klein, A. M. J. Koonen, G. D. Khoe, and H. de Waardt, Simulation results of dynamically reconfigurable broadband photonic access networks (BBPhotonics), *Proc. International Conference on Access Networks (ICAT) 2006*, pp. 93-96, June 2006, Cambridge, UK.

Regional conferences and workshops

27. N. Calabretta, P. J. Urban, D. H. Geuzebroek, E. J. Klein, H. de Waardt, and H. J. S. Dorren, Exploiting micro-ring resonators for all-optical label extractor/eraser of inband labels and 160 Gbit/s payload, *Proc. Annual Symposium LEOS Benelux Chapter 2008*, pp. 11-14, November 2008, Enschede, The Netherlands.

28. L. Xu, X. J. M. Leijtens, P. J. Urban, E. Smalbrugge, T. de Vries, Y. S. Oei, R. Nötzel, H. de Waardt, and M. K. Smit, Novel reflective SOA with MMI-loop mirror based on semi-insulating InP, *Proc. Annual Symposium LEOS Benelux Chapter 2008*, pp. 43-46, November 2008, Enschede, The Netherlands.

29. L. Xu, M. van Heijningen, G. van der Bent, P. J. Urban, X. J. M. Leijtens, E. Smalbrugge, T. de Vries, R. Nötzel, Y. S. Oei, H. de Waardt, and M. K. Smit, 4 Gbit/s hybrid InP-SiGe photoreceiver for the user access network, *Proc. Annual Symposium LEOS Benelux Chapter 2008*, pp. 83-86, November 2008, Enschede, The Netherlands.

30. P. J. Urban, A. M. J. Koonen, G. D. Khoe, and H. de Waardt, Rayleigh backscattering-suppression in a WDM access network employing a reflective

semiconductor optical amplifier, *Proc. Annual Symposium LEOS Benelux Chapter 2007*, pp. 147-150, December 2007, Brussels, Belgium.

31. P. J. Urban, E. J. Klein, L. Xu, A. M. J. Koonen, G. D. Khoe, and H. de Waardt, 1.25 - 10 Gbit/s reconfigurable access network, *Proc. ePhotonOne Summer School 2007*, July 2007 Brest, France.

32. P. J. Urban, E. G. C. Pluk, A. M. J. Koonen, G. D. Khoe, and H. de Waardt, First design of dynamically reconfigurable broadband photonic access networks (BBPhotonics), *Proc. Annual Symposium LEOS Benelux Chapter 2005*, pp. 117-120, December 2005, Mons, Belgium.

Non-refereed contributions

Regional events

33. P. J. Urban, 10 Gbit/s Wavelength Flexible Access Network Architecture, *Proc. Broadband Photonics Workshop 2008*, April 2008, Eindhoven, The Netherlands.